JRC Scientific and Technical Reports

Project PISA: Phosphorus influence on steel ageing

Analysis of data from work-packages 2, 4, 5, 6, 7 and 8

AMES Report N. 20

AMES
Ageing Materials European Strategy

JRC
EUROPEAN COMMISSION

ie
Institute for Energy

EUR 23450 EN - 2008

The Institute for Energy provides scientific and technical support for the conception, development, implementation and monitoring of community policies related to energy. Special emphasis is given to the security of energy supply and to sustainable and safe energy production.

European Commission
Joint Research Centre
Institute for Energy

Contact information
Beatriz ACOSTA-IBORRA
Address: Westerduinweg 3, 1755 BL, Petten (the Netherlands)
E-mail: beatriz.acosta-iborra@jrc.nl
Tel.: 00-31-224-565435
Fax: 00-31-224-565636

http://ie.jrc.ec.europa.eu/
http://safelife.jrc.nl/ames/
http://www.jrc.ec.europa.eu/

JRC 46587
EUR 23450 EN
ISSN 1018-5593

Luxembourg: Office for Official Publications of the European Communities

Printed in Netherlands

Analysis of PISA data from WPs 2, 4, 5, 6, 7, and 8

Work Package No. 9: ***Final Data Analysis***

Project Deliverable: ***D10***

PROJECT PISA
PHOSPHORUS INFLUENCE ON STEELS AGEING

Contract No.: FIKS-CT-2000-00080

nexiasolutions
Nuclear expertise intelligently applied

Analysis of PISA data from WPs 2, 4, 5, 6, 7, and 8

Checked by : S.R Ortner

Approved by :J Hyde

10/00912

SAP Number

July 2005

VERIFICATION STATEMENT

This document has been verified and is fit for purpose. An auditable record has been made of the verification process. The scope of the verification was to confirm that: -

- The document meets the requirements as defined in the task specification/scope statement
- The constraints are valid
- The assumptions are reasonable
- The document demonstrates that the project is using the latest company approved data
- The document is internally self consistent

HISTORY SHEET

Issue Number	Date	Comments
Issue 1	July 2005	

Title:	**Analysis of PISA data from WPs 2, 4, 5, 6, 7, and 8**
Programme:	Fifth Framework of the European Atomic Energy Community (EURATOM)
Project:	Phosphorus Influence on Steels Ageing (PISA)
Work Package:	WP09 – Final Data Analysis
Deliverable:	D10
Report No.	**PISA/R(15)**
Report Status:	Final
Author(s):	**C.A.English, Ferenc Gillemot, Peter Kizler, Milan Brumovsky, Pertti Nenonen, Filippo Sevini, Sebastien Saillet, Milos Kytka, S. R. Ortner, Andrew Donaldson, Peter Binkele, Reinhard Langer, Antonio Ballesteros, David Bacon, Marta Horvath**

EXECUTIVE SUMMARY

The PISA project has generated significant amounts of data on both the segregation of P and C during irradiation and thermal treatments, and the associated mechanical property changes. The new data cover a range of bulk P levels, irradiation temperatures and fluences, steel types and product forms. In all cases only modest increases of P level on the grain boundary have been observed in commercial steels. Segregation is higher in pre-strained than in unstrained material.

A model for P segregation under irradiation has been developed, and shown to be capable of fitting the experimentally observed changes in P level after irradiation. Significant insight into the development of the microstructure under irradiation has thereby been obtained. In particular, the fraction of point defects surviving cascades is found to be very low.

The model indicates that P reaches the grain boundaries predominantly via the diffusion of P-point defect complexes, and their annihilation at sinks. This leads to a strong dependence of irradiation-induced P segregation on fluence, but any dependence of P segregation on flux or irradiation temperature is low. (These dependences are in accordance with data in the literature, and acquired during the PISA program.) The interaction between P and the point defects produced by irradiation does not allow for P leaving a boundary while the flux continues.

It is apparent that the C levels on the boundary reflect changes in carbide precipitation and C trapping in the matrix resulting from irradiation. A dynamic equilibrium is possible between C available in the matrix and C in the boundary, since C can diffuse independently of, and in conjunction with, the point defect flux. There is no evidence in the irradiated steels or from modelling for a relation between C and P segregation in the steels under irradiation.

The comparisons made during PISA between grain boundary chemistry and mechanical properties show that both P and C are important in determining boundary strength. High P levels and / or low C levels are detrimental to boundary strength, and lead to intergranular failure.

A very important result of the PISA program is that the $\Delta T_{41J}/\Delta\sigma_y$ or $\Delta T_{41J}/\Delta H_v$ data analysed give no indication of non-hardening embrittlement in any of the steels examined, even at very high doses. (VB step-cool may be an exception). In some cases, this could be ascribed to the small amounts of P accumulating in the boundaries, but several instances were observed in which the grain boundary P and C levels were such that significant amounts of IGF would be expected. Even in these cases, the embrittlement: hardening ratios showed no signs of segregation-related embrittlement. This suggests that irradiated steels could exhibit IGF without this having a detrimental effect on the resistance to cracking.

CONTENTS

LIST OF TABLES

LIST OF FIGURES

INTRODUCTION

The CEC has funded a program to study the effects of phosphorus (P) on the microstructure and mechanical properties of reactor pressure vessel (RPV) steels. The program is entitled “Phosphorus In Steel Ageing” (PISA). The main aim of the PISA program is to add data to that currently available on radiation-induced segregation and embrittlement, doing so in such a way as to clarify the dependence of segregation and embrittlement on parameters such as flux, fluence, irradiation temperature, time-at-temperature and composition. More quantitatively, the program aims to provide key data against which current models of P segregation, and those derived within PISA, can be tested.

This report is written in fulfilment of Work Package 9 (WP9) of the PISA program – Final Data Analysis. The object of this report is to analyse and assess the data acquired on the PISA project WPs 2 – 8. The organisation of the report is as follows:

- Section 2 describes in more detail the purpose and organisation of the PISA contract.
- Section 3 details the sources of the data to be reviewed, and provides an overview of the material selection. This includes information on composition, thermo-mechanical history and (where relevant) irradiation history. For convenience, some relevant information on materials is repeated in an abbreviated form in Sections 4-7.
- Section 4 provides an analysis of the significance of the mechanical property data, both that gathered during the course of the PISA project and also data supplied by the partners
- Sections 5, 6 and 7 provide an analysis of the significance of the segregation data collected on samples thermally treated, previously irradiated, and irradiated as part of the PISA project. In section 6, comparisons are also made with data on segregation supplied by the PISA partners from their archives.
- Section 8 provides an overview of the modelling of P and C segregation during thermal ageing and irradiation, and a comparison between modelling and experimental data is given.
- Section 9 provides an overall assessment of the significance of the data trends analysed in sections 4-8.

1. PURPOSE AND ORGANISATION OF THE PISA PROJECT

The integrity of the pressure vessel is vital to the safe operation of a nuclear reactor. It is therefore necessary to monitor or predict the changes in the reactor pressure vessel (RPV) material during operation. Exposure to irradiation (or elevated temperatures) causes the segregation of phosphorus to internal grain boundaries in RPV steels. This, in turn, encourages brittle intergranular failure (bIGF) of the material. The CEC has funded the PISA program to study the effects of P on the microstructure and mechanical properties of RPV steels. The overall objective of this program is to reducing the uncertainties associated with the impact of bIGF on the properties of the RPV, both during service and at the end-of-life (EOL).
Predicting the impact of the bIGF mechanism on RPV properties up to EOL requires the prediction of both the process of segregation, and the changes in mechanical properties resulting from segregation. The approach employed within PISA involves improving predictability by further developing our physical understanding of both these aspects, through focussed experimental investigations of irradiated steels and model alloys, and also through associated modelling studies. The approach to achieving improved predictability is given in Figure 1.

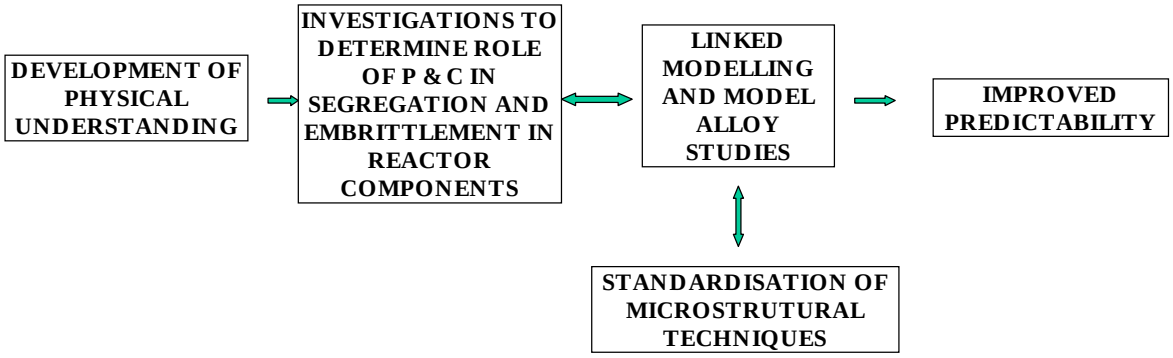

Figure 1. Schematic of the Aims of the PISA Program

The main elements of the PISA project are illustrated in Figure 2. In addition to the elements on modelling and analysis of selected materials, Figure 2 includes an element on technique standardisation. A critical aspect of the experimental measurements is the determination of the level of segregants on the grain boundaries, particularly P and C, and different methodologies are currently used by different laboratories. A comparison has been made within PISA of the segregation quantification techniques employed in the different laboratories, and initial steps have been taken towards optimising and standardising the measurement procedures.

A wide range of RPV steels has been considered within the PISA program, including the MnMoNi steels employed in European PWRs, the mild steels used in UK Magnox (steel) RPVs, and the low-alloy steels employed in VVERs. Intergranular fracture and/or P segregation is considered to be important in plant applications involving all three reactor types. The steel forms under consideration are plates, forgings, weld metals and weld heat-affected zones. In addition, some model alloys have also been examined, to help clarify processes occurring in the more complex steels.

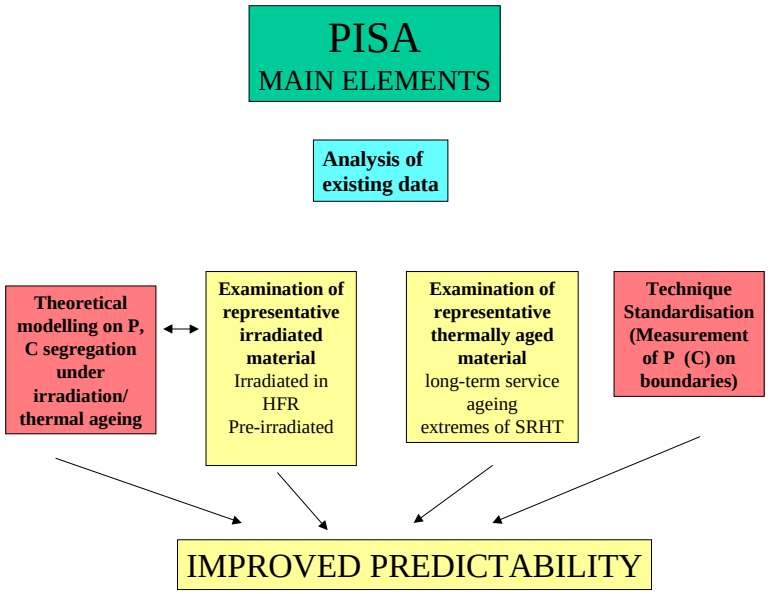

Figure 2. Elements of the PISA Program.

The elements of the PISA project illustrated in Figure 2 were divided into a number of Work Packages. These are illustrated in Figure 3.

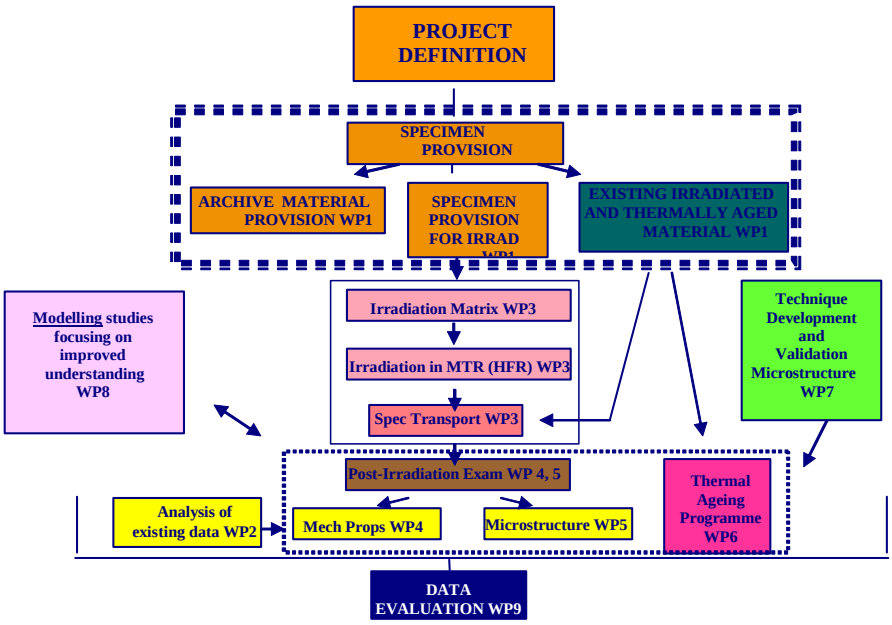

Figure 3. Work Package Structure.

2. SOURCES OF DATA TO BE REVIEWED

Several sources of data were employed in the different work packages (WPs) of PISA. These were:

a) Critical unpublished data from Partners on segregation and mechanical property changes in relevant irradiated RPV steels;
b) Data acquired during the PISA program on grain boundary segregation of P and C in material irradiated prior to the PISA program;
c) Data on mechanical property changes (ΔT_{41J} and ΔH_v), and on grain boundary segregation of P and C in material irradiated in irradiation rigs in HFR Petten during PISA;
d) Data on grain boundary segregation of P and C in thermally treated samples

Unpublished mechanical property and microstructural data from a number of different partners were collected and analysed as part of WP2 and WP9. In the latter this was in response to specific technical issues that arose out of the data acquired as part of the PISA project. These data are discussed in [1] and section 7. The information on the materials employed to acquire the data referred to in b) to c) above is detailed in Table 3.

2.1. Material irradiated prior to the PISA program

Microstructural measurements of grain boundary phosphorous (and carbon) coverage were made on materials irradiated prior to the PISA program. The primary aim was to select material that extended the parameter space available to the PISA project. Thus, samples were acquired which had been irradiated at higher fluences or lower fluxes than could be obtained in HFR Petten or during the period of the program. Details of these materials, and the reasons for their selection, are given in the Table below.

Table 1. Justification of selection of previously irradiated material (WP5).

Material	Irradiation condition	Reason for selection
PWR A533B plate JRQ	Start Of Life (SOL) 10^{20}ncm^{-2} at 270°C	The dose is higher than the EOL dose for most PWR RPVs. No material of this high a dose has been examined previously, and it is important to investigate what, if any, segregation is occurring.
VVER-440 weld # 502	SOL 3x10^{19} ncm^{-2} at 270°C	These high-P welds enable the inclusion of VVER 440 material in the PISA program.
VVER-440 test weld #501	SOL 2.4x10^{19} ncm^{-2} at 276°C.	
22 NiMoCr 37 PWR base metal heat ID 174 Data set ID –103 Data set ID – 725	103: 3.38x10^{19}ncm^{-2} @ 1.14x10^{11}ncm^{-2}s^{-1} 725: 3.20x10^{19} ncm^{-2} @ 2.26x10^{12}ncm^{-2}s^{-1} 285°C	A unique opportunity to examine material which has been irradiated in both surveillance programmes and in an accelerated MTR irradiation, to assess the influence of flux on segregation.
A508 Class 3 parent from ghost line	6.8x10^{19}ncm^{-2} @~4.4x10^{12}ncm^{-2}s^{-1}	Enables different microstructures (forging and HAZ) to be examined, and expands the composition range studied.
HAZ from ghost line	7.7x10^{19}ncm^{-2}@~4.4x10^{12}ncm^{-2}s^{-1}	
HAZ out of ghost line		

Table 2. Composition of previously irradiated steels (WP5).

Material	ID	Element (wt. %)										
		C	Mn	Si	P	S	Cr	Ni	Mo	V	Cu	Al
22 NiMoCr 37 PWR base metal	Heat ID 174	0.27	0.76	0.29	0.015	0.010	0.36	0.82	0.64	0.014	0.10	0.046
A533B PWR base metal	JRQ	0.07	1.34	0.21	0.020	0.002	0.11	0.70	0.49	0.002	0.15	0.014
Macrosegregated A508 Class 3	Material A (base)	0.18	1.31	0.24	0.011	0.007	0.18	0.70	0.50	0.006	0.08	0.06
	Material B (HAZ)	0.16	1.29	0.28	0.008	0.006	0.21	0.70	0.49	0.007	0.09	
VVER 440 test weld	501	0.03	1.17	0.40	0.038	0.014	1.38	0.12	0.49	0.19	0.17	0.003
	502	0.03	1.10	0.5	0.30	0.017	1.60	0.14	0.45	0.20	0.12	-

2.2. Material irradiated in HFR Petten

Segregation was studied in a number of RPV steels, to provide data relevant to several types of reactor. Different heat treatments were applied to the steels in order to assess the influence of microstructure and SOL segregation levels on subsequent segregation under irradiation [7]. A number of model alloys were also irradiated during the PISA program, so that the behaviour of simpler systems could be used to help interpret the behaviour of the more complex steels. Of these, segregation analyses were carried out on an Fe-P-C alloy in several heat treatment conditions. The materials examined are summarised in Table 3, and their compositions are given in Table 4.

Table 3. Materials irradiated during PISA program, and subsequently analysed for grain boundary segregation.

Steel / Alloy	Reactor Type	Heat Treatment Condition	Material ID
15Kh2NMFAA forging	VVER-1000	Base (Normalised, tempered and stress-relieved)	VA
		As VA, then step-cooled	VB
		Simulated Coarse-Grained Heat-Affected Zone (SCGHAZ)[1]	VC
CMn plate (Si-killed)	Magnox	Simulated works treatment	M1
A533B Class 1 (JRQ)	PWR	Plate	JX
		SCGHAZ[2]	JC
		Strained SCGHAZ	JE
Fe-P-C	-	Billet-cooled (M2A)	BC
		RPV cooled (M2B) (As M2A, + 10h 650°C, furnace cooled)	RPV
		Water quenched M2C (As M2A, + 10h 650°C, WQ)	WQ

[1] SCGHAZ treatment for VC = 1200°C/1h, air cool + 650°C/10h furnace cool
[2] SCGHAZ treatment for JC = 1200°C/0.5h oil quench + 615°C/25h, oil quench

Table 4. Compositions of materials irradiated during PISA program, and subsequently analysed for grain boundary segregation.

Element (wt. %)	Material			
	Magnox	JRQ	VVER 1000	FePC*
C	0.145	0.07	0.15	0.003
Mn	1.130	1.34	0.56	< 0.02
Si	0.195	0.21	0.27	0.01
P	< 0.015	0.020	0.010	0.12
S	0.041	0.002	0.011	< 0.002
Cr	0.036	0.11	2.17	< 0.02
Ni		0.70	1.23	0.03
Mo		0.49	0.59	< 0.005
V		0.002	0.09	
Cu	0.035	0.15	0.04	0.006
Co	< 0.015		0.006	
Sn	< 0.015		< 0.001	
Sb	< 0.015		< 0.001	
Al		0.014		< 0.005
Ti	< 0.015			0.03
N				< 0.0015
B				0.15ppm

* Heat treatment of FePC alloys is given in Section 2.4.3

2.3. Irradiation Conditions

Irradiations were carried out in the High Flux Reactor at JRC Petten (The Netherlands), using the LYRA facility. The conditions in which specimens were analysed are summarised in Table 5, and are described in detail in the material irradiation reports for the PISA program [2, 3, 4, 5]

Table 5. Irradiation conditions in which specimens were analysed in PISA program.

Irradiation Condition	Dose Seen By Auger Specimens		Irradiation Temperature (°C)
	$10^{22}nm^{-2}$; E>1MeV	dpa	
PISA 1	7.190	0.011	195
PISA B	30.02	0.0443	288
PISA C	6.78	0.010	287
	Dose Seen By Charpy and Hardness Specimens*		
PISA 1	10.0	0.015	195
PISA B	23.4	0.035	288
PISA C	8.04	0.012	287

*significant variability about these mean values due to specimen-to-specimen and material-to-material variation

2.4. Thermally Aged Samples

Two thermally-aged steels were chosen for examination in WP6, as shown in Table 6. The first was a PWR material owned by one of the partners which had been aged at the RPV operating temperature for several years. Examination of this material was intended to allow better differentiation between thermally-induced, and radiation-induced segregation in RPV materials. An equivalent VVER-1000 material was not available. Instead, base metal was step-cooled to encourage segregation in a relatively short time.

Table 6. Justification of material choice for WP6.

Material	Owner	Reason For Selection
PWR Weld 1D 200 Aged 2700 days at 290°C	Framatome	Unique opportunity to examine material that had undergone long term ageing at RPV operating temperature.
VVER 1000 Base Metal As-received or step cooled.	NRI Rez	Enabled the sensitivity of VVER 1000 base metal to slow cooling to be examined
Fe-0.012P-0.003C Model Alloy Water quenched, air cooled or RPV cooled.	BNFL	Thermal controls for PISA irradiations of model alloy. The different quench rates were intended to affect the start-of-life levels of P and C segregation.

2.4.1. Weld Metal ID 200

This material, supplied by Framatome, came from the core weld of a RPV. The weld was produced with the wire / weld flux combination NiCrMo 1 UP/LW 320, which is typical of submerged arc welds used in German RPVs. It was subjected to soaking and post-weld heat treatment prior to ageing at 290°C. The weld composition is given in Table 7, and further material details are to be found in [6].

Table 7. Compositions of materials studied in WP6.

Element (wt. %)	Material		
	PWR weld ID200	VVER-1000 base metal	Fe-P-C model alloy
C	0.06	0.15	0.003
Mn	1.85	0.56	<0.02
Si	0.18	0.27	0.01
P	0.010-0.016	0.010	0.12
S	0.004	0.002	<0.002
Cr	0.36	2.17	<0.02
Ni	0.86	1.23	0.03
Mo	0.52	0.59	<0.005
V	<0.01	0.09	
Cu	0.10	0.04	0.006
Al	0.011	-	<0.005

2.4.2. VVER-1000 Base Metal

The VVER-1000 base metal provided by NRI was taken from a cylindrical ring forging of 15Kh2NMFAA type steel. The composition is given in Table 7. The forging was normalised and tempered before being given a supplementary heat treatment at 620°C – 650°C characteristic of the final heat treatments seen by a RPV (condition VA).

Some of the forging material was given a subsequent step-cooling treatment of

593 °C – 1 hr
538 °C – 15 hrs
524 °C – 24 hrs
496 °C – 48 hrs
468 °C – 72 hrs,

followed by furnace cooling to 315 °C, and cooling in air to room temperature, in order to increase the grain boundary P levels (condition VB).

Further material details are given in [7].

2.4.3. FePC Model Alloy

In addition to the steels, an Fe-P-C model alloy, extensively studied in other programs [8, 9, 10], was chosen for examination. The alloy was provided by BNFL in three heat treatment conditions:

Condition M2/A
980 °C
Oil quench to 100 °C
650 – 670 °C – 10 hrs
Air cool to room temperature
(Referred to as Billet cooled (BC))

Condition M2/B
As M2/A +
650 °C – 10 hrs
Slow cool at approx. 5 °C/hr to 300 °C
Furnace cool to room temperature
(Referred to as RPV cooled (RPV))

Condition M2/C
As M2/A +
650°C - 10 hrs
Water quench to room temperature
(Referred to as Water Quenched (WQ))

The different tempering times and quench rates were designed to put different levels of P and C on the grain boundaries, prior to irradiation within the PISA program. The billet-cooled model alloy (condition M2/A) was used as a thermal control for the PISA 1 irradiation [11] (i.e. aged at 200°C for 75days) to further differentiate between thermally-induced and radiation-induced segregation.

2.5. Modelling

The objectives of the modelling were agreed to be:

- Improved prediction of the effect of flux, fluence and irradiation temperature for P segregation. Here, predictions for low fluxes are absolutely critical. The modelling of the data from the project on the influence of irradiation temperature and dislocation density will provide critical tests of the models.
- Modelling of the role of carbon on phosphorus segregation is a key aspect of WP8. Here, the aim is to understand the conditions when it is likely to be important, and to develop a potential methodology for treating carbon or phosphorus segregation under thermal ageing.
- Improved evaluation of input parameters required for modelling.

3. MECHANICAL PROPERTY DATA

3.1. Overall trends

3.1.1. CMn steels

In the PISA programme Charpy data were obtained from an unirradiated CMn plate BW78B, and from BW78B plate irradiated at 290°C in PISA B and C. The 41J transition temperatures for CMn plate in these conditions are given in Table 8. The doses associated with each irradiation are the averages taken over all specimens of CMn plate in each irradiation.

Table 8. Charpy data obtained on CMn plate BW78B (Cu = 0.035 wt%)

Condition	T_{41J} (°C)	ΔT_{41J} (°C)
Unirradiated	2.7	-
PISA C (14.3mdpa)	76.5	73.8
PISA B (39mdpa)	80.1	77.4

Considerable embrittlement occurred during the first 15mdpa of irradiation, with much less embrittlement occurring during the subsequent 34mdpa.

It is of interest to compare these data with the mechanistically based dose-damage relationships used to predict irradiation hardening/embrittlement of Magnox pressure vessel steels. Dose-damage relationships of the following form are applied for Magnox pressure vessel steels and weld metals [12]:

$$\Delta\sigma_y \text{ (or } \Delta T_{40J}) = B + A F_T \sqrt{(\text{dose})}$$

Equation 1

where B represents the peak hardening effect of copper,
A is a material dependent constant,
F_T is the irradiation temperature factor.

Neutron damage dose units are dpa, with thermal neutrons (<1 keV) having a damage effectiveness factor that is twice that of fast neutrons (>1 keV) i.e. dose is evaluated in terms of $dpa_{fast} + 2*dpa_{thermal}$. The trend curve and the associated data are plotted in Figure 4.

It can be seen from Figure 4 that the embrittlement of the lower-dose PISA C material is in keeping with the dose damage relationship, whilst the PISA B material exhibits lower embrittlement than expected. Similar behaviour is observed in the hardness measurements made on the individual Charpy specimens. Charpy specimens in a given PISA rig experienced a range of doses. Taking hardness measurements from these samples thus allowed hardness data to be obtained from material irradiated from ~10mdpa to ~50mdpa. The hardness data so acquired are shown in Figure 5. Although there is considerable scatter in each data set, a trend line through the data shows that there was an increase in hardness on going from PISA C to PISA B, though it is only a small. The hardening and embrittlement data thus appear qualitatively consistent.

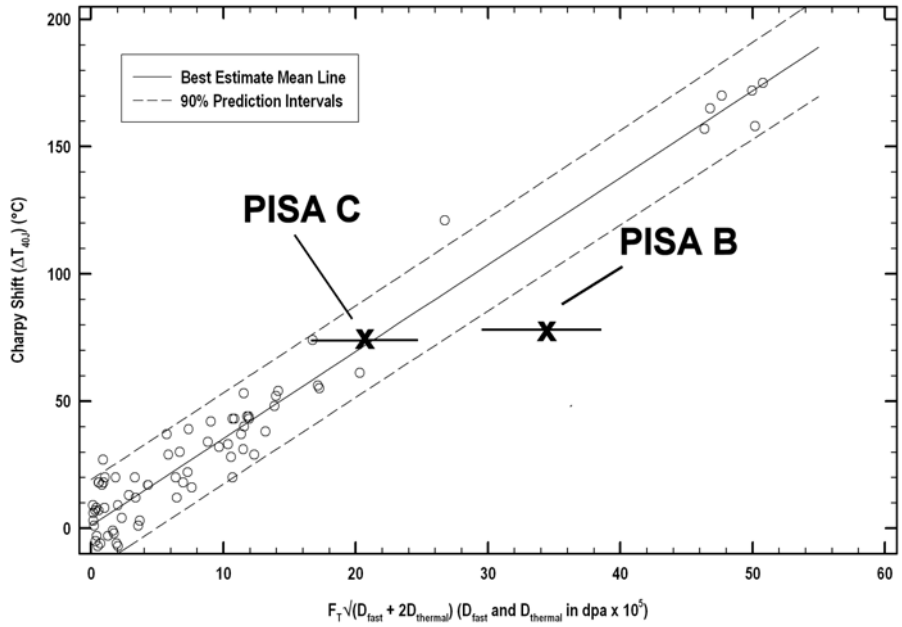

Figure 4. Comparison of Charpy shift data for CMn plate BW78B irradiated in PISA B and C with the surveillance data and dose damage relationship for Si-killed plate [Wootton private communication].

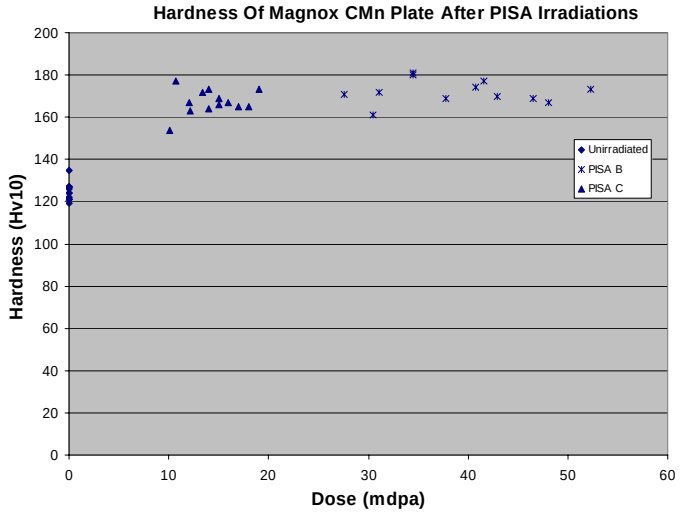

Figure 5. Hardness data (HV10 Equostat) obtained on CMn plate BW78B.

Quantitative correlations between Charpy and hardness shifts under irradiation have been published by Williams et al [13], although these correlations were for A533B plate and weld, rather than CMn plate. They used a linear fit to data involving ΔT_{41J} shifts up to 300°C. The derived expressions were

$\Delta T_{41J} = 1.64 \times \Delta H_v$ **(plate)**

Equation 2

and

$\Delta T_{41J} = 2.225 \times \Delta H_v$ **(weld)**

Equation 3

In Figure 6 the hardness data from the individual Charpy specimens have been converted to equivalent Charpy shifts using Equation 2, and compared to the measured Charpy shifts. It can be seen that the measured Charpy data, and the Charpy shifts predicted from hardening are quantitatively as well as qualitatively consistent. The lower-than expected embrittlement measurement thus appears reliable.

Also plotted on Figure 6 are data obtained on BW78B by Chivers [14] in an irradiation in the IVAR irradiation facility at the University of Virginia. It can be seen that the highest dose corresponds closely to that obtained in the PISA C irradiation, and the two measured shifts are also in keeping. Like the PISA C datum, the embrittlement data obtained by Chivers agree with the dose damage relationship of Jones and Bolton, and exhibit a square root dependence on dose.

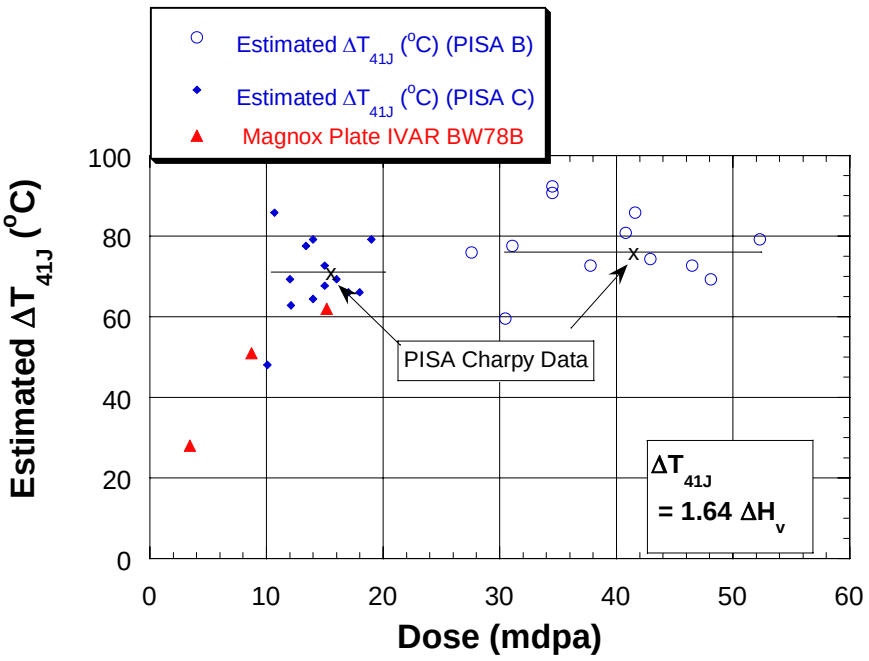

Figure 6. Comparison of Charpy and 'converted' hardness data for CMn plate BW78B. The hardness data have been converted to a ΔT_{41J} equivalence using Equation 2

Although the embrittlement of the higher-dose PISA B material is lower than predicted by the Magnox dose-damage relation, Equation 1, the change in embrittlement between 10mdpa and ~50mdpa is similar to that predicted by the USNRC correlation (for matrix damage only since BW78B is very low in Cu) for a 0.015wt.% P steel. This is illustrated in Figure 7. This result is unexpected.

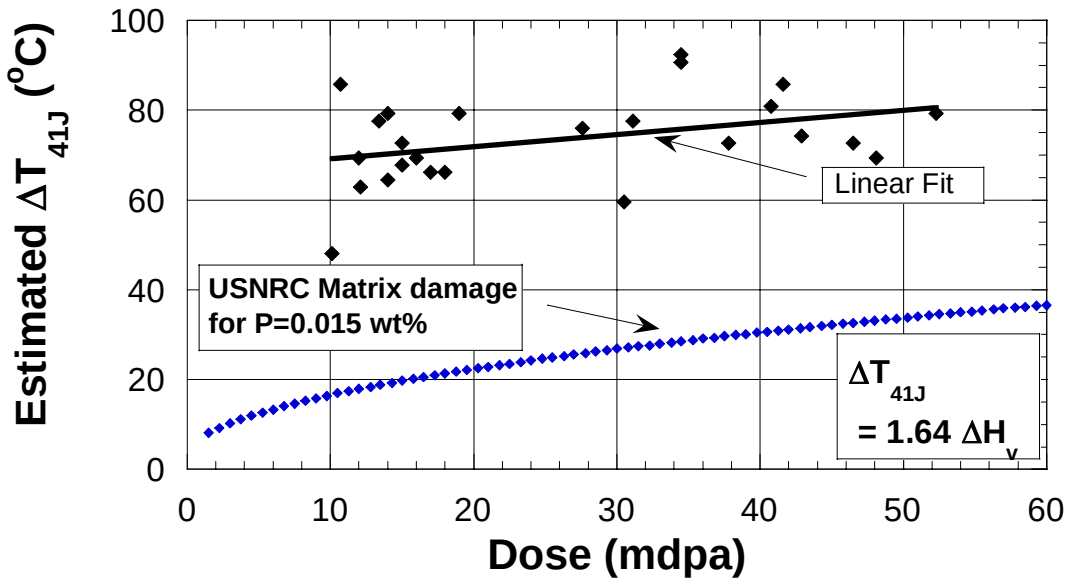

Figure 7. Comparison of 'converted' hardness data for CMn plate BW78B from PISA B and C with the predictions of the hardening from matrix damage by the USNRC correlation for a plate steel with P=0.015 wt% P.

The similarity of the increase in embrittlement between PISA C and PISA B to the USNRC prediction may be coincidental but, together with the unexpected result seen in Figure 4, may indicate an effect of dose on the embrittlement rate in CMn steels. It is worth noting that the data in Figure 4 data are plotted using F_T*√dose rather than simply √dose. (F_T is the Jones and Williams [15] expression describing the temperature dependence of matrix damage: $F_T = 1.869 - 4.57 \times 10^{-3}T$). Although there are higher F_T*√dose data in Figure 4 than the PISA B datum, these were obtained at lower irradiation temperatures. The PISA irradiations at 290°C are the highest dose data acquired at this temperature for CMn plate (Bolton private communication). The higher matrix hardening seen in CMn plates rather than MnMoNi plates is due to the higher free N levels in the former. It is possible that the free N present at SOL is gradually pinned at matrix defects as radiation proceeds, so that the initial high hardening rate gradually diminishes to the level seen in MnMoNi steels. If the dose at which the value of A in Equation 1 effectively diminishes is itself temperature-dependent, then the location of the PISA B datum in Figure 4, and the similarity between the slopes of the lines in Figure 7 (despite the higher initial shift in the CMn plate) could be justified.

Fractography was carried out on the CMn plate prior to irradiation, and after the PISA B and PISA C irradiations. Some intergranular fracture (IGF) was present, although transgranular cleavage dominated, as shown in Figure 8, and it was not possible to determine if the proportion of IGF changed with irradiation.

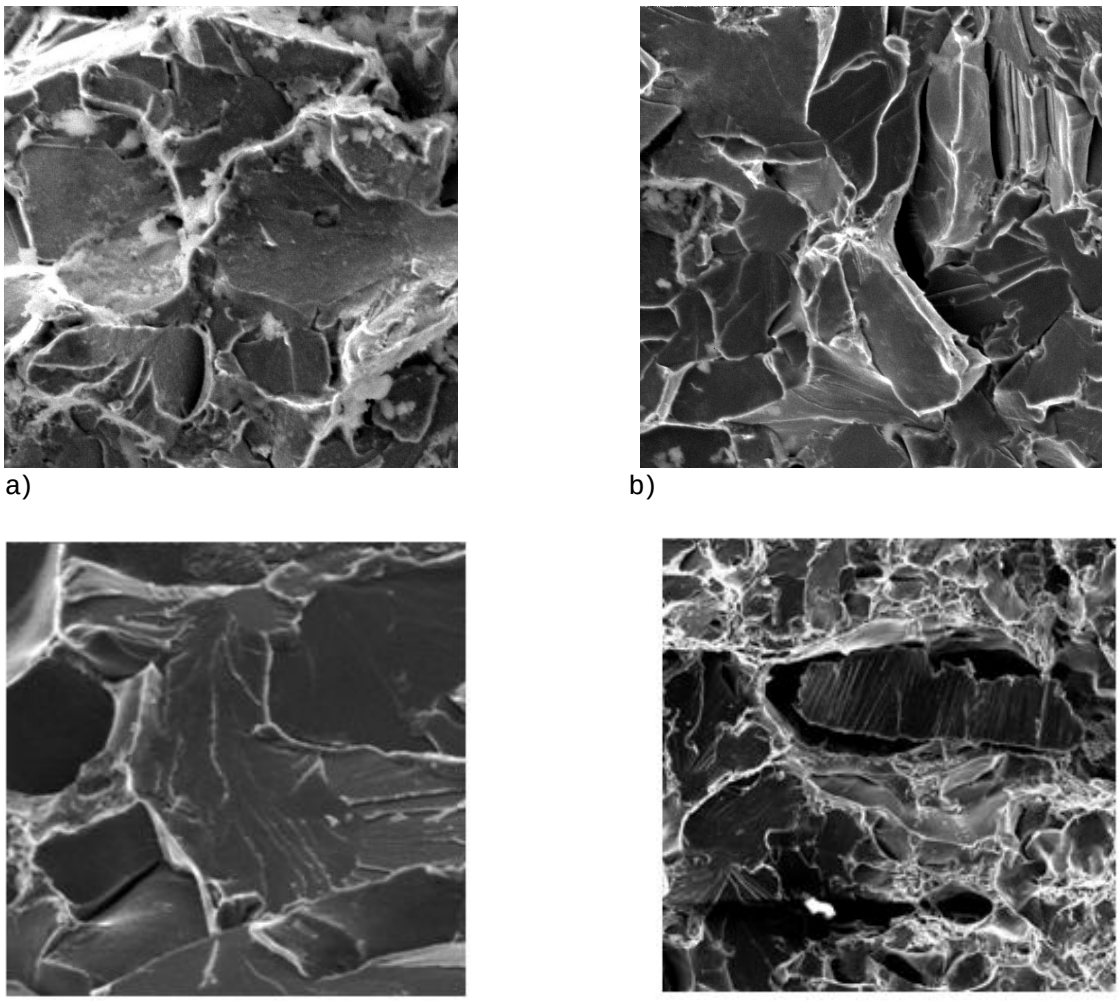

a) b)

c) d)

Figure 8. Fracture surfaces of CMn plate Charpy specimens (a, b) at SOL, tested at 0°C (Absorbed energy = 43J) (c, d) after PISA C irradiations, tested at 84°C (Absorbed energy = 44J).

3.1.2. MnMoNi Plate JRQ.

The MnMoNi plate JRQ containing 0.15wt% Cu and 0.02 wt% P was irradiated in three conditions; as-received, after a thermal treatment to generate SCGHAZ microstructure, and then in this condition but with 5% compressive pre-strain. The Charpy data obtained are given in Table 9 and Table 10. The radiation doses described in the Tables are the averages over all the different JRQ Charpy samples exposed during a given irradiation.

Table 9. Charpy data (T_{41J} (°C)) obtained from samples of JRQ irradiated in PISA I, B and C.

SOL Condition	Irradiation Condition			
	Unirradiated	PISA I 16mdpa @ 195°C	PISA C 12mdpa @ 290°C	PISA B 30.3mdpa @ 290°C
As-received (JX)	-14.4		24.7	
SCGHAZ (JC)	-88.3	10.6	-63.4	5.9
SCGHAZ + ε (JE)	-75.5		-18.7	

Table 10 ΔT_{41J} (°C)) obtained from samples of JRQ irradiated in PISA I, B and C.

SOL Condition	Irradiation Condition		
	PISA I 16mdpa @ 1950°C	PISA C 12mdpa @ 290°C	PISA B 30.3mdpa @ 290°C
As-received (JX)		39.1	
SCGHAZ (JC)	98.9	24.9	82.4
SCGHAZ + ε (JE)		56.8	

Trends in the SCGHAZ data

The Charpy data from JRQ SCGHAZ demonstrate that as expected the embrittlement increases with increasing fluence at 290°C and with decreasing irradiation temperature at ~10mdpa (PISA I *vs*. PISA C). The hardness data for JRQ SCGHAZ after irradiation at 290°C are also consistent with hardening increasing with increasing fluence (Figure 9). As was found for the CMn plate, the hardening and embrittlement data are qualitatively consistent, even though the unirradiated (and irradiated) hardness data exhibit significant scatter.

In Figure 10 the Charpy data measured after the 290°C irradiations, and the hardness data converted to a ΔT_{41J} shift using Equation 2, are compared to the predictions of the ASTM E900-02 and USNRC embrittlement correlations for MnMoNi steels in US BWRs and PWRs [16, 17 and 18]. In Figure 10, the converted hardness data appear to be largely consistent with expectation, as does the embrittlement measured after the higher-dose PISA B irradiation. The embrittlement measured on the lower-dose PISA C-irradiated specimens appears lower than expected from either the embrittlement versus dose correlations or the embrittlement versus hardness correlation. In this material, then, the lower-than-expected embrittlement measurement appears to be related more to scatter than to any particular embrittlement mechanism.

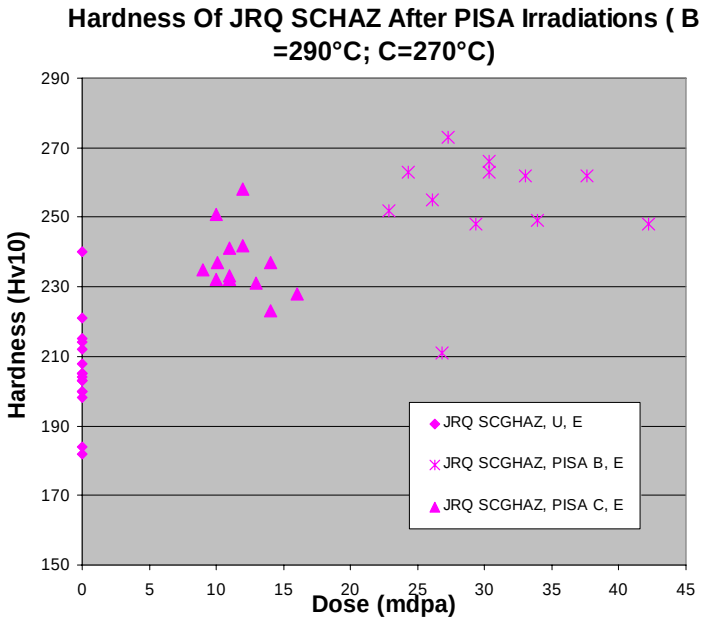

Figure 9 Hardness data (HV10 Equistat) for JRQ SCGHAZ

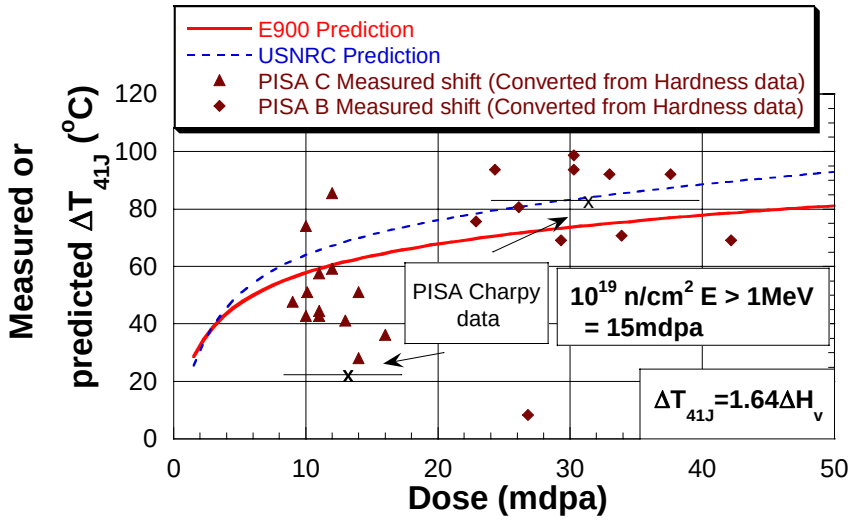

Figure 10 Comparison of Charpy and 'converted' hardness data for JRQ SCGHAZ with the predictions of the E900 and USNRC embrittlement correlations. The experimental hardness data have been converted to a ΔT_{41J} equivalence using Equation 2.

The hardening after irradiation at ~200°C is compared with that after irradiation at 290°C in Figure 11. Hardening is clearly significantly greater after irradiation at the lower temperature.

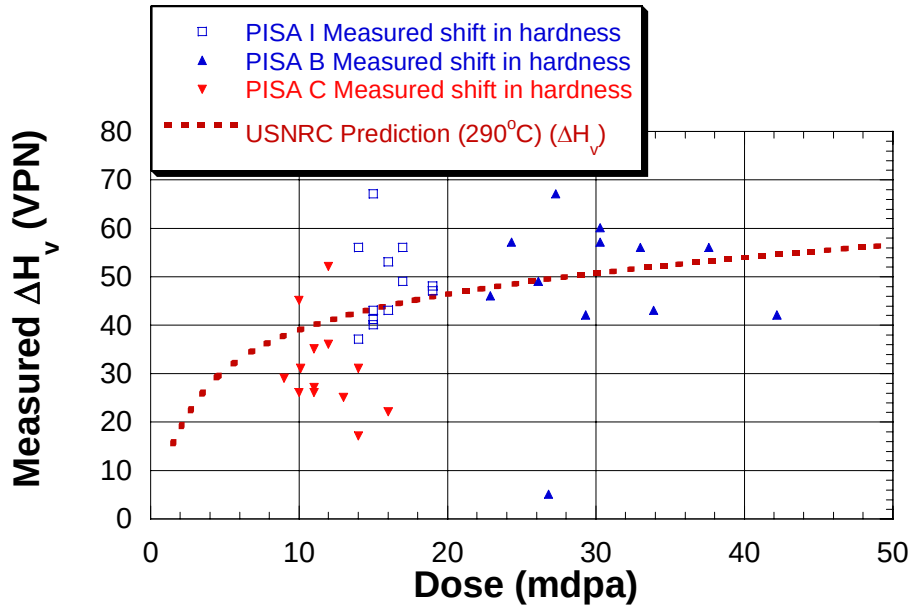

Figure 11 Comparison of the measured hardness for JRQ SCGHAZ irradiated in PISA I (195°C), PISA B and PISA C (290°C).

Although it is well-established that decreasing the irradiation temperature increases the hardening, the US embrittlement correlations were developed from Charpy data obtained in irradiations with a relatively restricted range of temperatures (~270-295°C). Thus they cannot be used to predict the effect of changing the irradiation temperature from 290°C to 200°C. The F_T parameter developed by Jones and Williams [15] can, however, be used to adjust the hardening for matrix damage over this large change in irradiation temperature. The following comparison was made: for each dose experienced by a PISA I-irradiated sample, the USNRC dose-damage correlation was used to predict a hardening increment (for 290°C). The matrix damage component of this hardening increment was then scaled by a factor F_{200}/F_{290} where $F_T=1.869-4.57\times10^{-3}T$, to determine what the equivalent hardening at this dose at 200°C would have been. The difference between the two calculated values of $\Delta\sigma$ was calculated (call it $\Delta\sigma_{difference}$). Each hardening increment actually measured after the 200°C irradiation was then reduced by its corresponding $\Delta\sigma_{difference}$ to estimate the hardening which would have occurred at 290°C. These data are shown in Figure 12.

In Figure 12, the temperature-adjusted PISA I data appear consistent with the PISA B and PISA C data. This indicates that the F_T parameter is applicable to MnMoNi steels as well as to CMn steels, and that the major effect of changing irradiation temperature is on the level of hardening from matrix damage (rather than an effect of the hardening from the formation of Cu enriched clusters).

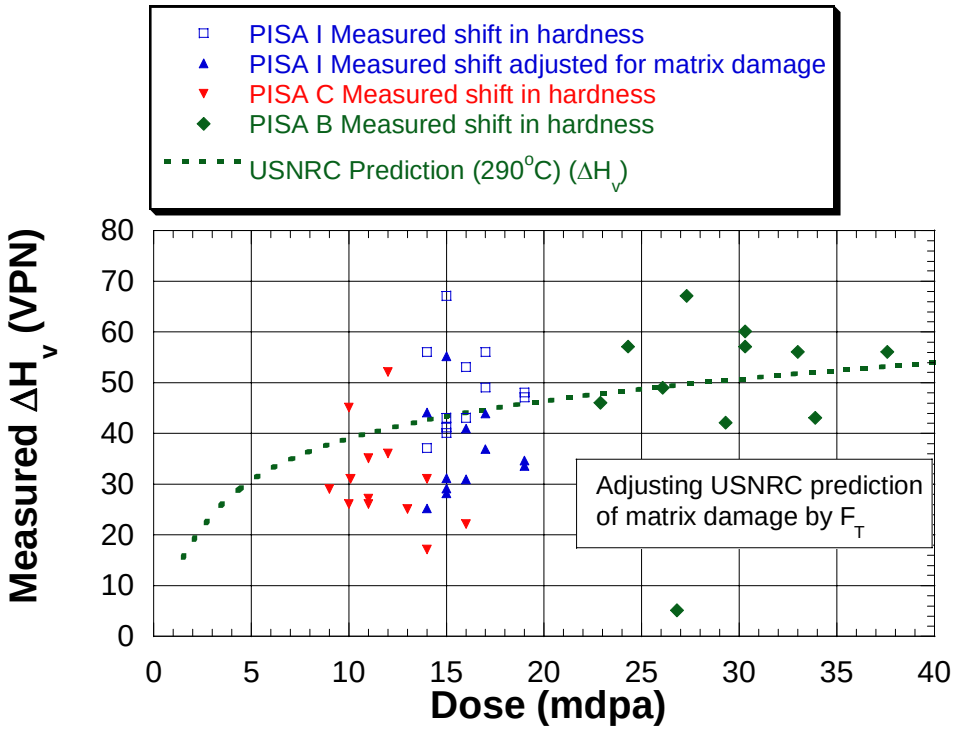

Figure 12. Comparison of the measured hardness (Hv10 Equistat) for JRQ SCGHAZ irradiated in PISA I, PISA B and PISA C. In addition, PISA I data are shown reduced by an amount that allows for the effect of irradiation temperature on matrix damage (see text above).

Table 9 and Table 10 compare the embrittlement induced by the PISA C irradiation in JRQ with different microstructures. They show that the embrittlement from JRQ in the SCGHAZ+ε condition was greater than that from JRQ plate or JRQ SCGHAZ. Some of this difference in embrittlement is due to the slightly different doses experienced by specimens with different microstructures (10.7mdpa on average for the plate specimens versus 11.9 for SCGHAZ and 14mdpa for SCGHAZ+ε). Figure 13, however, compares the hardnesses of the individual samples as a function of dose, and it may be seen that the hardening from JRQ in the SCGHAZ+ε condition was still greater than that from JRQ plate or JRQ SCGHAZ at equivalent doses. The difference between the hardening of plate and unstrained SCGHAZ is less marked once the different exposures are taken into account, but the SCGHAZ may still harden less than the plate.

The effect of prestrain on the radiation hardening of JRQ SCGHAZ is difficult to explain. One might expect that the additional dislocation lines in pre-strained material would act as extra sinks for the irradiation-induced point defects, thereby lowering the hardening and embrittlement if anything. Experimental data on other MnMoNi steels strained and aged at room temperature, however, do tend to show similar behaviour to that shown here by the JRQ SCGHAZ. The limited data available often show greater embrittlement in the pre-strained MnMoNi steels at moderate embrittlement levels. This is illustrated in Figure 14.

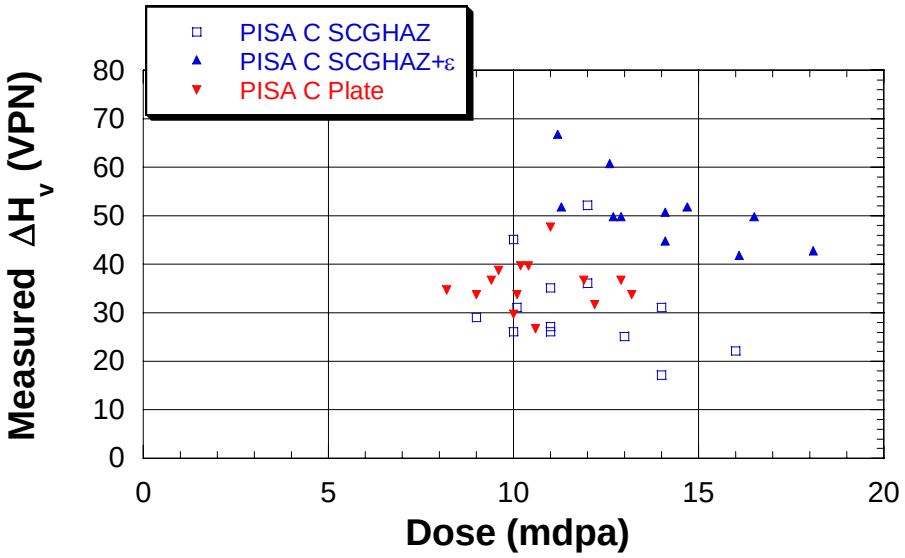

Figure 13. Comparison of the hardening from JRQ plate, JRQ SCGHAZ, and JRQ SCGHAZ + ε irradiated in PISA C

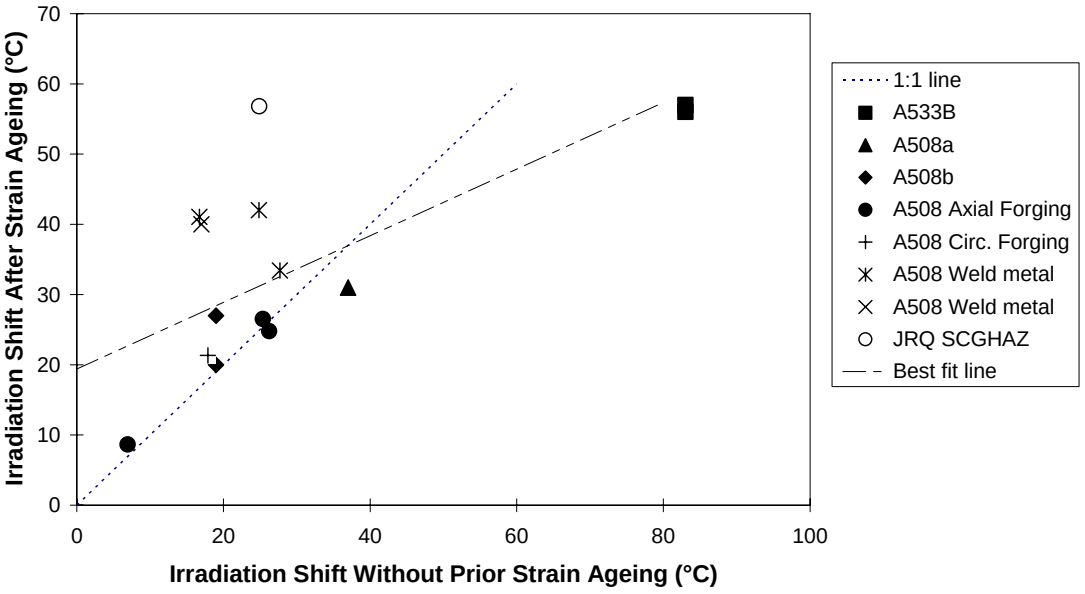

Figure 14. Effect of prestraining (or strain ageing) on the embrittlement produced by irradiation of MnMoNi steels, from various sources (A533B and A508a [19] A508b [20] forgings and weld metals [21]).

The fracture surfaces of JRQ Charpy specimens were examined. Only the pre-strained SCGHAZ samples showed any signs of intergranular failure prior to irradiation. Some IGF was also observed in JRQ SCGHAZ after the PISA B and PISA C irradiations, but the transgranular cleavage fracture mode clearly dominated.

3.1.3. VVER 1000 Base Metal

The measured transition temperatures are given in Table 11, and the corresponding Charpy shift, ΔT_{41J} °C, values are given in Table 12 for the base material in the three material conditions (VA as received, VB step cooled, and VC SCGHAZ) The radiation doses described in the Table are the averages over all the different VVER Charpy samples exposed during a given irradiation. The mean exposures of the different material conditions are in fact within 1mdpa of each other after the PISA I and PISA C irradiations. After the PISA B irradiation, the average exposures were higher for the base metal, VA (44.4mdpa) than for the SCGHAZ, VC (39.3mdpa) or the step-cooled base metal, VB (35.7mdpa).

It can be seen that, as expected, the observed embrittlement increases with increasing irradiation dose (PISA C vs PISA B) and decreasing irradiation temperature at ~15mdpa (PISA C vs PISA I) for all heat treatments. Step-cooling significantly increases the embrittlement (VB *vs* VA) caused by each irradiation. The step-cooling should have had the greatest effect on level of P on the boundaries, i.e. the increased embrittlement may be due to non-hardening embrittlement. It is interesting that the VVER SCGHAZ (VC) is more sensitive to radiation embrittlement than the base metal (VA) while the opposite was found to be true of the JRQ SCGHAZ and plate. After the 290°C irradiations the VVER SCGHAZ shows even greater embrittlement than the step-cooled steel (VB).

Table 11. 41J Charpy transition temperatures measured in VVER steels.

Material Condition	Irradiation Condition			
	Unirradiated	PISA I 11.5mdpa @ 200°C	PISA C 15.0mdpa @ 290°C	PISA B 39.8mdpa @ 290°C
Base metal, VA	-86	-46	-81	-68
Step-cooled, VB	-117	-49	-98	-90
SCGHAZ, VC	-21	+36	+15	+25

Table 12. Measured Charpy Shift ΔT_{41J} °C

Material Condition	Irradiation Condition		
	PISA I 11.5mdpa @ 200°C	PISA C 15.0mdpa @ 290°C	PISA B 39.8mdpa @ 290°C
Base metal, VA	40	5	18
Step-cooled, VB	68	19	27
SCGHAZ, VC	57	36	46

In Figure 15, the embrittlements measured after the 290°C irradiations are compared with the maximum embrittlement formula given for VVER 1000 base metal in [22]. Even the very sensitive VC microstructure lies below the maximum expected level.

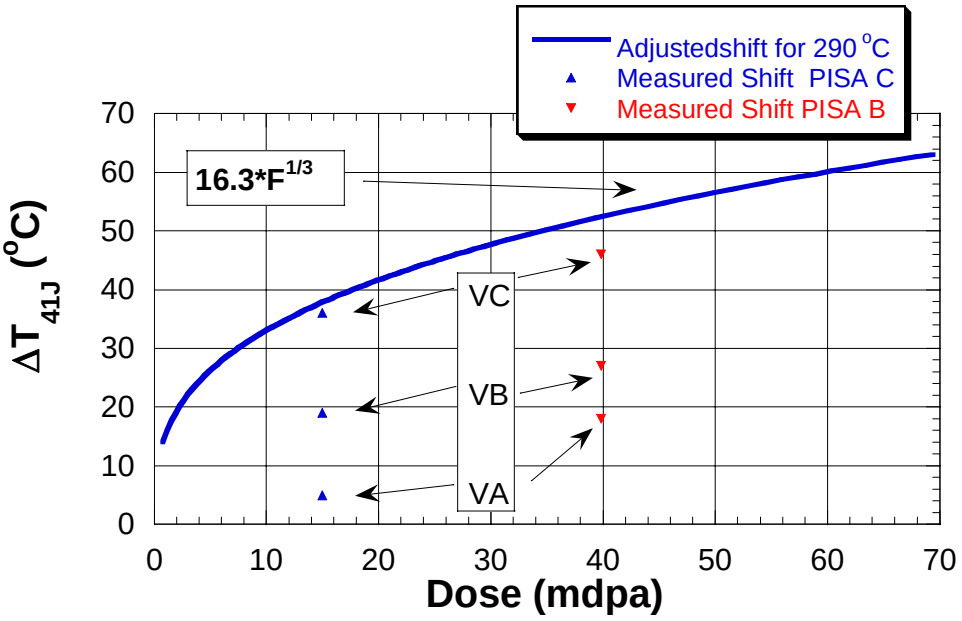

Figure 15. Embrittlement (ΔT_{41J}) caused in different VVER microstructures by radiation at 290°C.

3.1.4. Summary

In this section we have discussed the increase in Charpy shift on irradiation in the PISA irradiations at HFR Petten with the expected behaviour of these materials. In the case of JRQ and the CMn plate hardness data on individual Charpy specimens was available. On the basis of a generally accepted correlation between ΔH_V and ΔT_{41J} the shifts in hardness and Charpy data in these cases are consistent.

The following remarks may be made about each material.

1. For JRQ the general trends in hardening/embrittlement with dose are consistent with expected behaviour at different doses or irradiation temperatures. The initial microstructure clearly has a strong influence on the resultant embrittlement. It is interesting to note that pre-strain has increased the irradiation-induced shifts in both hardening and embrittlement.

2. For the CMn plate irradiated at 290°C, the data suggest that there is surprisingly little dependence on fluence for the fluence conditions studied, with the irradiation-induced shifts at higher fluence being lower than expected. (It is to be noted that the embrittlement observed in CMn plate after irradiations at 290°C at lower fluences is fluence dependent).

3. For the VVER 1000 base metal there is a strong role of initial microstructure in determining the irradiation induced shift. In particular material with an SCGHAZ microstructure exhibits a greater irradiation-induced shift than the parent material irradiated under identical conditions. The step-cooled material has a greater shift than the parent material.

3.2. The ratio of $\Delta T_{41J}/\Delta\sigma_y$ or $\Delta T_{41J}/\Delta H_v$

3.2.1. General Considerations

P segregation does not affect yield stress or hardness, although it can induce embrittlement. Irradiation usually causes an increase in the tensile properties which, itself, increases the ductile-brittle transition temperature (DBTT). Thus the ratio of the yield stress or hardness change to, say, the increase in DBTT measured by Charpy testing, is frequently a good measure of whether non-hardening embrittlement is occurring. For the samples irradiated in the PISA program, hardness measurements were made on either individual Charpy samples or on specially prepared slices. It is thus possible to make reasonable comparisons between the radiation-induced hardening and embrittlement. In addition, unpublished data on the effect of irradiation on the DBTT and yield stress were supplied by the partners for conditions of interest, in particular low dose rates (from vessel surveillance irradiations), and high fluences.

It is important first to establish the values of $\Delta T_{41J}/\Delta H_v$ (or $\Delta T_{41J}/\Delta\sigma_y$) that may indicate operation of non-hardening embrittlement. This topic was reviewed in [1] and it was concluded that, for hardening embrittlement the following ratios were typical:

$\Delta T_{41J} = 0.7\ \Delta\sigma_Y$ (°C/MPa) for welds

and

$\Delta T_{41J} = 0.6\ \Delta\sigma_Y$ (°C/MPa) for base metals.

Furthermore, from the data reviewed in reference [1] Ortner and English concluded that considerable scatter mighty be expected in the ratio of $\Delta T_{41J}/\Delta\sigma_Y$. Even so, a mean value of less than ~ 0.7 indicates that there is no evidence of non-hardening embrittlement. As the segregation is expected to increase with increasing fluence the most significant data are those measured at high fluences.

As discussed Williams et al [13] published hardness (H_v)/Charpy shift correlations for irradiated A533B plate and weld. Although, not explicitly stated it was believed that non-hardening embrittlement was not occurring in the steels employed to establish the correlations below.

$\Delta T_{41J} = 1.64\Delta H_v$ (plate)
$\Delta T_{41J} = 2.225\Delta H_v$ (weld)

In the IAEA CRP3 programme a small study was included to examine the effect of thermal ageing, irradiation and post-irradiation annealing, on simulated CGHAZ material of three model steels based on LWR RPV A533B [23]. These data provide further evidence of values of $\Delta T_{41J}/H_v$ that may indicate that embrittlement from non-hardening embrittlement is occurring (see Table 13). The data suggest that values of $\Delta T_{41J}/\Delta H_v > (2.5\text{-}3)$ are indicative of non-hardening embrittlement.

Table 13. Percentage Intergranular Fracture (IGF), Grain Boundary Phosphorus Monolayer Coverage, Hardness (H_v), and Transition Temperatures (ΔT_{41J}) as a Function of Alloy Composition and Heat Treatment in the Unirradiated and Irradiated Conditions. [23]

Alloy	Condition	Cu (wt%)	P (wt%)	ΔT_{41J} (°C)	ΔH_V (VPN)	IGF Unirrad. (%)	IGF Irrad. (%)	P Coverage Unirrad. (% monolayer)	P Coverage Irrad. (% monolayer)
JPC	Plate	0.01	0.007	15	9	< 1	< 1	<5	Not detected
	CGHAZ			20	-3	8	5	<5	6
	Aged CGHAZ			25	-5	86	86	15	16
JPB	Plate	0.01	0.017	22	19	< 1	< 1	5	Not detected
	CGHAZ			51	3	35	83	10	16
	Aged CGHAZ			54	2	98	94	35	44
JPG	Plate	0.16	0.017	33	38	1	<1	8	Not detected
	CGHAZ			69	31	20	25	8	17
	Aged CGHAZ			50	15	96	90	35	47

3.2.2. PISA Irradiations

Table 14 shows the values of ΔT_{41J} / ΔH_v from CMn and MnMoNi samples irradiated during the PISA program. Only for the data from JC SCGHAZ irradiated in PISA I is the ratio > 2. The presence of intergranular failure at the start of life (CMn plate and JRQ SCGHAZ+ε) does not appear to affect the ratio, nor does the appearance of some IGF after irradiation (JRQ SCGHAZ PISA B). With such low values of ΔT_{41J} / ΔH_v non-hardening embrittlement is not predicted for any of these steels and irradiations.

Table 14. Values of $\Delta T_{41J}/\Delta H_v$ from samples irradiated in PISA I, B and C.

Specimen	PISA I	PISA B	PISA C
JX (Plate)			1.08
JC (SCGHAZ)	2.02	1.68	0.79
JE (SCGHAZ+ε)			1.11
CMn Plate		1.61	1.66

The trends in the VVER 1000 material are difficult to assess because of the behaviour of the hardening data. The hardness data measured on the unirradiated and irradiated hardness tiles are shown in Table 15.

Table 15 Hardness data for the VVER 1000 steels (VA, VB, VC)

Material Condition	Hardness (measured by Equostat)				Change in Hardness		
	Unirradiated	PISA I	PISA B	PISA C	PISA I	PISA B	PISA C
VA	213.1	258	257	244.5	44.9	43.9	31.4
VB	197.1	225	203	203	27.9	5.9	5.9
VC	235.8	237.5	227	227	1.7	-8.8	-8.8

If the hardness data are as identified in Table 15, then softening has occurred in VC after the 290°C irradiations and only marginal hardening after irradiation at 200°C, despite significant embrittlement occurring in each case. In the PISA irradiations every effort was made to control specimen identity in each of the irradiation rigs. Nonetheless, it is possible that some specimen misidentification took place during the program. If we postulate that the relative hardnesses of the different microstructures at SOL are retained after irradiation[3], (i.e. VC is the hardest followed by VA, then VB), then we could tentatively suggest that the data from irradiated VA and VC should be transposed. The 'corrected' hardness data are shown in Table 16. There is now greater consistency between the trends in "corrected" hardening and the trends in the Charpy data. These data do not provide a basis for a detailed comparison of the $\Delta T_{41J}/\Delta H_v$ trends, although, it should be noted that VB irradiated at 290°C shows a little hardening (ΔH_v~ 6) for an appreciable Charpy shift (ΔT_{41J} = 27°C), possibly indicating non-hardening embrittlement.

Table 16. "Corrected" hardness data for the VVER 1000 steels (VA, VB, VC)

Material Condition	Hardness (measured by Equostat)				Change in Hardness		
	Unirradiated	PISA I	PISA B	PISA C	PISA I	PISA B	PISA C
VA	213.1	237.5	227	227	24.4	13.9	13.9
VB	197.1	225	203	203	27.9	5.9	5.9
VC	235.8	258	257	244.5	22.2	21.2	8.7

3.2.3. Data Supplied By Partners

In addition to the materials recorded in the PISA literature review [1], Gillemot has irradiated three steels to exceptionally high doses (> 150mdpa). The steels were JRQ, 15H2MFA (CS), 15H2MFA (Hg); JRQ is the same IAEA reference steel irradiated in the PISA program, CS is a SKODA heat of 15H2MFA, and Hg specimens were reconstituted from VVER-440 surveillance samples. The compositions of the three steels are given in Table 17, and data on ΔT_{41J}, ΔH_v and $\Delta\sigma_Y$ are presented in Table 18. The values of $\Delta T_{41J}/H_v$ (or $\Delta T_{41J}/\Delta\sigma_y$ for CS and Hg) do not give any indication of non-hardening embrittlement occurring at high doses in these steels. The values of JRQ are slightly higher than expected for plate without non-hardening embrittlement. It should be noted, however, that there are few data at such high doses and Odette et al [24] concluded that there should be a non-linear $\Delta T_{41J}/\Delta\sigma_Y$ relationship with $\Delta T_{41J}/\Delta\sigma_Y$ increasing with increasing $\Delta\sigma_Y$. The slightly high value of $\Delta T_{41J}/H_v$ for JRQ could thus reflect the high dose rather than non-hardening embrittlement.

[3] It was confirmed from independent testing that the relative hardness of unirradiated VA, VB, and VC were correct

Table 17. Composition of steels JRQ, 15H2MFA (CS), 15H2MFA (Hg) (wt%).

	JRQ	CS	Hg
C%	0.19	0.18	0.13
Si%	0.25	0.33	0.2
Mn%	1.41	0.45	0.51
P%	0.02	0.01	0.012
S%	0.004	0.018	0.014
Cu%	0.14	0.04	0.07
Ni%	0.84	0.05	0.06
Cr%	0.12	2.85	2.86
Mo%	0.5	0.64	0.6
V%	0.003	0.25	0.34

Table 18. Data on ΔT_{41J}, ΔH_V and $\Delta\sigma_Y$ in highly-irradiated steels.

Property	Value After Irradiation to					
	3.12×10^{20} n/cm² E> 0.5 MeV			**4.11×10^{20} n/cm² E> 0.5 MeV**		
	JRQ*	CS	Hg	JRQ*	CS	Hg
ΔT_{41J}	328	131	72	328	111	96
ΔH_v	140			168		
$\Delta\sigma_y$		178	179	345		205
$\Delta T_{41J}/\Delta H_v$	**2.3**			**2.0**		
$\Delta T_{41J}/\Delta\sigma_y$		**0.7**	**0.4**	**1.0**		**0.5**

* Unirradiated Hv for JRQ taken to be average of measurements made with Equostat on unirradiated JRQ within the PISA program (i.e. Hv = 187)

Saillet supplied Charpy and tensile data on an A508 forging of very uneven composition. Highly segregated regions in this forging are referred to as ghost lines. Material from several different regions was supplied: Material A was a base metal with segregated zones, and Material B was largely HAZ, also with ghost lines. The average compositions of these materials are given in Table 2, and their irradiation histories in Table 1. Data for three variants of Material B were provided, Z5 was the base metal, Z1 was decarburised HAZ, and Z4 was ICCGHAZ.

Table 19. Hardening and embrittlement in macro-segregated forging

Property	Value in material irradiated as described in text			
	Material A Base metal	Material B Z1 Decarburised HAZ	Material B Z4 ICCGHAZ	Material B Z5 Base metal
ΔT_{K7} (°C)[#]	55	55	75	66
$\Delta\sigma_{0.2}$ (MPa) [#]	183	95	89	115
$\Delta T_{K7}/\Delta\sigma_{0.2}$	**0.30**	**0.58**	**0.84**	**0.57**

[#] ΔT_{K7} is the Charpy shift measured at ~ 56J, $\Delta\sigma_{0.2}$ is the 0.2% proof stress

It can be seen that there is some variation in $\Delta T_{K7}/\Delta\sigma_{0.2}$ (Table 19) which may be related to the material type, or merely be evidence of experimental uncertainty. The $\Delta T_{K7}/\Delta\sigma_{0.2}$ for the ICCGHAZ in steel B gave a value of $\Delta T_{K7}/\Delta\sigma_{0.2}$ greater than that of the other conditions, but even this value is not sufficiently high to be taken as evidence for non-hardening embrittlement at radiation doses higher than those imposed during the PISA program.

Data from the Tecnatom surveillance program [25] also shows the scatter in the relationship between ΔT_{41J} and $\Delta\sigma_Y$ found by other workers, as seen in Figure 16. Again, within the intrinsic data variability, there is no indication that an additional embrittlement mechanism is introduced at high doses. Overall, significant P segregation-related embrittlement does not appear to have occurred in these base metals within the reactor surveillance doses. The Siemens surveillance database also shows no change in the embrittlement hardening ratio with dose [1]. See Figure 17, which includes surveillance data from both base and weld metal (identified as "surv."), and from weld metal irradiated at an accelerated rate ("VAK").

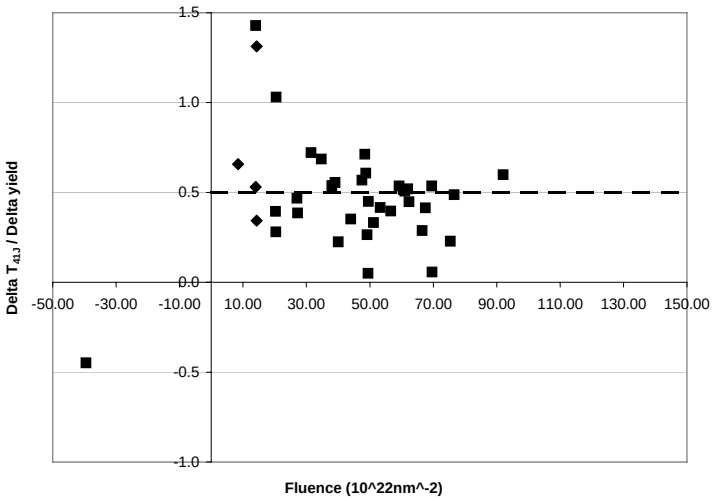

Figure 16 Ratios of Charpy shifts to yield stress increases in MnMoNi base metal in the data from Tecnatom surveillance database [25].

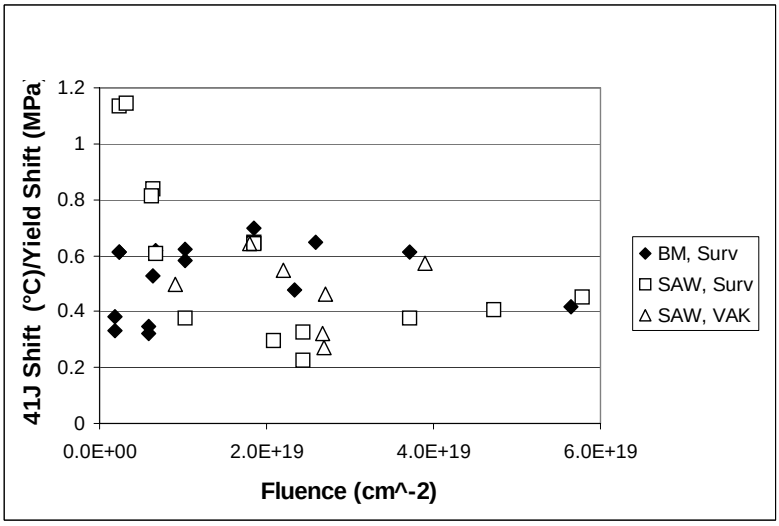

Figure 17. Relation between hardening and embrittlement in Framatome ANP database of surveillance specimens, and test reactor data (VAK).

3.2.4. Summary

$\Delta T_{41J}/\Delta\sigma_y$ or $\Delta T_{41J}/\Delta H_v$ data analysed to date give no indication of non-hardening embrittlement in samples irradiated as part of the PISA programme, in specific PWR surveillance samples irradiated as part of national programmes, or in samples irradiated prior to the PISA programme. In particular, PWR steels do not show any evidence for non-hardening embrittlement at surveillance doses up to ~ $1x10^{20}$ $n.cm^{-2}$ E> 1MeV. It has to be noted that the hardness data for the VVER 1000 base metal did not give a consistent pattern of behaviour. It cannot be ruled out that non-hardening embrittlement is affecting the embrittlement of the step-cooled material irradiated at 290°C.

4. Segregation in Thermally Aged Alloys

4.1. Introduction

The results of the segregation measurements in thermally aged steels and model alloys have been reported in detail in [26], and interpreted with reference to the literature.[≠] This section therefore only summarises the segregation information. Two thermally-aged steels were chosen for examination in WP6, as shown in Table 6 and Table 7, and repeated for convenience in Table 20, below. The first steel was a PWR material owned by one of the partners which has been aged at the RPV operating temperature for several years, the second was a VVER-1000 base metal, step-cooled to encourage segregation in a relatively short time. In addition, Fe-P-C alloys subject to different thermal heat treatments were analysed. These data will be reviewed first.

Table 20. Material examined in WP6.

Material	Composition (wt.%)		
	P	Ni	Cu
PWR Weld id 200 Aged 2700 days at 290°C	0.010-0.016	0.86	0.10
VVER 1000 Base Metal As-received or step cooled.	0.01	1.23	0.04
Fe-0.012P-0.003C Model Alloy Water quenched (WQ), air cooled (BC) or RPV cooled .(RPV)	0.12	0.03	0.006

4.2. Segregation During Thermal Ageing of Fe P C alloys

Figure 18 and Figure 19 show the levels of P and C (respectively) found on the grain boundaries of the Fe-P-C alloy after stress-relief and billet cooling (sample M2A condition BC), and after additional stress relief followed by furnace-cooling (sample M2B condition RPV) or water quenching (sample M2C condition WQ). The Figures also show the effect of thermal ageing on the billet-cooled material.

The additional stress-relief treatment (10h 650°C) seen by the WQ and RPV samples has increased the grain boundary P level, and decreased the grain boundary C level, with respect to the BC material. This is probably related to the precipitation of carbides in the matrix at 650°C. The reduction in grain boundary C permits the equilibrium grain boundary level of P to rise, while the diffusion rate of P at 650°C is fast enough to respond to this change in equilibrium P level within 10h.

[≠] A summary of WP7 is given in the Appendix. This WP focussed on technique development and a comparison of the use of Auger and FEGSTEM to measure P and C monolayer coverage. The analysis of the Auger data reported here takes account of the advances and recommendations made in this WP.

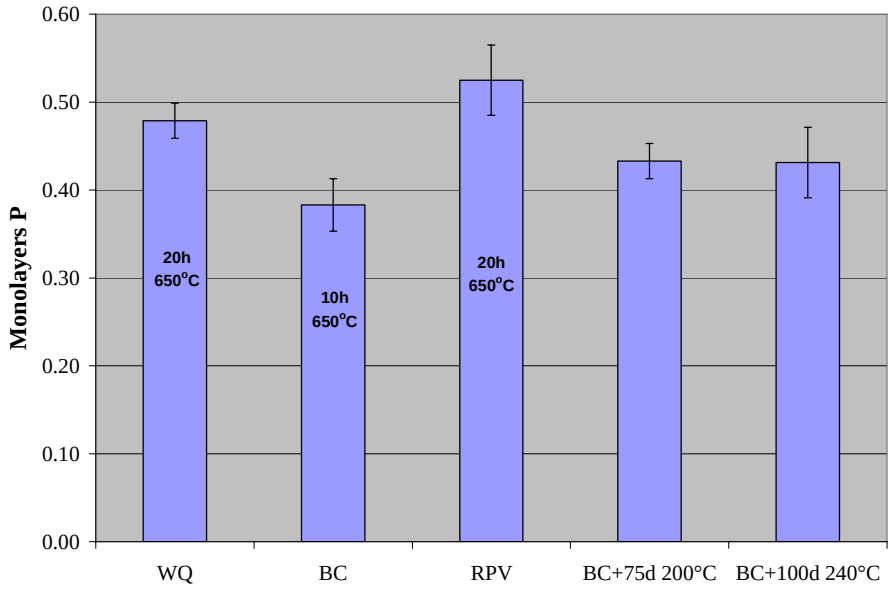

Figure 18. Effect of quench rate and ageing on grain boundary segregation of P in an Fe-0.012P-0.003C model alloy.

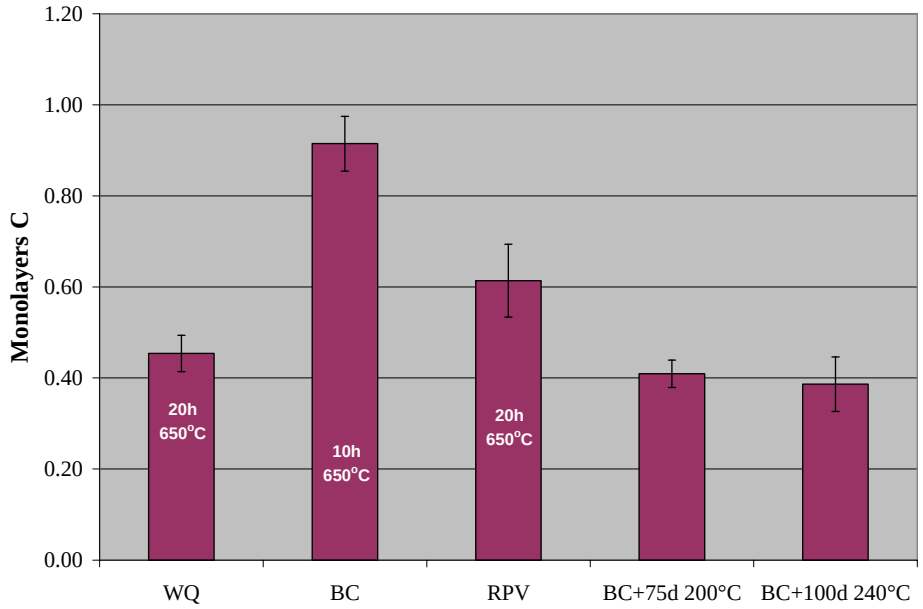

Figure 19. Effect of quench rate and ageing on grain boundary segregation of C in an Fe-0.012P-0.003C model alloy.

P is likely to continue to segregate during furnace cooling down to ~400°C [8]; C diffusion continues to <100°C. Figure 18 and Figure 19 thus show less P and less C segregation in the WQ sample than in the RPV-cooled samples, even though both experienced the same time at 650°C. The WQ sample shows the frozen-in grain boundary P levels produced by ageing 20h at 650°C, while the RPV-cooled material shows the additional segregation brought about during slow cooling.

Ageing the billet-cooled material at either 200°C or 240°C significantly decreased the C levels in the boundaries of the billet-cooled material. Again this is may be due to carbide precipitation. At these low temperatures, however, clustering of C atoms, or trapping in dislocation atmospheres may also contribute to the reduction in the amount of C left free to segregate.

The ability of P diffusion to compensate for C precipitation and desegregation is much less at 200-240°C than at 650°C. Ageing the billet-cooled material at 200°-240°C therefore increased the P levels in the boundaries slightly, but did not bring them up to the levels seen in the (additionally-stress-relieved) WQ or furnace cooled samples.

In summary there is evidence that, in the Fe-P-C model alloy

- P_{gb} increases and C_{gb} decreases during time at 650°C, 200°C, 240°C
- P is likely to be in equilibrium with C in the grain boundaries at 650°C.
- the decrease in free C is probably due to additional carbide precipitation during the additional time at 650°C.
- the decrease in C_{gb} after ageing at 200/240°C may be due to carbide precipitation or to C clustering in the matrix. P diffusion is too slow at these temperatures for P to remain in equilibrium with C in the grain boundaries.

Figure 20 shows the P and C levels measured on the grain boundaries of VVER base metal before (VA) and after (VB) the step-cooling treatment. The final tempering treatment for VA was 650°C 18.25h. During this time, the boundary was likely to reach close to the equilibrium P level for 650°C. The step cooling would have put the boundary P level into equilibrium with only a locally-depleted region at 468°C, although the change in temperature would be expected to dominate the segregation behaviour. Figure 20 shows that, as intended, the step-cooling treatment of the VVER-1000 steel markedly increased the grain boundary P levels. The decrease in grain boundary C could again be due to carbide precipitation.

Unfortunately, of the two samples of the long term thermally aged PWR weld ID200 only one sample fractured in a brittle manner in the AES. The P segregation levels in weld ID200 were low with 0.03 $\pm$ 0.06 of a monolayer of P. Such a low level, typical of start of life levels, suggests that little if any segregation to boundaries has occurred during the thermal ageing for 2700d at 290°C. The diffusion rate at 290°C is sufficient for significant segregation within 2700d. It appears that the P available to segregate in this weld is less than the bulk P level i.e. there are traps for P within the grains (precipitates, dislocation atmospheres etc.).

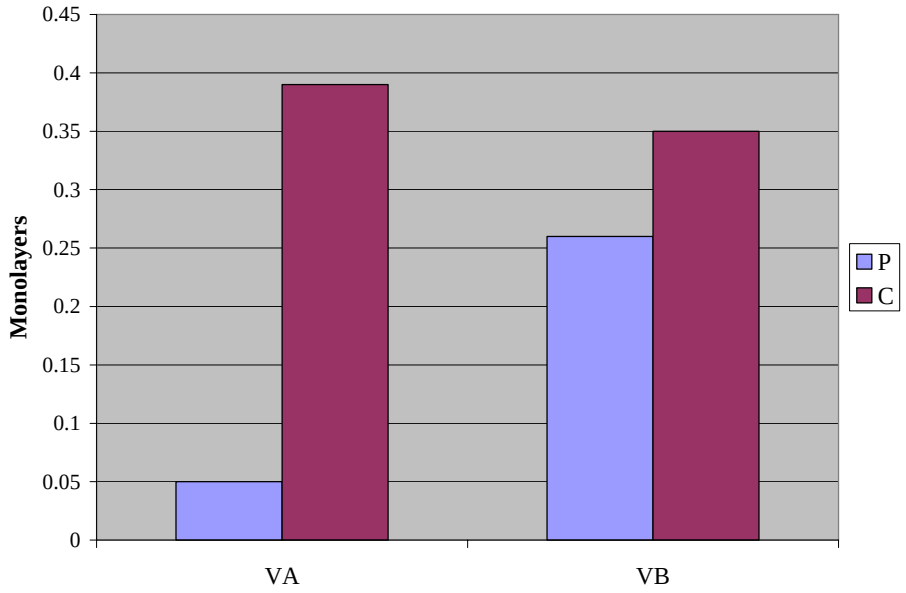

Figure 20. Effect of step-cooling on grain boundary P and C levels in VVER-1000 steel (VA is before step cool, VB is after step cool).

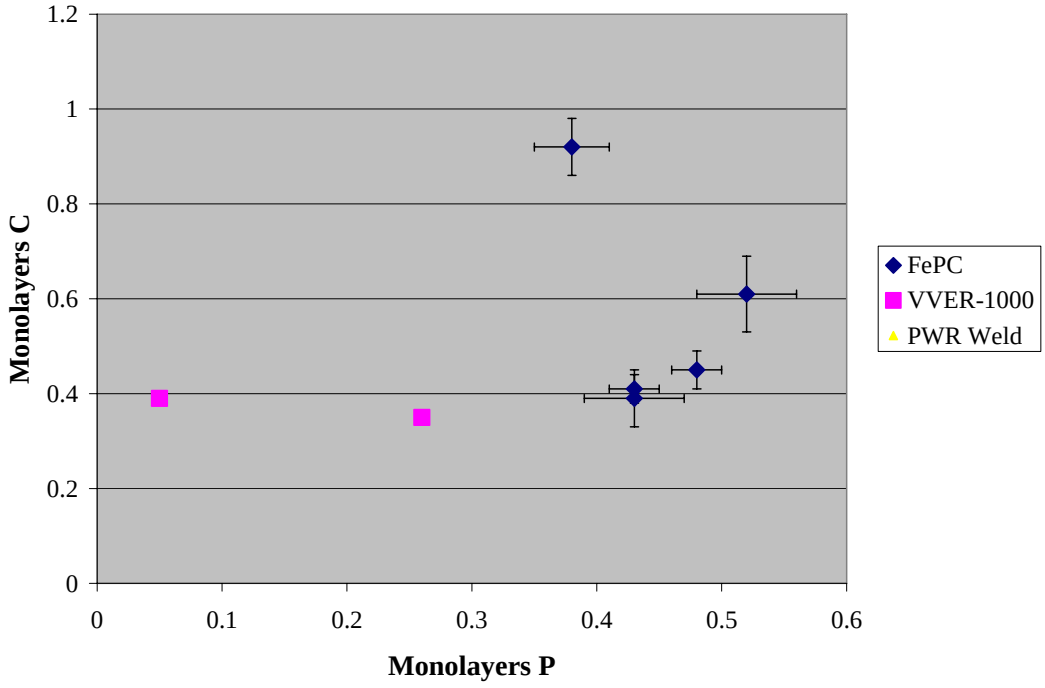

Figure 21. Comparison between P and C levels in grain boundaries after thermal ageing.

Figure 21 compares the grain boundary P and C levels measured in the thermally-aged materials. It shows no clear relationship between the P and C levels in the grain boundaries since the data convolute effects of different dissolved P and C levels with different heat treatment temperatures. In the case of the Fe-P-C alloy, the behaviour of P is dominated by the changes in the levels of its competing co-segregant, C, brought about by changing time at temperature. In the case of the VVER steel, the extended heat treatments at 620° - 650°C, in the presence of strong carbide formers (Cr and Mo) left a very low initial level of dissolved C in VA, despite the higher bulk level. The heat treatment for VB did not therefore change the dissolved C level by very much, and the behaviour of P was dominated by the effect of temperature on the equilibrium segregation level.

4.3. Summary and Conclusions

An Fe-0.012P-0.003C model alloy, a 5Kh2NMFAA VVER-1000 base metal and a German PWR weld were supplied by PISA partners for an examination of thermal effects on P and C segregation in RPV steels and associated materials. The materials were examined by Auger electron spectroscopy.

The free C level in the Fe-P-C alloy dominated P segregation. The free C level was reduced by precipitation during tempering or subsequent ageing. As the free C level dropped, so did the segregated C level, and the segregated P level was able to rise.

Analyses showed that the Fe-P-C alloy would not be in a stable state with respect to carbide precipitation at the start of the PISA irradiations. Even in the absence of irradiation, carbide precipitation would reduce the grain boundary C levels during the times / temperatures of the PISA irradiations, but purely thermal segregation of P would only partly offset this, and could increase the grain boundary P levels by only a few %monolayer in the same time.

In the VVER-1000 base metal, the initial free C level was low due to the presence of strong carbide formers, and an extended preliminary heat treatment. Segregation of P during step-cooling was therefore dominated by the effect of temperature on the driving force for P segregation and on the diffusion rate of P.

The P segregation levels in weld ID200 were low with 0.03 $\pm$ 0.06 of a monolayer of P. Such a low level, typical of start of life levels, suggests that little if any segregation to boundaries has occurred during the thermal ageing for 2700d at 290^{o}C.

5. PREVIOUSLY IRRADIATED MATERIAL

Microstructural studies of grain boundary phosphorous (and carbon) coverage were obtained on material irradiated prior to the PISA program. The details of these materials are given in Table 1**,** Table 2 and Table 19 , some of which are reproduced for convenience in the Table below.

Table 21 Previously irradiated material examined in WP5.

Material	Irradiation condition
PWR A533B plate JRQ	Start Of Life (SOL)
	10^{20}ncm^{-2} at 270°C
VVER-440 weld # 502	SOL
	3 10^{19} ncm^{-2} at 270°C
VVER-440 test weld #501	SOL
	2.4x10^{19} ncm^{-2} at 276°C.
22 NiMoCr 37 PWR base metal heat ID 174 Data set ID –103 Data set ID – 725	103: 3.38x10^{19}ncm^{-2} @ 1.14x10^{11}ncm^{-2}s^{-1} 725: 3.20x10^{19} ncm^{-2} @ 2.26x10^{12}ncm^{-2}s^{-1} 285°C
A508 Class 3 parent from ghost line	6.8x10^{19}ncm^{-2} @~4.4x10^{12}ncm^{-2}s^{-1}
HAZ from ghost line	7.7x10^{19}ncm^{-2}@~4.4x10^{12}ncm^{-2}s^{-1}
HAZ out of ghost line	

Since data from both SOL and irradiated samples were obtained from the VVER welds and JRQ, the levels of segregation in these steels are considered first. The behaviour of the grain boundary P and C on irradiation of the VVER 440 welds and JRQ are plotted in Figure 22 and Figure 23.

Figure 22 shows that, during irradiation to 2.4x10^{19}ncm^{-2}, the amount of P segregation in weld 501 has barely changed. The segregation of the carbide formers Mo and Cr to the grain boundaries has decreased during the irradiation. The average grain boundary enrichment of Ni has decreased, but there was a great deal of variability between individual measurements (~ 5 measurements taken). (No information on the segregation of C itself is obtained in the TEM.)

In Figure 23a, irradiation to 3x10^{19}ncm^{-2} has caused the level of segregation of P to increase in weld 502. The levels of Mo and C have decreased. In these measurements the mean Ni increases somewhat. Figure 23b shows that, in A533B plate JRQ, irradiation to 10^{20}ncm^{-2} causes a slight increase in P segregation, and a decrease in Mo and C levels.

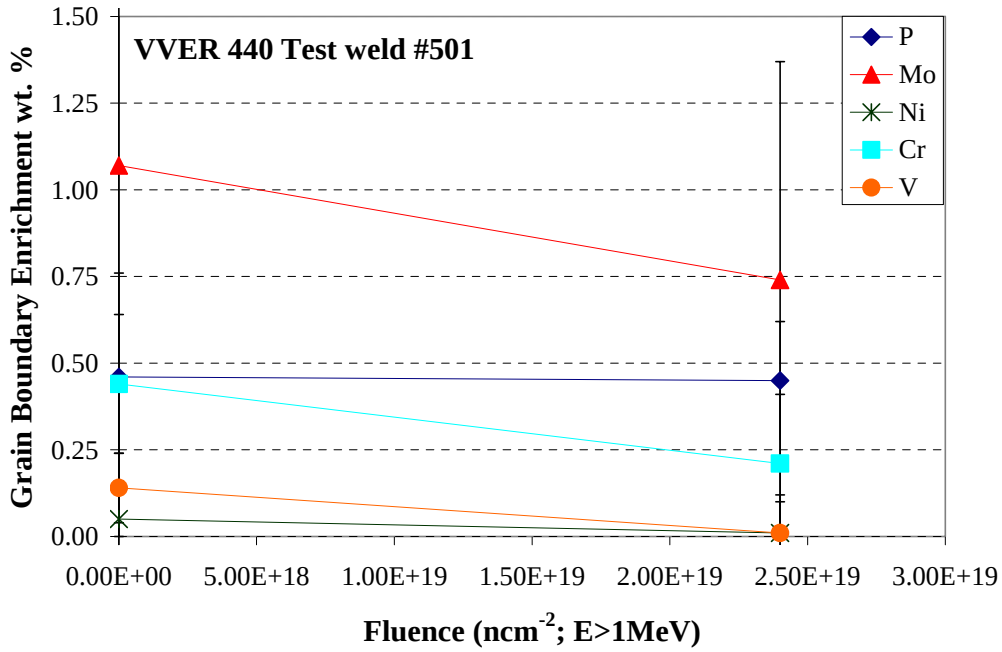

Figure 22. TEM measurements of grain boundary enrichments (wt%) in VVER 440 test weld #501.

(a)

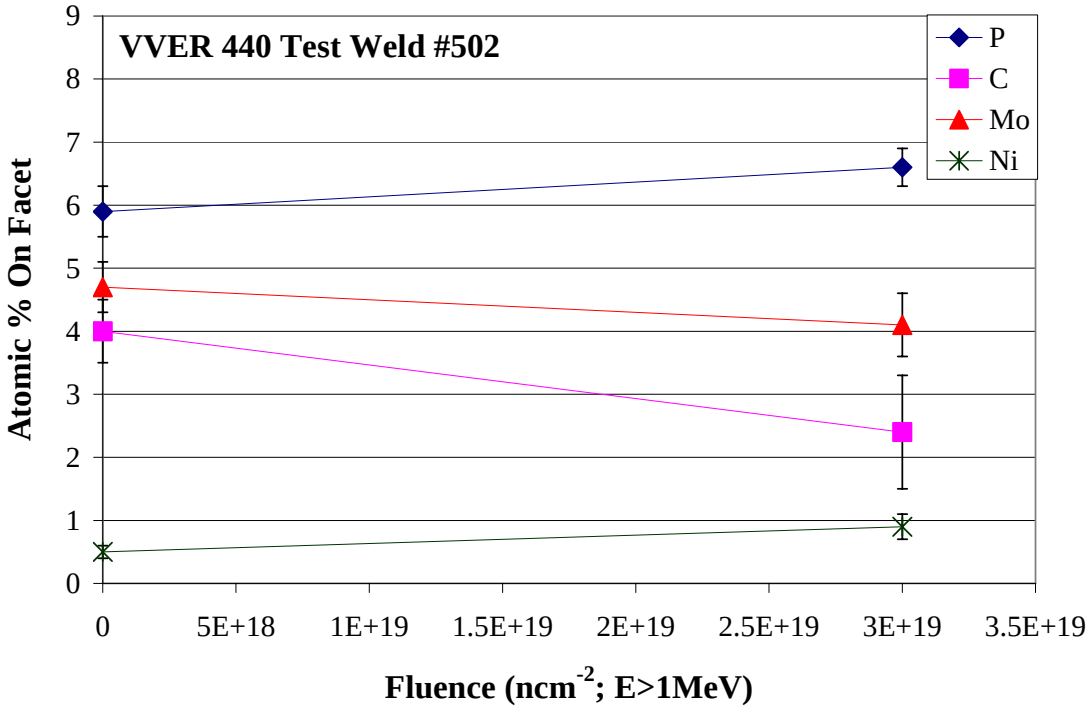

(b)

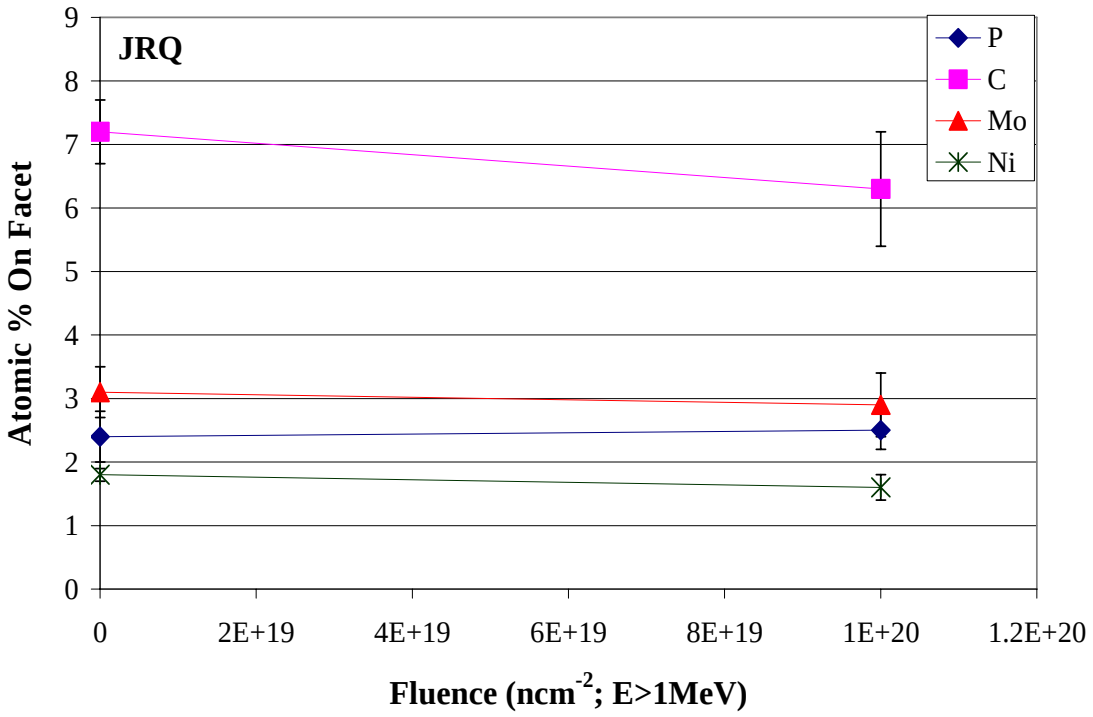

Figure 23. AES measurements of facet composition (in atomic %) in (a) VVER-440 test weld #502, and (b) JRQ.

The decrease in grain boundary C levels on irradiation indicates a reduction in free C in the matrix. This may be due to irradiation-induced carbide precipitation and / or to the trapping of free C at point defects, point defect clusters in dislocation atmospheres (i.e. trapping at the irradiation-induced matrix defects). It is likely that carbide precipitation dominates in the VVER welds, as irradiation also causes a reduction in the grain boundary levels of the carbide forming elements, Mo and Cr (Cr levels only determined in weld 501). In general, the level of segregated Mo increases with increasing P segregation [27]. That overall Mo segregation does not increase when the VVER-440 welds 501 and 502 are irradiated, despite the associated increase in P segregation, suggests that the free Mo level has decreased during irradiation (i.e. carbide precipitation is occurring). This is confirmed when data from individual facets are compared, as in Figure 24. The data show scatter, but fall into clear groups, as shown by the trend lines. For each material condition, Mo segregation tends to increase as P segregation increases. After irradiation, however, the amount of Mo segregation in weld 502 is decreased. Conversely, in JRQ, C segregation decreases on irradiation but the change in mean Mo segregation with irradiation (see Figure 23) is minimal. In addition, the relation between Mo and P segregation on individual facets does not change with irradiation. In JRQ, therefore, the reduction in free C on irradiation is more likely to be associated with trapping at matrix defects rather than with carbide precipitation.

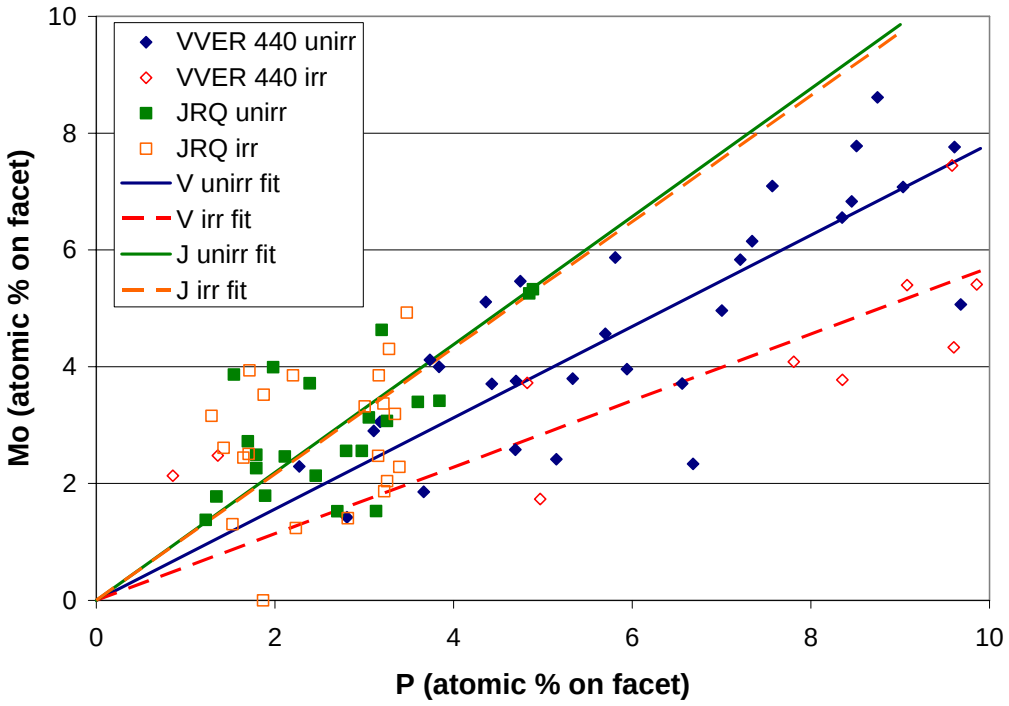

Figure 24. Comparison between P and Mo levels measured on individual facets in VVER 440 test weld 502 and A533B plate JRQ.

Comparing JRQ and weld 502 further, the SOL grain boundary P levels are lower, and C levels higher in JRQ, consistent with its lower bulk P level, and lower level of strong carbide formers. On irradiation, the grain boundary C level decreases more strongly in weld 502 than in JRQ, indicating that carbide precipitation is more effective at reducing free C levels than trapping at matrix defects. Compensating increases in P segregation are more evident in weld 502 than in JRQ, in which radiation barely affects the segregated P level. Radiation also has a negligible effect on the grain boundary P levels in weld 501.

The P and C data on all the previously-irradiated steels are shown in Figure 25 and Figure 26. In all cases where to SOL levels are known, the grain boundary C level decreases on irradiation. The P level generally increases, but the increases in JRQ and the A508 IGHAZ are well within the measurement uncertainty (as is the marginal decrease in P observed in VVER 440 test weld 501).

Figure 27 compares the P and C levels in the grain boundaries of the different materials. There appears to be an inverse relation between P and C segregation in the more strongly segregated materials.

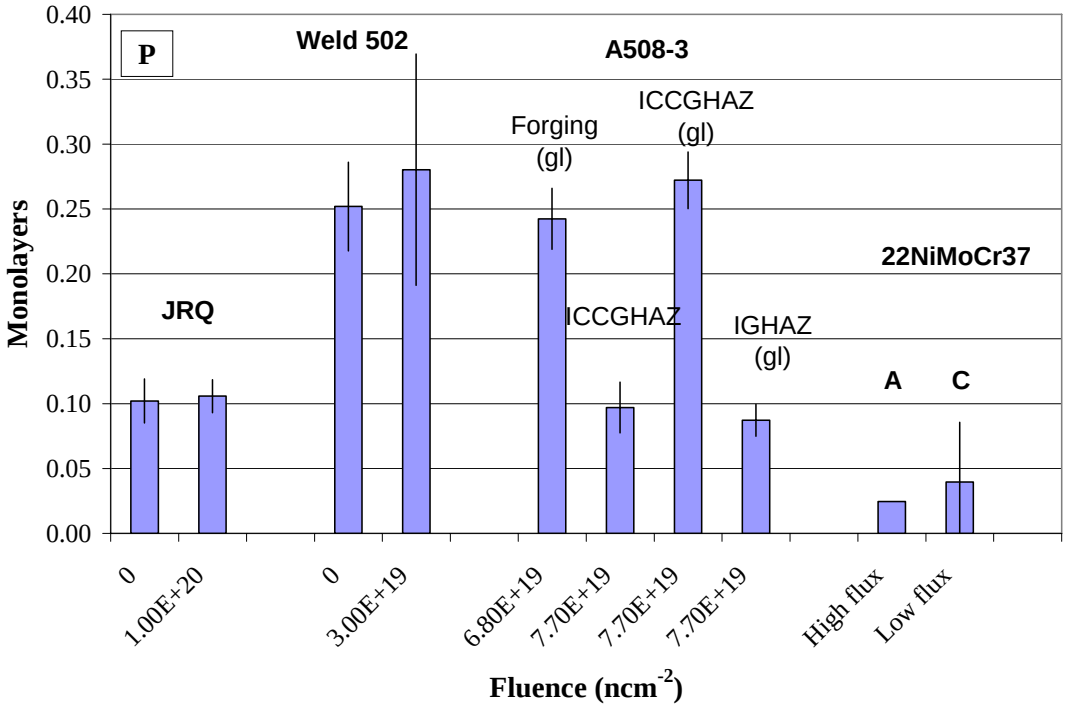

Figure 25. Monolayer coverage of P derived from AES measurements on steels irradiated prior to the PISA program.

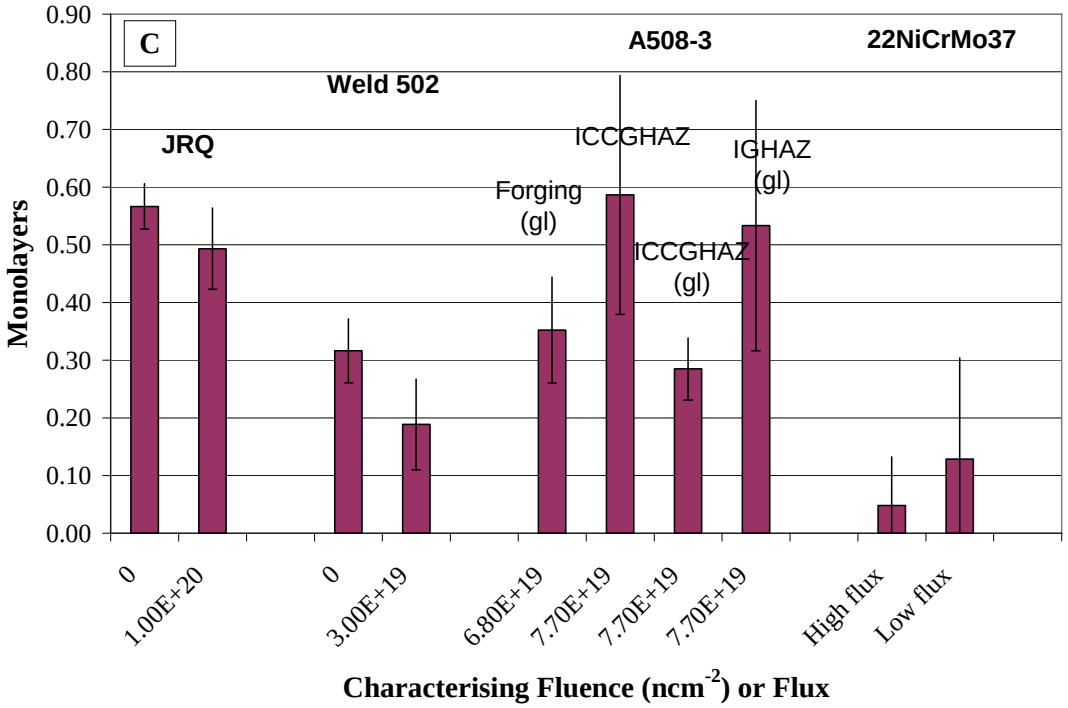

Figure 26. Monolayer coverage of C derived from AES measurements on steels irradiated prior to the PISA program

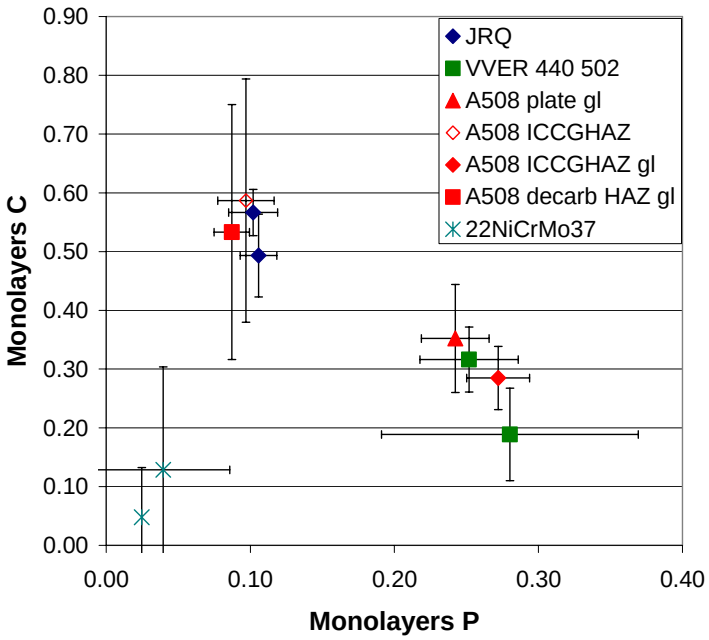

Figure 27. Comparison between grain boundary P and C levels in irradiated RPV steels.

P segregation in the two 22NiCrMo37 base metal samples is even lower than in JRQ and VVER 440 weld 501, indicating that the higher concentration of carbide formers has not sufficiently offset the higher bulk C level and lower bulk P level in enhancing P segregation. Within the measurement uncertainty, it is not possible to observe any effect of flux on the level of P or C segregation.

EdF have supplied data, from previous work by Brillaud and co-workers, on the P segregation observed on grain boundaries of a Auger samples machined from broken halves of Charpy surveillance samples of an A508 forging containing 0.008 wt% P (see Figure 28). The specimens were irradiated at a low dose rate of (between 1.6 and 2 10^{11} n/cm^2/s E > 1 MeV) to irradiation doses of up to ~5 10^{19} n/cm^2 E> 1MeV. It can be seen that there is appreciable scatter in the data and Brillaud et al concluded that, within the measurement uncertainties, any increase in P on irradiation was negligible or very small. There is certainly no evidence from both these data and the data on the material from Framatome on 22NiCrMo37 base metal that irradiation at low dose rates leads to significant increases in P levels on grain boundaries.

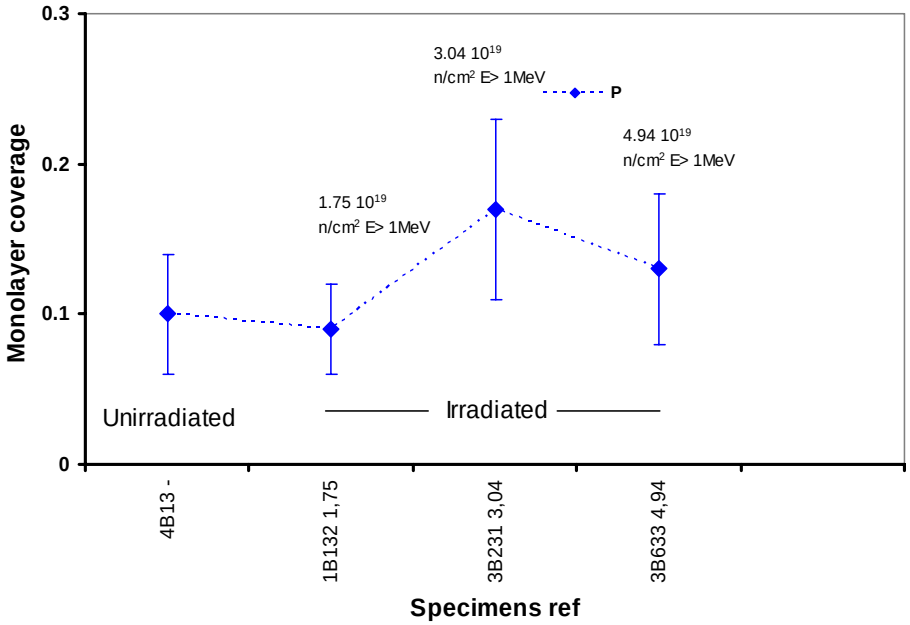

Figure 28. Fraction of a monolayer coverage of P for unirradiated and irradiated A508 surveillance samples. Samples were irradiated at ~290°C to doses of upto 5 10^{19} n/cm² and at dose rates between 1.6 and 2 10^{11} n/cm²/s E > 1 MeV.

The (post-irradiation) levels of P in the A508 Class 3 materials vary according to the local solute contents. Within the solute-rich ghost lines, in both plate and ICCGHAZ, the levels of P segregation resemble those seen in the high-P weld 502. Outside the ghost lines, the level of segregation in the ICCGHAZ resembles that in the lower-P JRQ plate. The levels of C segregation are inversely related to the levels of P segregation.

5.1. Implications For Mechanical Behaviour Under Irradiation

The grain boundary P increase in JRQ is within the measurement uncertainty despite the high dose (10^{20}ncm^{-2}); the C decrease is clearer, but the uncertainties on the SOL and as-irradiated measurements still overlap. For the A508 HAZ outside ghost lines, and in the decarburised zone, the P levels after ~7x10^{19}ncm^{-2} are still below 10% monolayer, and the C levels significant. The P threshold above which intergranular failure occurs in MnMoNi steels appears to be ~10% monolayer [1]. Thus, for moderate-P MnMoNi steels, it is unlikely that irradiation-induced segregation during plant operation will affect the fracture path to any significant extent. In the macrosegregated regions of A508 – 3 forging and ICCGHAZ, IGF is present at SOL, and the irradiation-induced P segregation and C desegregation must be expected to weaken the grain boundaries further.

Although the 22NiMoCr37 samples were only irradiated to ~3x10^{19}ncm^{-2}, the grain boundary P levels were so low after this dose, that this low-P base metal is also likely to avoid non-hardening embrittlement during typical reactor lifetimes.

5.2. Summary and Conclusions

Material irradiated prior to the PISA program has been supplied by PISA partners, so that the range of RPV materials examined within the program may be extended. In some cases, the material has been supplemented by previously-acquired segregation data.

Auger data have been acquired to determine the levels of both P and C segregation to grain boundaries before and after irradiation.

The steel microstructure (i.e. plate versus forging or HAZ) has less effect on the SOL P segregation than the free C level. This, in turn, is controlled by the presence and strength of carbide forming elements, and the thermal history. High levels of P segregation require high bulk P levels, but this segregation will only occur in the presence of low free C.

Irradiation leads to a decrease in the segregated C levels. In the VVER-440 steels, this is predominantly due to irradiation-induced carbide precipitation. In steels with lower levels of carbide-forming elements, or weaker carbide formers, the importance of matrix damage in trapping interstitial solutes at point defects or defect clusters is greater.

P segregation generally increases on irradiation. This is most evident in the higher P materials.

Increasing the flux from 1.4×10^{11} to 2.26×10^{12} $ncm^{-2}s^{-1}$ had no discernible effect on P and C segregation in 22NiCrMo37 base metal after ~$3.3 \times 10^{19} ncm^{-2}$; E>1MeV.

On the basis of the observations made here and elsewhere, it appears unlikely that non-hardening embrittlement will influence RPV condition during normal operation for homogeneous MnMoNi steels (i.e. A508 Class 3, A533B, 22NiMoCr37) of <0.02 wt.% P.

6. SAMPLES IRRADIATED IN PISA IRRADIATIONS AT HFR PETTEN

Microstructural studies of grain boundary phosphorous (and carbon) coverage were obtained on material irradiated HFR Petten as part of the PISA programme. The details of these materials are given in Table 3, Table 4 and Table 5.

6.1. Fe-P-C alloys

A particularly important set of data were obtained from the FePC alloys containing 0.12 wt% P and 0.03 wt% C. The data are plotted in Figure 29 and Figure 30. The main trends are that

- P increases with irradiation and (slightly) with time at 200°C; the increases under irradiation at 200°C are greater than in the corresponding thermal control.
- The increases in P are more dependent on the dose, ϕt, than on the irradiation temperature, T_{irr}. This trend is clearest in the data on the billet cooled material, in which similar increases in monolayer coverage are observed after the irradiations at ~10mdpa at 200° and 290°C.[≠]
- C decreases with irradiation and with time at 200°C; the decreases under irradiation at 200°C are greater than in the thermal control.
- The degree of C desegregation does not show any consistent trend with ϕt. It may increase with increasing T_{irr}, but the effect is within the scatter of the data.

The segregation of P and the desegregation of C show some dependence on SOL segregation levels / quench condition (see Figure 31). Figure 32 shows that this effect (for P at least) is visible only at low dose (<~10mdpa). Between 10mdpa and 44.3mdpa, the amount of P segregation is the same for all heat treatment levels. Figure 31 also indicates that most C desegregation occurred within the first 10mdpa. These data may suggest that C desegregation itself influences P segregation at the relatively low doses, and further support the insensitivity of P segregation to T_{irr}. (It is difficult to plot the data from the water quenched material irradiated to ~11mdpa in Figure 31 because of an apparent grain boundary depletion of C during the PISA C irradiation.)

The dose dependence of the P segregation observed in the FePC alloys is plotted in Figure 33; an approximate linear dependence on fluence can be observed, and that there is little evidence for a strong dependence on irradiation temperature. Further, the data obtained on the P segregation on this alloy after irradiation at 240°C by Cowan et al [8] has also been included on this plot. It can be seen that the level of segregation observed is in keeping with the data obtained from the PISA irradiations.

[≠] The data from the sample of FePC irradiated at 200°C in PISA C showed very high C levels on the cleavage facets and a lower level of C on the facets versus the regions exhibiting cleavage. This suggests the carbon data on the facet levels are unreliable and that the P levels may be under-estimated because of the covering layer of C. In the observation of this sample on the Auger the C did not increase with time, suggesting a contamination layer formed on the initial fracture of the sample (I.A. Vatter private communication) . The data on this material have not been included in the subsequent analysis.

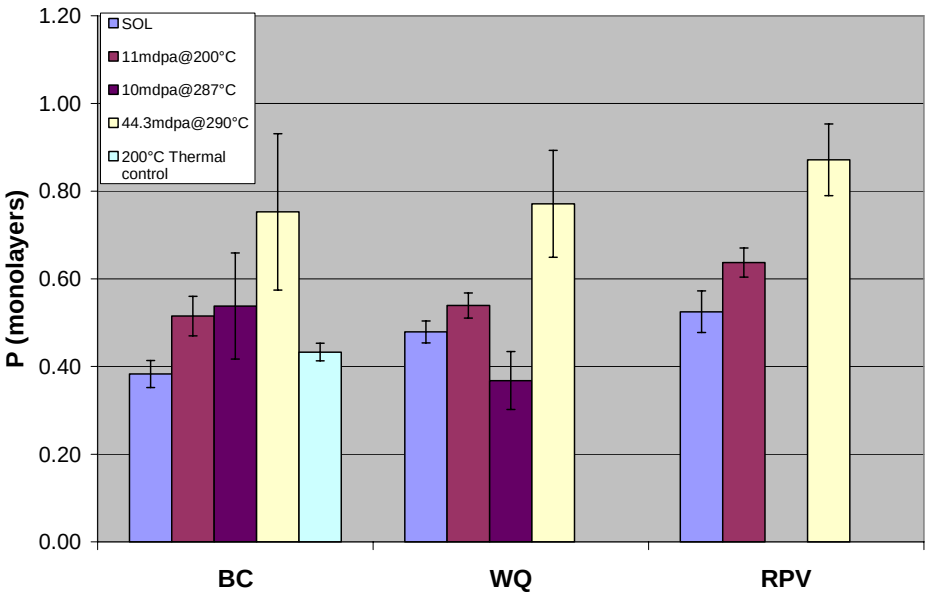

Figure 29. Monolayer coverage of P derived from AES measurements on FePC alloys irradiated at HFR Petten in PISA 1, PISA B and PISAC.

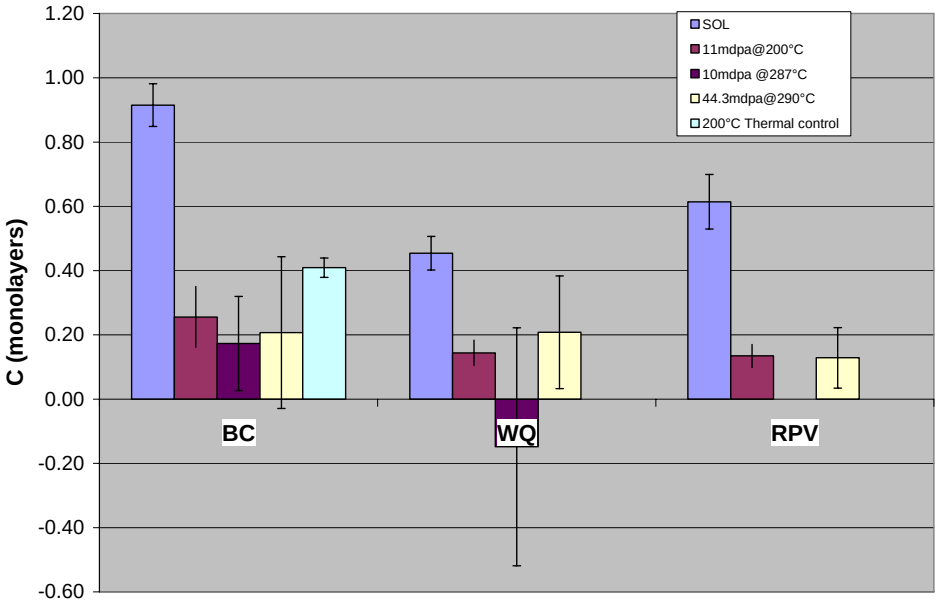

Figure 30. Monolayer coverage of C derived from AES measurements on FePC alloys irradiated at HFR Petten in PISA 1, PISA B and PISA C.

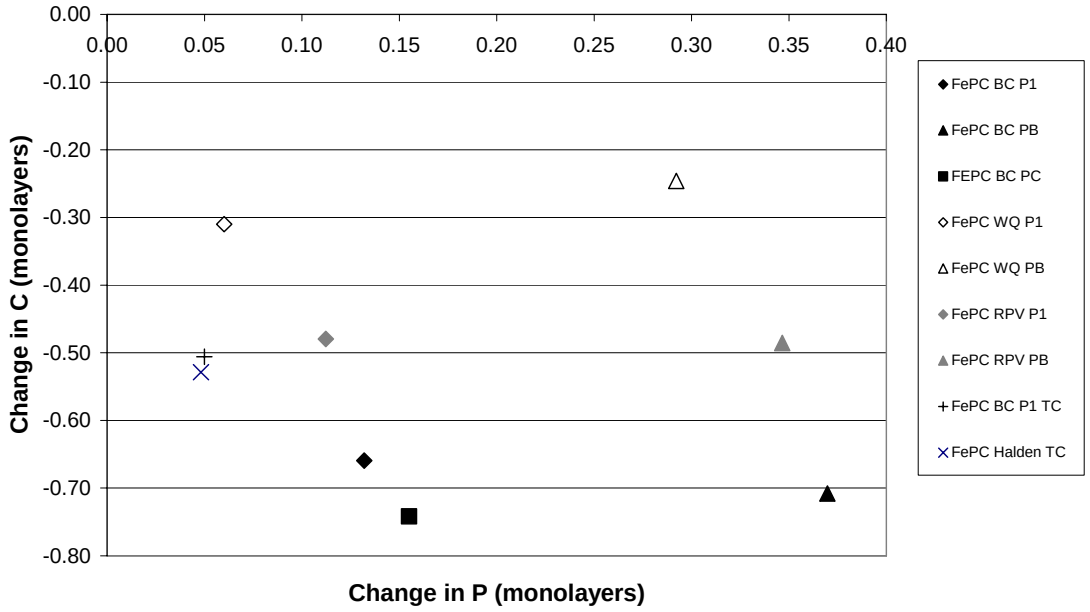

Figure 31 Plot of change in C versus change in P monolayer coverage for FePC alloys irradiated at HFR Petten in PISA 1, PISA B and PISA C.

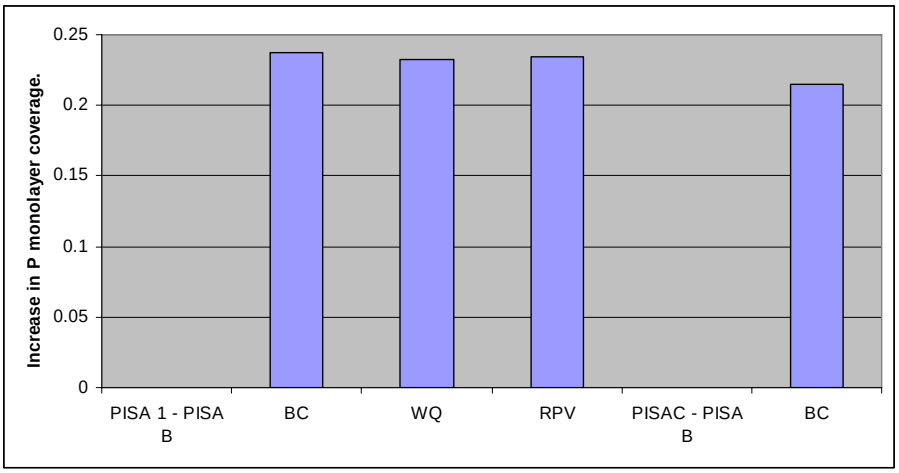

Figure 32. Plot of the difference in P monolayer coverage from high dose irradiation (PISA B) to coverage in low dose irradiation PISA 1 or PISA C.

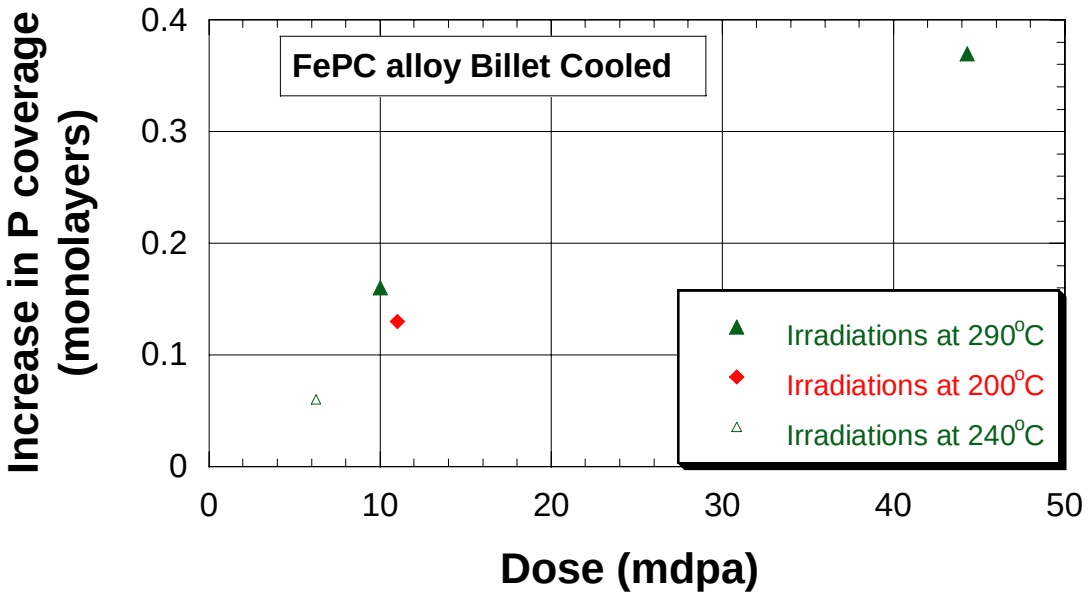

Figure 33. Plot of the increase in P monolayer coverage versus dose for the billet cooled FePC alloy.

6.2. Commercial Steels

The data on the P and C monolayer coverage in the commercial steels are plotted in Figure 34 and Figure 35 respectively. It is difficult to discern trends in the C segregation or de-segregation under irradiation. In the C-Mn plate steel, the mean C level initially decreases under irradiation, but the degree of desegregation later reduces. Within the uncertainties there is no observable dependence on irradiation dose or T_{irr}. In the MnMoNi steel JRQ, in all heat treatment conditions, C segregation is actually higher after irradiation to 44.3mdpa at 290°C than at SOL, but shows no other consistent trend with material condition, dose or irradiation temperature. In the VVER 1000 base metal it is difficult to discern any trends, as the changes in C level on irradiation are small and within experimental uncertainty.

The trends in the change in P monolayer coverage on irradiation are easier to identify. In general, the P monolayer coverage increases on irradiation, but the increase in P segregation is smaller in these commercial steels than in the FePC alloys. This is demonstrated most clearly in the data from steels heat treated to produce a SCGHAZ microstructure, which are plotted versus dose in Figure 36. Figure 36 shows that, within the scatter, there is an almost linear dependence of P segregation on fluence, but it is much weaker than that shown for the FePC alloys in Figure 33. Figure 36 also shows that, for the SCGHAZ specimens irradiated at doses close to 10mdpa, there is very little dependence on T_{irr}.

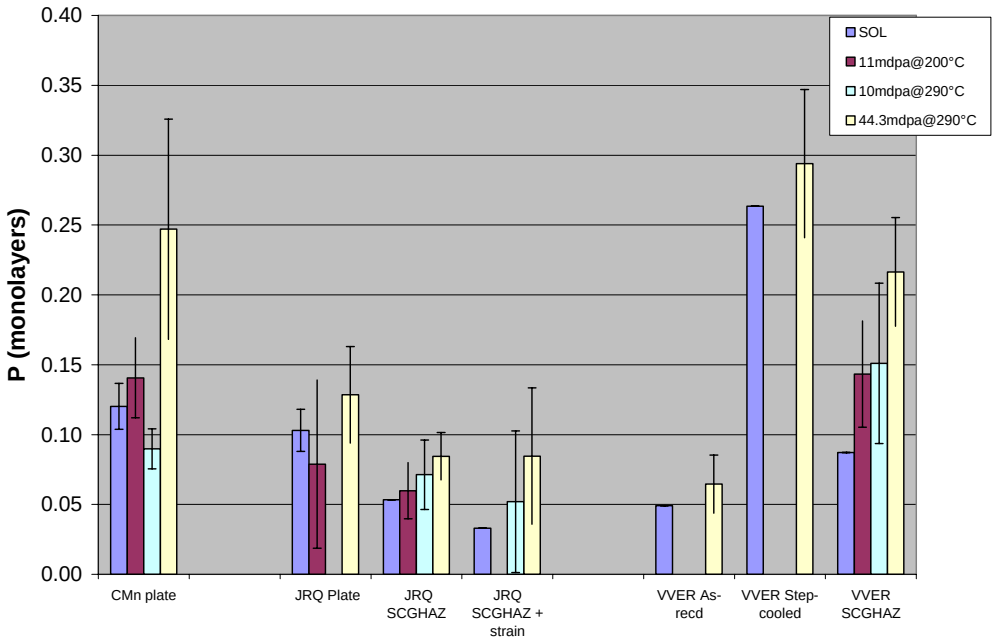

Figure 34. Monolayer coverage of P derived from AES measurements on commercial steels irradiated at HFR Petten in PISA 1, PISA B and PISA C

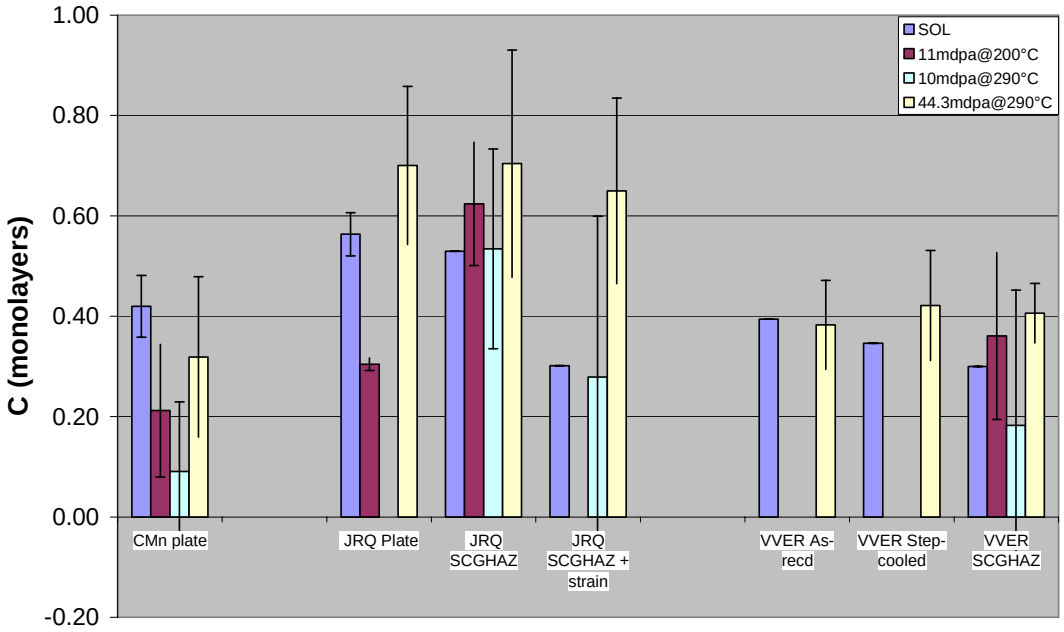

Figure 35. Monolayer coverage of C derived from AES measurements on commercial steels irradiated at HFR Petten in PISA 1, PISA B and PISA C

Since there is a clear trend of increasing P with dose, but no clear trend of C with dose, no clear relation between the degree of P segregation and that of C segregation during irradiation can be discerned (See Figure 37).

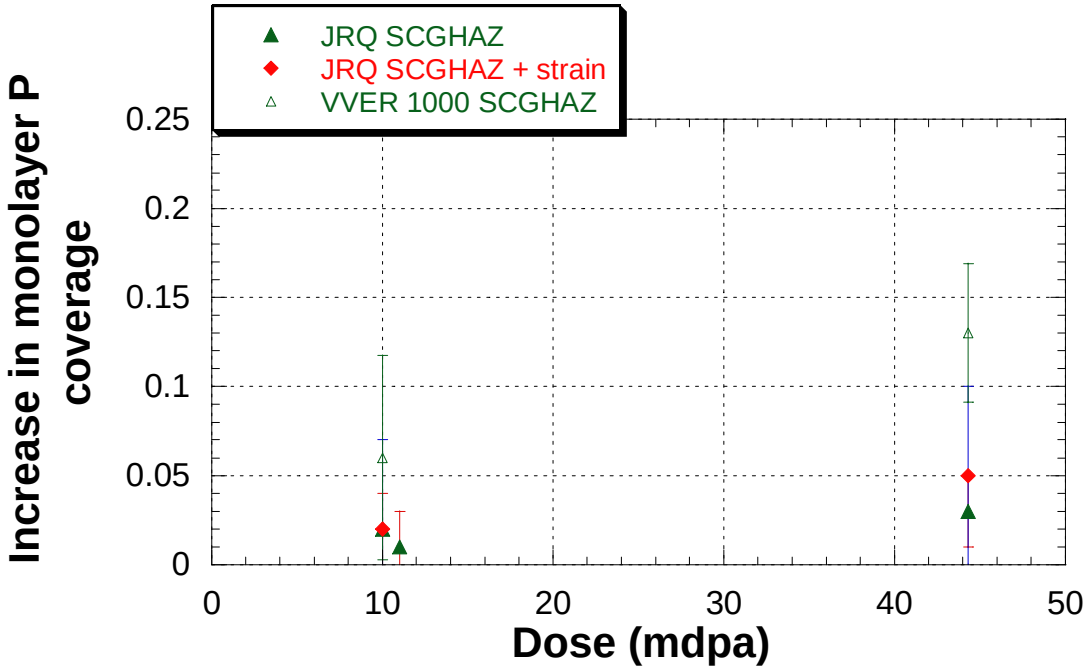

Figure 36. Plot of the increase in P monolayer coverage in JRQ SCGHAZ, JRQ SCGHAZ + strain, and VVER 1000 base metal SCGHAZ

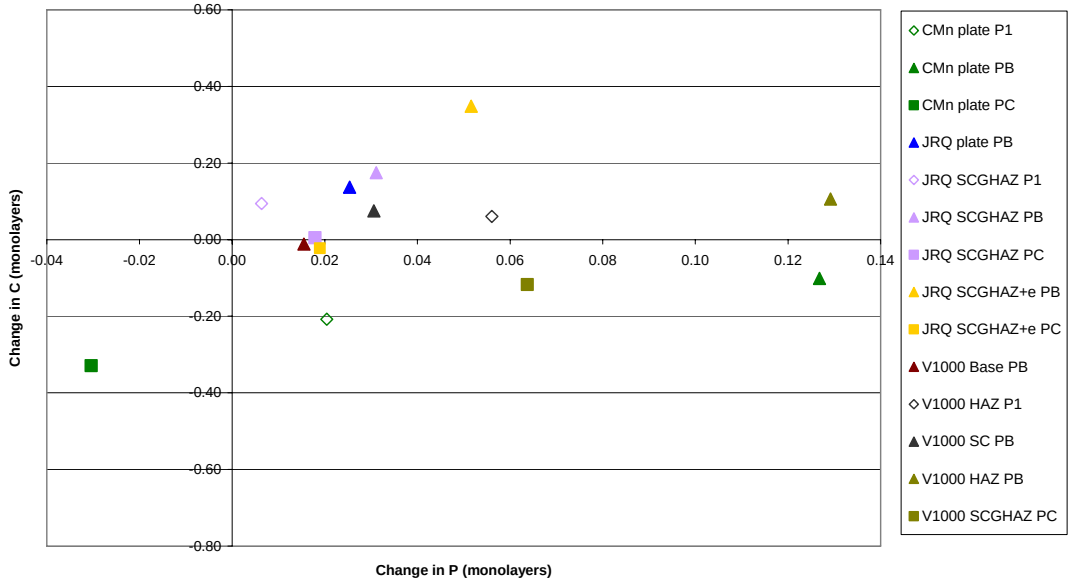

Figure 37. Relation between change in P segregation and change in C segregation during the various PISA irradiations.

The dependence of segregation during irradiation on SOL microstructure is clearest in the VVER base metal irradiated at 44.3mdpa. Here, within the experimental scatter, the increases in segregation in the as-received and step-cooled base metal are very similar (Figure 38). This is of interest as, although the general microstructure of these two materials were the same, and the SOL grain boundary C levels similar, the SOL levels of monolayer P were very different. Figure 38 also shows that the increase in P levels in the material with the SCGHAZ microstructure is significantly higher than that observed in the as-received and step-cooled base metal.

Equivalent data are plotted in Figure 39 for JRQ. The increase in P is again greater in the material given the SCGHAZ treatment than in the base metal, but the large uncertainties on the data on the base metal make it difficult to say that this trend is as well founded as in the case of the VVER 1000 material.

The comparison between the segregation observed in JRQ SCGHAZ with that in JRQ SCGHAZ+ε was intended to show the effect of dislocation density on segregation during irradiation. Irradiation to10 or 44.3mdpa at 290°C does, indeed, increase segregation in both materials, but only by a small amount. No effect of strain can be seen in the segregation within 10mdpa (0.02 monolayers in both cases). After 44.3mdpa, the increases in P level were0.03±0.02 monolayers in the SCGHAZ and 0.05±0.05 in the prestrained SCGHAZ. The prestraining appears to have increased segregation, but the scatter between individual measurements affects the security of the assessment.

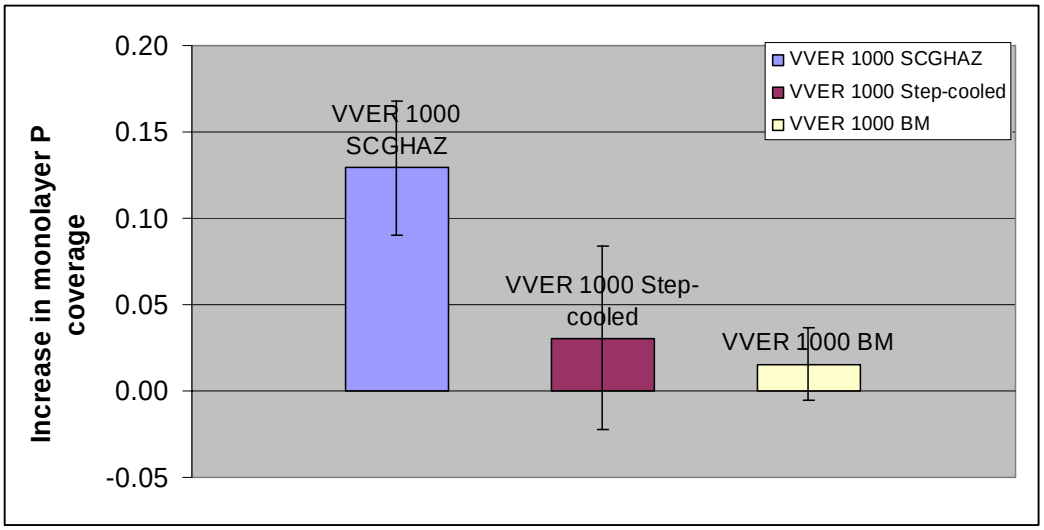

Figure 38. Plot of the increase in monolayer coverage of P after irradiation at 44.3 mdpa at 290°C for the VVER 1000 material.

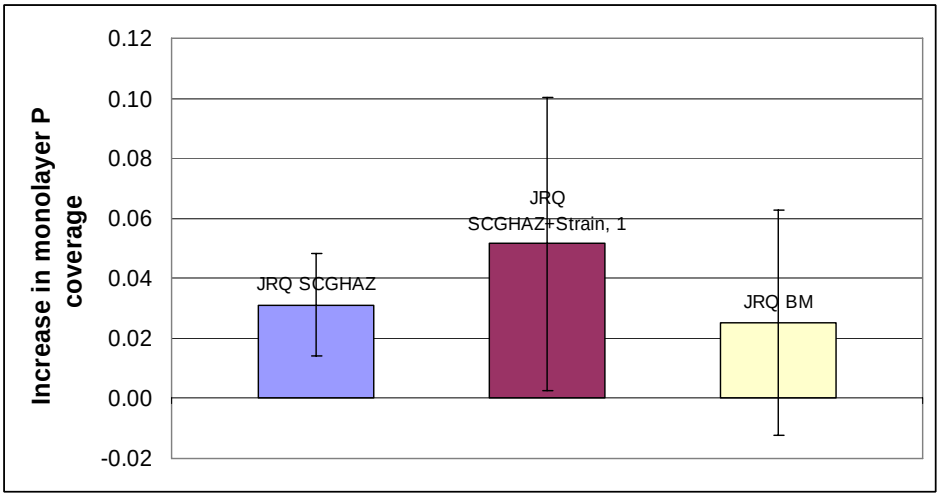

Figure 39. Plot of the increase in monolayer coverage of P after irradiation at 44.3 mdpa at 290°C for JRQ.

A correlation between the level of Mo on an individual facet and the level of P was found in the highly-irradiated VVER 440 weld 501 and JRQ (see Figure 24). A similar correlation was found for the JRQ and VVER materials irradiated in PISA 1, PISA B, and PISA C. This is illustrated in Figure 40 for the VVER 1000 base metal in the as received and step-cooled conditions before and after irradiation to 44.3mdpa at 290°C. In none of these cases, however, was there a pronounced effect of irradiation on the correlation, as observed in the VVER 400 weld 501 (Figure 22 -Figure 24). This suggests that C did not precipitate during the irradiation of these VVER 1000 steels, which is consistent with the insignificant change in boundary C in these two materials.

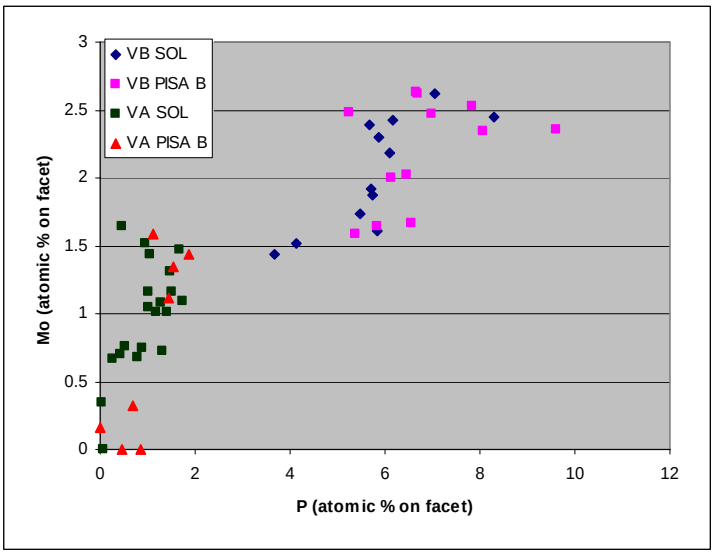

Figure 40. Comparison between P and Mo levels measured on individual facets in the as-received (VA) and the step-cooled (VB) VVER base metal.

The precise correlation between P and Mo in the VVER 1000 base metal depended on the material and precise heat treatment, if not on irradiation. In both heat treatment conditions there is a tendency for higher P on an individual facet correlating with higher Mo. More P is associated with a given level of Mo in the step cooled condition. It is apparent that, during the step-cooling of VB, P was segregating to boundaries at temperatures where Mo is immobile.

6.3. Summary of trends in data in samples irradiated in HFR Petten

In Fe-P-C model alloys, and CMn plate, the grain boundary C levels decrease and the grain boundary P levels increase with irradiation (within measurement uncertainty). This behaviour is similar to that observed in VVER 440 welds and JRQ irradiated prior to PISA.

In JRQ (all heat treatment conditions) irradiated within PISA, both the grain boundary C and P have increased after irradiation to the highest fluence (44.3mdpa). This may also be true of the VVER-1000 steels (all heat treatment conditions), although the increases in C are minimal.

In the FePC alloys and the steels with an appreciable increase in P segregation on irradiation (SCHAZ), segregation appears to increase approximately linearly with fluence.

Changing irradiation temperature (195°C – 287°C) at ~10mdpa has a relatively small effect on P or C segregation in the steels or the FePC alloys. No consistent trends can be detected.

The degree to which P segregation increases during irradiation is lower in the steels than in the model alloys. The increase is strongly influenced by the microstructure of the steel, and possibly by the behaviour of C during irradiation. This can lead to an influence of the initial C level on P segregation during irradiation, but there is no evidence for an effect of the initial grain boundary P level.

7. Modelling

The modelling of P segregation carried out within the PISA program is described in detail in [28 and 29], and summarised here.

7.1. Rate theory modelling

A rate theory model of P segregation to grain boundaries has been developed at the University of Liverpool that takes account of:

- recent developments in the determination of the Fe-P inter-atomic potential and, hence, new predictions of the coupling of P to interstitial and vacancy point defects.
- insight into interstitial and vacancy production, survival, and clustering from Molecular Dynamic (MD) simulations of cascades in iron.

A particular focus has been the effect of the accumulation of irradiation-produced interstitial clusters in the matrix on both the point defect concentration and the P level in the matrix.

In reference [29] an analytical equation is proposed for the increase in grain boundary coverage of P during irradiation as a function of irradiation dose, dislocation density, diffusion parameters etc. The simplicity of this model is partly based on careful analysis of the kinetics of the process, partly on quantum mechanical, molecular dynamics (MD) and Monte Carlo (MC) calculations of the interaction of P atoms with point defects, and partly on the analysis of experimental data arising from the PISA project.

To fit the experimental data (obtained over a range of compositions, irradiation temperature and fluences) it has been necessary to make a number of simplifying assumptions. More specifically it is assumed that:

- P atoms migrate in complexes with vacancies and interstitial atoms in a material with constant dislocation density.
- The grain boundaries are perfect sinks for point defects.
- Thermal vacancies, and recombination reactions between vacancies and single interstitial atoms (SIAs), are negligible.
- The possible depletion of P near grain boundaries, i.e. diffusion profiles set up by segregation during initial heat treatment of the samples, is ignored.

The diffusion properties of P atoms in complexes with vacancies and interstitial atoms are taken from calculations published in [30]. These are based on the potential set developed in collaboration with Ackland [31]. The binding energy, E_b, between a P atom and a <110> dumb-bell is taken to be 1.02 eV, and the migration energy, E_m, is 0.27eV. A vacancy-P atom complex is formed because of the significant binding energy when a vacancy is either in the 1st or 2nd nearest neighbour site of a P atom, binding energies are 0.35 and 0.37 eV respectively.

It is important to note that the high binding energy of P atoms with interstitials implies that there will be no thermally-activated dissociation of P-interstitial atom complexes.

In addition, the high binding energy of P atoms and vacancies in first and second nearest-neighbour positions suggests that P may be dragged by vacancies. These insights are critical for understanding the segregation of P under irradiation.

MD simulations of cascades in Fe suggest significant clustering of interstitial point defects occurs in the cascade. Fewer mobile SIAs than vacancies are left at the end of the cascade. Further Monte Carlo simulations of the subsequent annealing of these cascades suggest that a significant fraction of the SIAs will be lost through recombination with vacancies or lost to the interstitial clusters. Specifically,

After MD cascades $G \approx 0.25 G^{\mathrm{NRT}}$

After MC annealing $G_{\mathrm{V}}^{\mathrm{single}} \approx 0.15 G^{\mathrm{NRT}}$

$G_{\mathrm{I}}^{\mathrm{single}} \approx 0.015 G^{\mathrm{NRT}}$

It is to be noted that G^{NRT} is the same for vacancies and interstitials. An implication of this is that the transport of P by mobile SIAs (which are assumed to be the primary carriers of P in the previous models) may not be important.

The increase of grain boundary P (in monolayers) after an irradiation time, t, due to its diffusion in complexes with vacancies and interstitials, is described by Barashev in reference [32] as

$$\Delta C_{\mathrm{P}}^{\mathrm{GB}}(t) \approx \frac{2C_{\mathrm{P0}}}{\sqrt{\rho} d} \ln\left(1+\Gamma G^{\mathrm{NRT}} t\right)$$

Equation 4

Where C_{P0} is the bulk atomic fraction of P atoms,

d is the monolayer width (half lattice parameter),

ρ is the dislocation density

G^{NRT} is the NRT dpa rate

and Γ accounts for the diffusion properties of P atoms in complexes with vacancies and interstitial atoms. It follows from MC calculations [30] based on the potential set developed in collaboration with [31] that Γ can be expressed as

$$\Gamma = \left[\varepsilon_{\mathrm{I}}^{\mathrm{Single}} + \frac{\varepsilon_{\mathrm{V}}^{\mathrm{Single}}}{1 + C_{\mathrm{P0}}^{-1} \exp(-E_{\mathrm{b}}\beta)} \right] \frac{1}{C_{\mathrm{P0}}}.$$

Equation 5

where $\beta = (k_B T)^{-1}$,

E_b =0.37 eV is the binding energy of a vacancy-P atom complex,

ε_V^{Single} =0.2 and ε_I^{Single} =0.02 are the fractions of vacancies and interstitial atoms that escape the cascade in single form (values were estimated by the Monte Carlo 'short-term annealing' of the cascades simulated by MD, [33]).

The fitting of experimental data were performed assuming a dislocation density of $\rho = 2 \times 10^{14}$ m^{-2}.

The critical experimental data to describe were the data on P segregation levels in the Fe-P-C model alloys and in the VC SCGHAZ. These data cover a range of bulk P levels, irradiation temperatures, and fluence, and show the greatest range in P levels with irradiation.

The most striking feature of the experimental data is the low segregation levels observed, as compared with the number of vacancies produced by irradiation and arriving at a grain boundary. A significant reduction in the vacancy-P binding energy from the values employed above would result in the required low segregation levels, but would also lead to a significant temperature dependence of the segregation, which is not observed. This left only the parameters ε_V^{Single} and ε_I^{Single} as the parameters which could be varied to obtain a fit between the model prediction and the data. The best fit was obtained with the defect production efficiencies reduced by 20 times: ε_V^{Single} =0.02 and ε_I^{Single} =0.002, without changing any other parameters. Thus, the total vacancy production rate is 0.01 of the NRT standard. The fits between data and prediction using these single defect production rates, are shown in Figure 41.

It is important to note that the model used to successfully fit the data has a weak dependence on irradiation temperature and the predicted segregation does not depend on dose rate. The segregation is largely determined by the bulk level of P, the dose and the local dislocation density (i.e. the distance from the boundary of a competing fixed sink for the point defect).

A key feature of this model is that both interstitials and vacancies form complexes with P, and segregation results from the flux of point defects (and point defect complexes) to the boundary. Since the flow of both kinds of point defect is towards the boundary, there is no mechanism for removing P from the boundary. Thus no "equilibrium" level of P may be defined. The level of P in the boundary increases with the number of complexes arriving, regardless of the "equilibrium" level of P defined by the temperature etc. This is possible because P segregation is driven by the reduction in the total free energy of the system. Under thermal conditions, the dominant cause of excess free energy is the distribution of solutes amongst the various microstructural constituents.

An equilibrium balance between P (and other solutes) in the matrix and P in a grain boundary may therefore be defined and, since vacancies flow both into and out of the boundary, P may move both into and out of the boundary, and that equilibrium balance may be achieved. Under irradiation, the dominant cause of excess free energy is the supersaturation of point defects. It is acceptable for the level of P in the boundary to rise above that required by thermal equilibrium in unirradiated steel, if the total free energy of the system is reduced more by the concomitant destruction of the point defects than it is increased by the over-segregation of P. With no mechanism for removing P from the boundary in the presence of a flux of point defect complexes to the boundary, and little effect of P over-segregation on suppressing the flux, P levels in the boundary continue to rise until the supply of P is exhausted. For the dose range applied within the PISA program, the rate of increase in P at the grain boundaries in close to linear with dose.

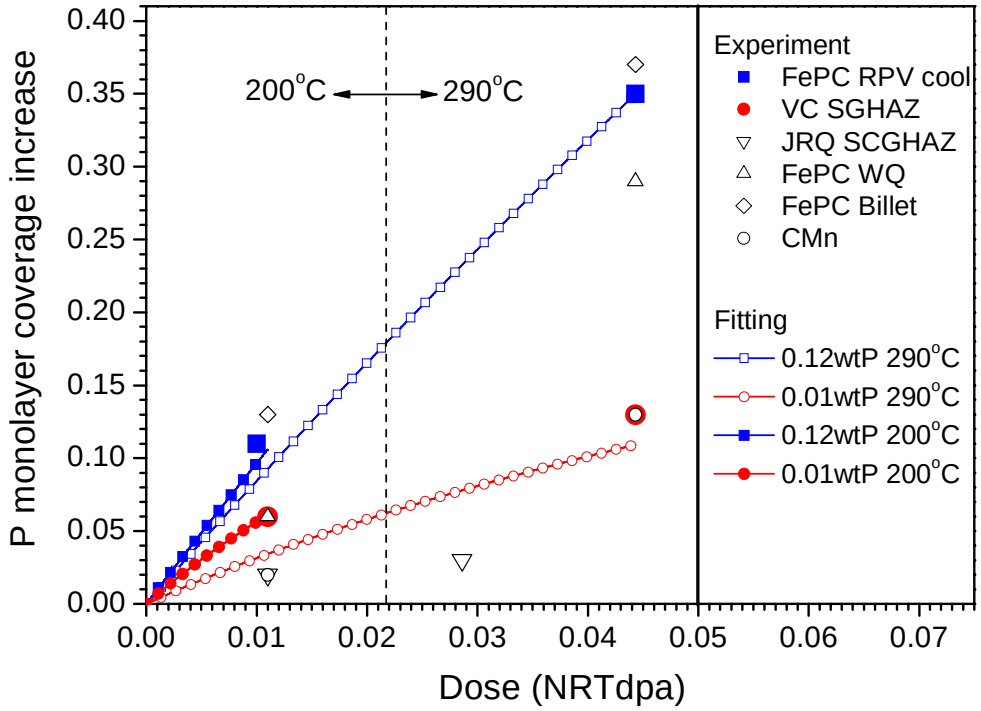

Figure 41. Comparison between data on P segregation in FePC model alloys (0.12wtP) and VVER-1000 SCGAZ (0.01wtP) and predictions of the model produced within PISA.

7.2. Monte Carlo Calculations

Modelling has been undertaken at MPA Stuttgart aimed at generating insight into the thermal segregation of P and C under conditions which simulate the experimental conditions studied in the PISA project. More specifically, atomistic Monte Carlo simulations of time-dependent segregation of P and C to grain boundaries in bcc Fe have been performed. The diffusion of Fe and P atoms is assumed to occur via a vacancy mechanism, and C diffuses by an interstitial mechanism, whereby a thermally activated C atom jumps from an octahedral position to the next nearest neighbour octahedral position.

A comparison between simulated and AES segregation data, for an Fe-P-C alloy aged at a variety of temperatures, shows good agreement for the P data (see Figure 42). For C the simulation yields nearly constant low segregation levels, in contrast to the variation observed by AES. It is believed that this is caused by the fact that there are probably too few C atoms in the simulation box, i.e. the movement of C to the grain boundary exhausts the C, whereas in the real material C can diffuse into the grain boundary region from 'deeper' in the matrix.

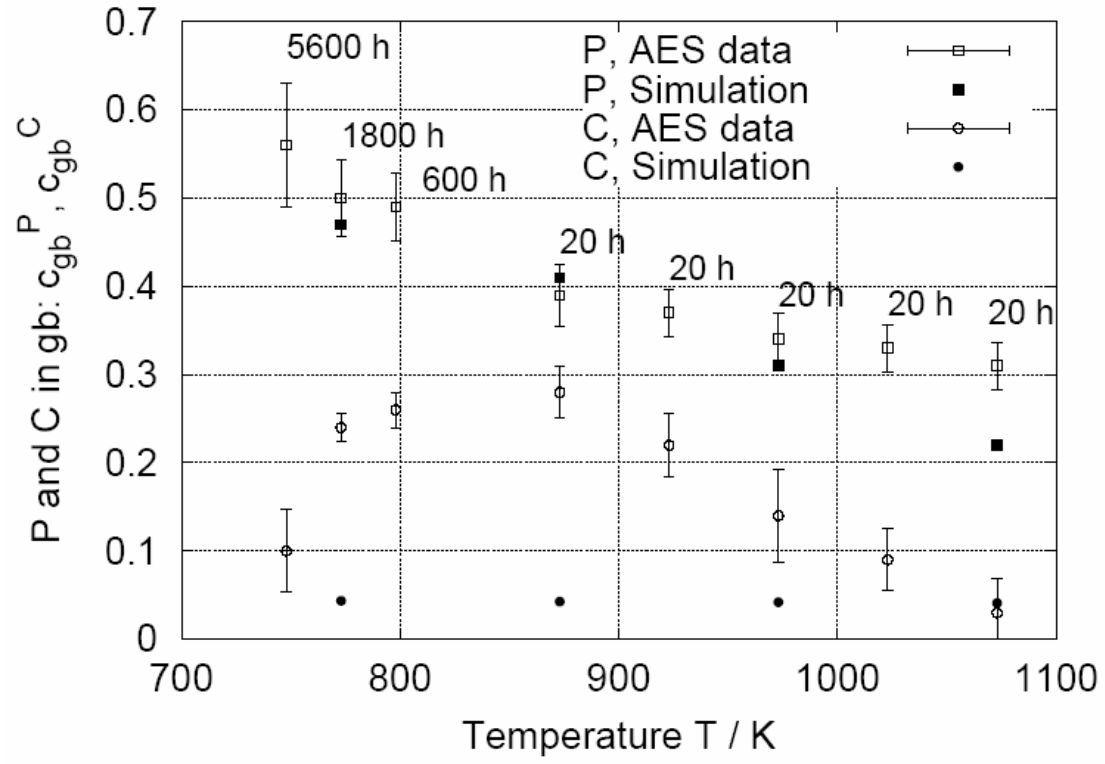

Figure 42. Comparison of simulation and AES data.

Simulations were undertaken of P and C segregation under thermal ageing conditions starting with no P or C on the boundary (an empty boundary), or with a fixed initial level of P or C on the boundary. These showed that:

- The simulated P segregation could be described using a Johnson-Mehl-Avrami (JMA) equation in all simulations, i.e. the equations for the time-dependent P and C concentrations in the grain boundary can be written as:

$$c_{gb}^{P}(t) = c_{gb}^{P}(0) + (c_{gb}^{P}(\infty) - c_{gb}^{P}(0))\left(1 - \exp\left\{-\left(\frac{t}{\tau^{P}}\right)^{n}\right\}\right)$$

$$c_{gb}^{C}(t) = c_{gb}^{C}(0) + (c_{gb}^{C}(\infty) - c_{gb}^{C}(0))\left(1 - \exp\left\{-\left(\frac{t}{\tau^{C}}\right)^{n}\right\}\right)$$

  The constants τ^{C}, τ^{P} and n were derived from the simulations.

- In the case of C this was only established for cases where there was a high level of C on the grain boundary at t=0, i.e. the decrease of the initially high C coverage followed the JMA law in these simulations.

- The simulations showed that the C level on the grain boundary after thermal exposure depends on
  - the level of free C in the matrix,
  - temperature, annealing time, grain size
  - SOL grain boundary coverage.

- In simulations starting with an empty boundary, the equilibrium level of P in the grain boundary increases with decreasing temperature while the time to reach equilibrium increases.

A key aspect of the work at MPA Stuttgart was to investigate the interaction between P and C atoms, in particular how this influenced the segregation at grain boundaries. The simulations have shown that the movements of P and of C at such low concentrations do not depend on each other. Further, at the temperatures of interest, C atoms moved to their new equilibrium positions at much shorter times than P atoms. This is illustrated in Figure 43. The ratio τ^{P}/τ^{C} is a measure of the different speeds of grain boundary segregation of P and C, e.g. for 200°C the segregation of C is 10063 times faster than the segregation of P. The ratio τ^{P}/τ^{C} significantly decreases at higher temperatures. This plot illustrates the influence of temperature on the different speeds of P- and C- segregation, due to their different diffusion mechanisms.

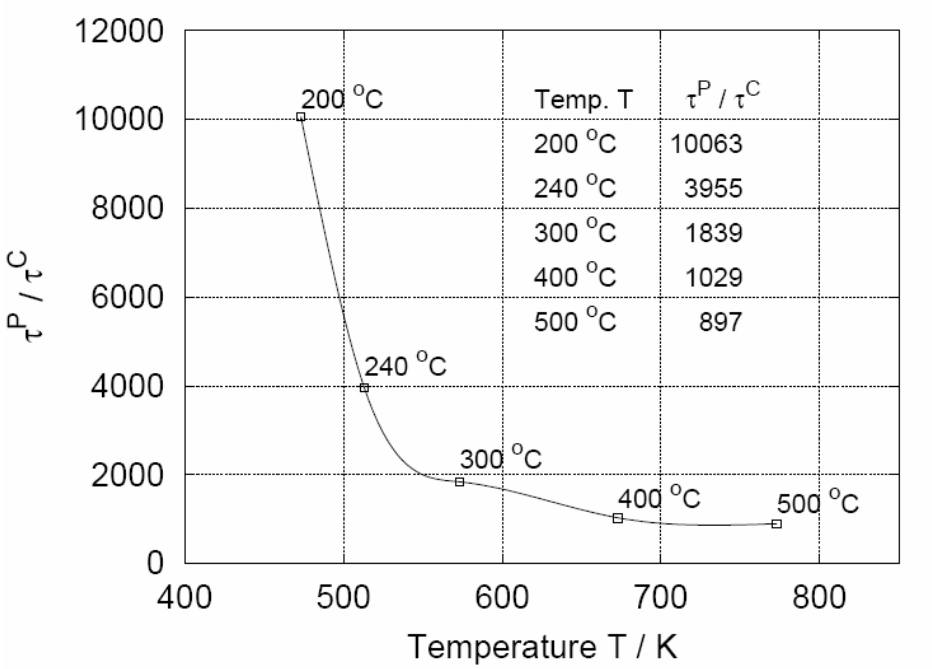

Figure 43. Plot of the ratio of τ^P / τ^C as a function of temperature for an Fe-P-C alloy containing a pre-filled boundary.

The simulations suggested that there is no consistent relation between the levels of P and C on the grain boundary as a result of thermal ageing.

8. Overall summary

In this section we review the data trends observed within the PISA experimental and modelling program, and compare them with observations reported elsewhere.

8.1. Dependence of P segregation on irradiation and material variables

8.1.1. Dose and dose rate

A major observation made on the material irradiated in HFR Petten is that the increase in monolayer P coverage increased ~linearly with increasing dose. This observation was justified in the light of the modelling, which indicated that both vacancy- and interstitial-type defects would complex with P, and drag it to the point defect sinks.

Support for this comes from data on VVER steels reviewed as part of WP2. For example, Gurovich et al [34] examined 25Kh3NM base metal after irradiation at 270-290°C. The amounts of segregated P increased with fluence, as shown in Figure 44. It can be seen that within the error bars the increase is consistent with a linear increase with fluence.

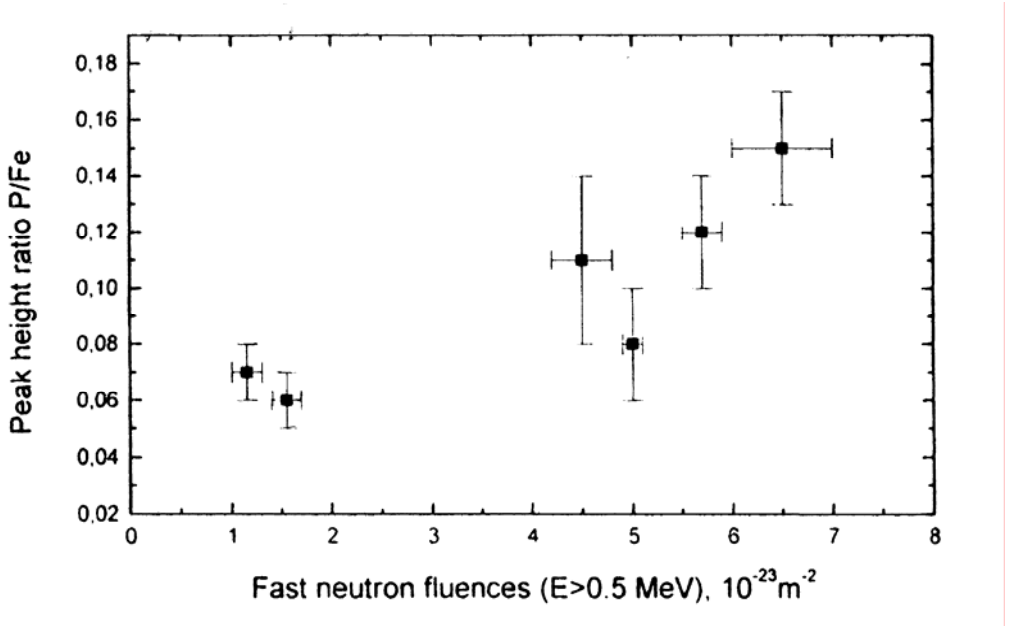

Figure 44. Increase of segregated P with irradiation of 25Kh3NM base metal.

In addition, Nikolaeva et al. [35] examined the change in grain boundary P with irradiation in a high-Cr, low alloy VVER RPV steel, containing 0.018 wt% P, irradiated to high doses at 275°C. The Auger data revealed an increase in P grain boundary concentration with damage dose. Although, the authors' model did not predict a linear increase with fluence, it can be seen from Figure 45 that the data are consistent with a linear increase over the fluence range examined. Further support is found for a linear increase with dose in the work of Ortner et al [1] who reported Auger measurements of the P segregation in base metal from the Novovoronezh-2 VVER-440 [36] (see Figure 46).

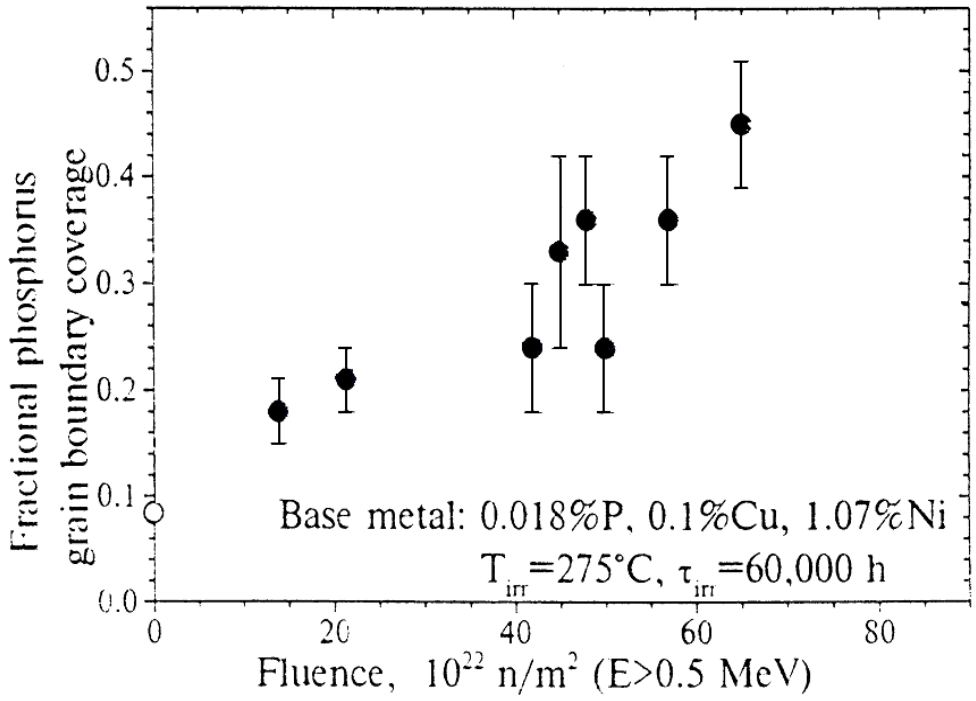

Figure 45. Increase of segregated P with irradiation of low-alloy Cr-Ni-Mo steel.

Within the observations made during the PISA program, no effect of dose rate on the rate of P segregation could be observed. The levels of segregation in the steel irradiated at two different fluxes were, however, sufficiently low that any effect could have been masked by scatter. The modelling indicates that no effect of flux should be observed, at least within the flux range in which point defect recombination occurs predominantly at fixed sinks. There are no other data in the literature that have compared the same material irradiated at two different dose rates but at the same dose.

8.1.2. Irradiation Temperature

The measurements of P segregation in the material irradiated in HFR Petten indicate that the increase in monolayer P coverage is not significantly dependent on irradiation temperature between 200 and 290°C. There are no other studies in the literature that have undertaken a systematic examination of irradiation temperature. However, the ternary alloy, Fe-0.12P-0.003C included in the PISA irradiations was previously irradiated at 240°C [10]. This datum is added to Figure 33, where it is clearly consistent with the data from this alloy irradiated at 200°C or 290°C.

8.1.3. Bulk P content

The greatest insight here comes from equation 4 developed in section 8.1 to describe the segregation under irradiation. Here, the rate of increase in grain boundary P is linearly dependent on the bulk level of P.

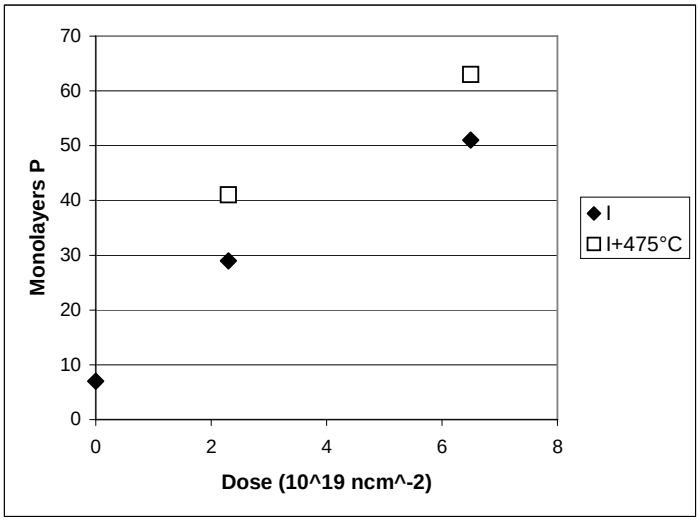

Figure 46 Effect of dose and PIA at 475°C on P segregation (measured by AES) in VVER-440 base metal.

8.1.4. Microstructure

That microstructure affects segregation during irradiation is particularly clear when P segregation in VVER 1000 base metal is compared with that observed in the corresponding SCGHAZ. Greater segregation is observed in the SCGHAZ microstructure. It is not clear which aspects of the microstructure changed by the HAZ simulations have most affected the segregation during irradiation. Further comparisons are, however, available within the PISA program.

The HAZ-simulating treatment on VB decreased the SOL C level with respect to VA, though only slightly, and the P level was increased. No other data in the PISA program have shown an increase in P segregation (under thermal ageing or irradiation) associated with an increase in SOL P level, and no relation of any kind between segregation under irradiation and SOL P level is predicted by the model described in section 7.1. The SOL C level appears to affect P segregation at low doses in the FePC alloys but, in these alloys, the lower the initial C level, the lower the P segregation (and the C desegregation) during irradiation. Overall, then, the influence of the SCGHAZ treatment on the sensitivity of the microstructure to irradiation-induced segregation, does not appear to have been via its effect on the SOL grain boundary composition.

The HAZ-simulating heat treatment could have affected the dislocation density. The comparison between the segregation observed in JRQ SCGHAZ with that in JRQ SCGHAZ+ε was intended to show the effect of dislocation density on segregation during irradiation. As described in Section 6.2 the effect of straining was probably to cause an increase in segregation. This is contrary to the predictions of the simple model by Barashev reported in section 8.1, in which it was predicted that the increase in dislocation density (i.e. fixed sinks for point defect annihilation) caused by straining would lead to a reduction in irradiation-induced segregation.

The only systematic study in the literature on the effect of dislocation density (reviewed as part of WP2) was that of Cowan, who studied an Fe-0.06P-0.002C alloy aged at 500°C [9]. Here, the thermal segregation, hardening and precipitation behaviour of as-

quenched material was compared with that of material strained +10% prior to ageing. After short ageing times (4h), the increased dislocation density produced by tensile pre-straining increased the rate of P segregation. The rate of increase was consistent with the near-boundary dislocation density, and local P movement being by pipe diffusion. After longer ageing times, the grain boundary P levels decreased, probably due to precipitation on dislocations. Thus after extended ageing, the effect of the dislocations was "thermodynamic" rather than "kinetic". The complex effect of increasing the dislocation density in thermal ageing demonstrates that it is possible that for dislocations to play more than one role in affecting segregation. At the low levels of P segregation observed in the JRQ SCGHAZ, it is plausible for (pseudo-thermal) pipe diffusion down dislocations to grain boundaries to occur even under irradiation. In summary, it is necessary to understand the effect of increasing dislocation density on all aspects of the radiation-induced microstructure if we are to fully understand the result.

The central result of both the experimental data and the associated modelling is that, for a given microstructure, the main variables controlling the increase in P are the dose and the bulk level of P. Thus by comparing the increase in monolayer coverage per wt% P per mdpa the effect of 'microstructure' may become more apparent. The latter is plotted in Figure 47 for the FePC (BC) alloy, the CMn plate, JRQ, the VVER 1000 base metal and the VVER weld 501. In the commercial steels the amount of segregation per wt% P per mdpa is lower in the strong carbide formers JRQ and VVER 1000 base metal.

Overall, the experimental data clearly demonstrate that the microstructure at SOL has an important effect on the resultant segregation. The data collected as part of the PISA programme have established that the microstructural variables of interest may not be limited to simply the dislocation density of the material.

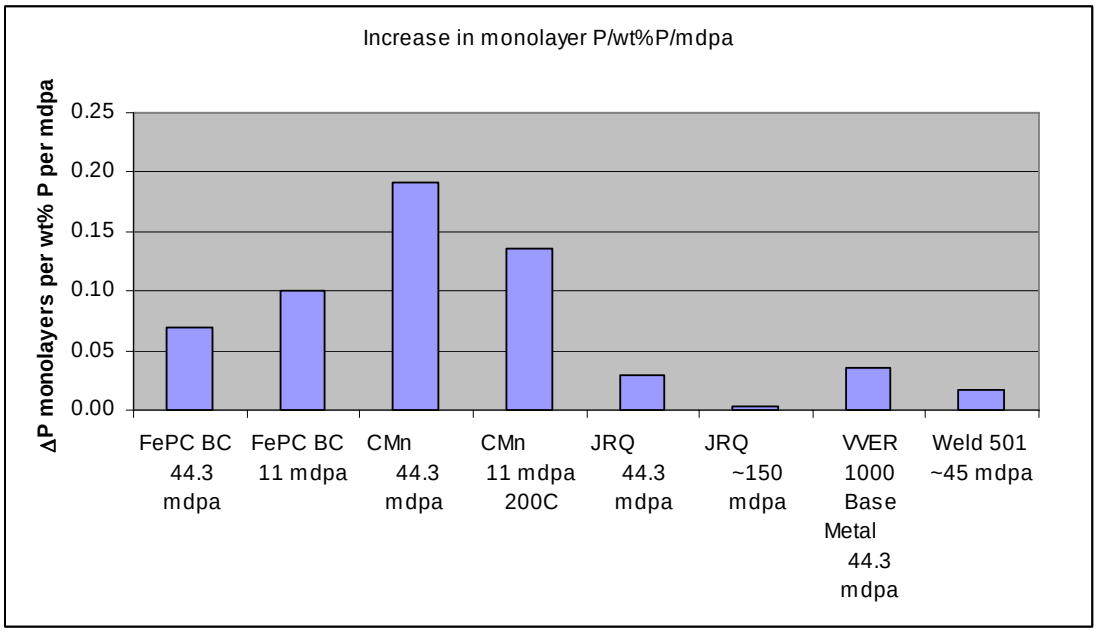

Figure 47 Plot of the increase in monolayer coverage per wt% P per mdpa for the FePC (BC) alloy, CMn plate, JRQ, VVER 1000 base metal and VVER 440 weld 501.

8.1.5. Comparison of mechanical property and segregation data

The PISA literature review suggested that the shift in the DBTT with segregation was better correlated with the grain boundary chemistry than with the %IGF, as the latter very rapidly increased past the threshold, and saturated. The ratio $\Delta T_{41J}/\Delta H_v$ is therefore plotted versus grain boundary P and C coverage (in fractions of monolayers) for JRQ and CMn plate irradiated in HFR Petten (Figure 48). The accepted correlation for $\Delta T_{41J}/\Delta H_v$ for base metal is also given in the Figures. For all combinations of material and monolayer coverage there is no suggestion of such abnormally high values of $\Delta T_{41J}/\Delta H_v$ as would indicate non-hardening embrittlement. It is to be noted that the highest P coverage in this Figure is ~0.24monolayer, in a CMn plate sample which had 0.31 monolayers C after irradiation – a boundary composition which (from [1] and Figure 48) would be expected to lead to IGF.

The ratio $\Delta T_{41J}/\Delta \sigma_y$ is plotted in Figure 49 versus P and C coverage for previously irradiated A508 ClIII materials from EdF. The accepted correlation for $\Delta T_{41J}/\Delta \sigma_y$ for base metal is also given in the Figure. Once again, for all the combinations of material and C/P coverage there is no suggestion of abnormally high values of $\Delta T_{41J}/\Delta \sigma_y$ or non-hardening embrittlement. In this Figure, Material A (grain boundary composition 0.24monolayers P, 0.35monolayers C) and Material B ICGHAZ (gl) (0.27 monolayers P, 0.28 monolayers C) would be expected to exhibit IGF after irradiation. Fractography has been performed on Material B by EdF prior to the PISA programme; IGF was observed in ICGHAZ (gl) which had the high P on the boundary, no or a small percentage of IGF was observed in the other two Material B samples (Saillet private communication). EdF also reported that, in each case, no significant increase in the level of IGF was observed on irradiation.

These figures and the fractographic observations reviewed above and in section 3 may indicate that some level of IGF may be tolerated in irradiated steels before additional embrittlement is observed. Recently, Chivers has reported [37] irradiation of a thermally aged C-Mn submerged-arc weld. The Charpy shifts due to in-service thermal ageing were not known, but the subsequent shifts due to accelerated irradiation are considerably less than predicted for irradiating unaged weld (even assuming Cu was precipitated during thermal ageing). It was observed that the amount of IGF increased dramatically during irradiation but did **not** seem to cause embrittlement. Further, Chivers reported that large increases in IGF without apparent embrittlement have also been seen elsewhere, e.g. in C-Mn plate after accelerated irradiation at 270/290°C to 0.003 - 0.015 dpa. The percentage IGF increased from 1% to 37-53% without non-hardening embrittlement.

a)

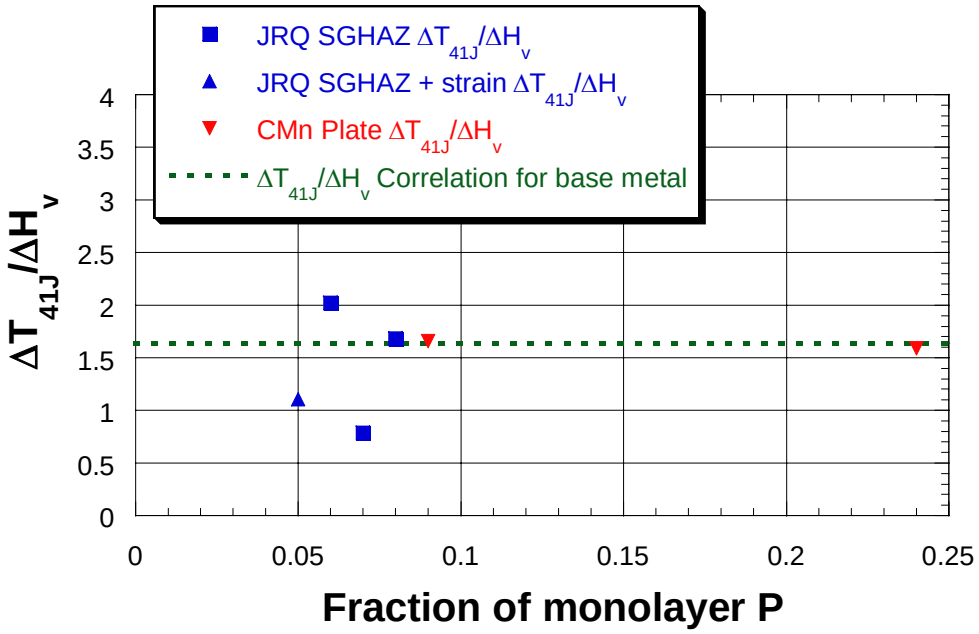

b)

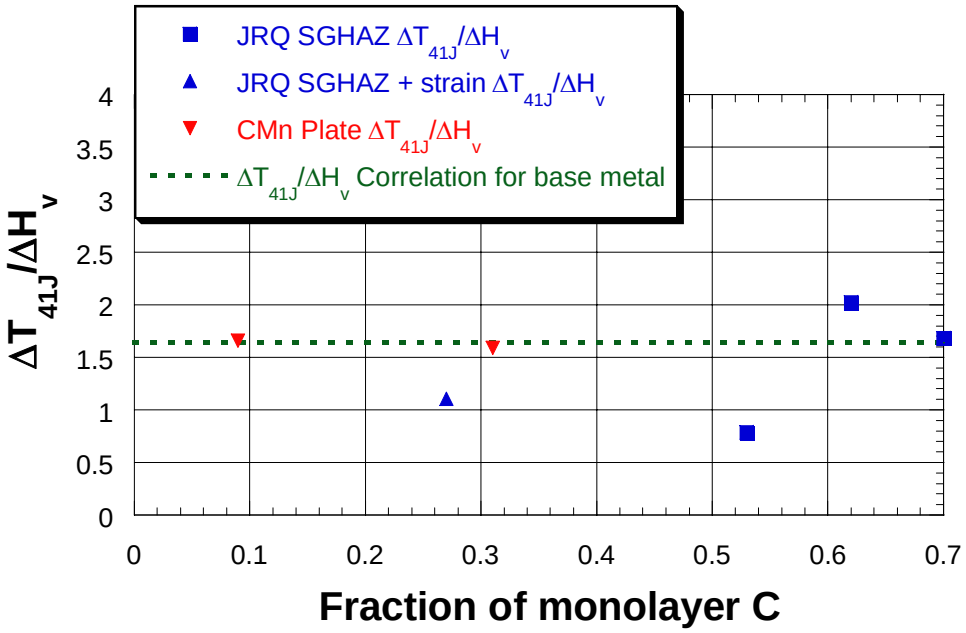

Figure 48. Plot of $\Delta T_{41J}/\Delta H_v$ vs fraction of a) monolayer P coverage and b) monolayer C coverage, for JRQ and CMn plate irradiated in HFR Petten.

a)

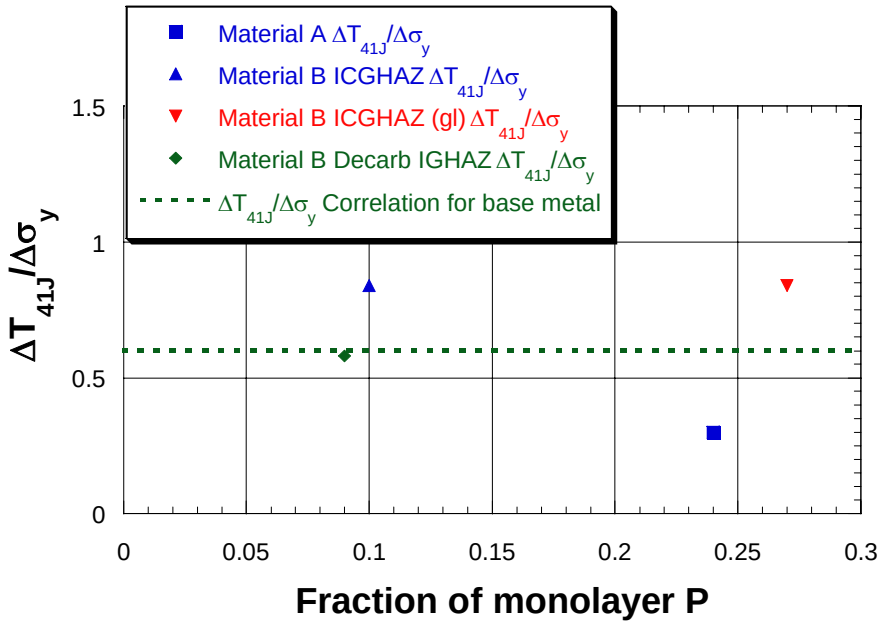

b)

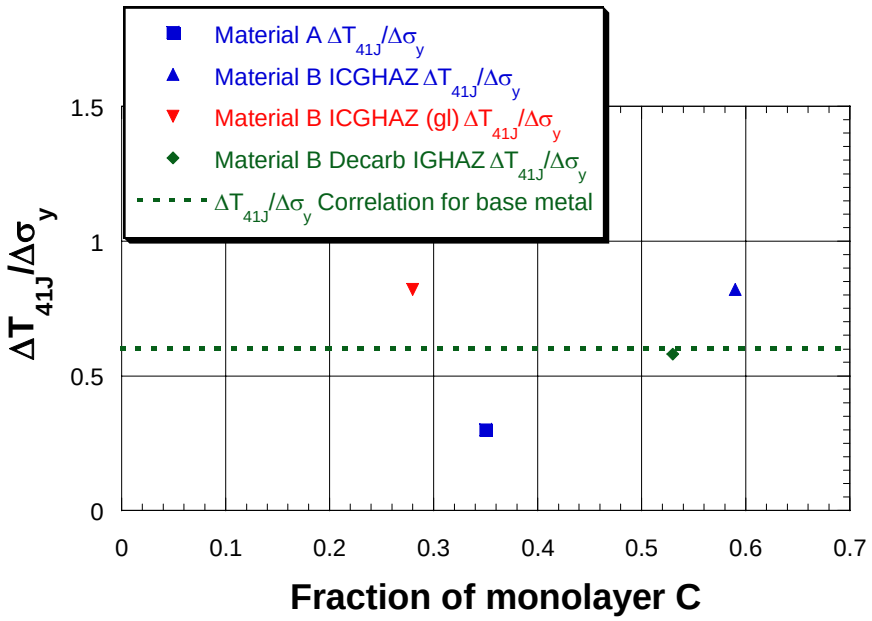

Figure 49. Plot of $\Delta T_{41J}/\Delta\sigma_y$ versus fraction of (a) monolayer P coverage and (b) monolayer C coverage, for previously irradiated A508 Cl. III materials from EdF.

8.2. Mechanistic insight into the role of C

The greatest insight into the influence of C on P segregation arises from studies of the FePC alloys and the results of the MC modeling. The MC modeling does not explain why C segregation is high at SOL but the results of the AES analyses do support the de-segregation of C from the boundary during thermal ageing. The C desegregation in the thermally-aged FePC alloys is probably the result of precipitation at 650°C, and a combination of precipitation and strain ageing at 200° and 240°C. This C desegregation influences the P segregation occurring during the heat treatment, although the effect is relatively small.

More specifically, thermal ageing of FePC alloys shows that, if the time at temperature is sufficient for the grain boundary P levels to reach equilibrium, then this equilibrium level seems to be affected by the amount of C on the boundary. At short P diffusion times, the absence of C has little effect on the amount of P arriving at the boundary. Since C diffusion is so much faster than P diffusion, the P level on the boundary does not have the same opportunity to affect the behaviour of C. KMC modeling also finds that C segregation is effectively independent of the behaviour of P.

Measurements on JRQ and VVER-440 weld 502 irradiated prior to PISA, indicate that C may desegregate from grain boundaries during irradiation due to both precipitation (in the VVER weld) and trapping at matrix defects. The measurements of C and P segregation in FePC alloys irradiated within PISA further show that the desegregation of C occurs predominantly at low doses. This may also be occurring in the PISA-irradiated CMn plate.

The behaviour of C in the PISA-irradiated steels is complex, as any initial desegregation of C appears to be replaced by an increase in grain boundary C segregation by 44.3mdpa. Even the CMn plate irradiated to 44.3mdpa shows an increase wrt 10mdpa, though not wrt SOL. It is possible that the rapid diffusion of C to matrix defects is occurring, followed by the much slower diffusion of the C-point defect complexes to the grain boundary sinks. The fact that C increases above the SOL level after high doses in some materials / irradiation conditions, but not in others, is difficult to explain. In particular, the consistent decrease in C wrt SOL seen in the materials irradiated prior to PISA is difficult to reconcile with the increases seen in the same materials irradiated to similar or lower doses within the PISA program. A complicated interaction may be postulated, between absorption of C by point defect clusters (dominant at low doses), the partial destruction of carbides and dislocation atmospheres (increasing with increasing dose), diffusion of C-point defect complexes to the grain boundary sinks (at intermediate and high doses), and carbide formation at complexes (during post-irradiation room temperature ageing), but there is insufficient evidence to render this more than a postulate.

Overall, there is no evidence in the irradiated steels for a consistent relation between C and P segregation, similar to that observed in thermally-aged materials. There is strong evidence that the level of C (and Mo) on grain boundaries in irradiated steels is influenced by the changes in the internal microstructure during irradiation, (i.e. the formation of the irradiation induced microstructure, and changes in the carbide distributions). C could be diffusing both independently (mainly away from the boundaries) and in association with point defect complexes (mainly towards the boundaries). The grain boundary P level is more simply determined by the flux of P-bearing point defect complexes to sinks. The levels of the two elements in the boundaries thus develop largely independently of one another.

It is also important to note that from the review of the literature on segregation and brittle fracture, it was suggested that intergranular fracture would be introduced above ~0.1monolayers in MnMoNi steels, with a possibly higher threshold in CMn plate [1]. It was recognised, however, that the level of IGF did not depend on P alone, so the P level would be a somewhat uncertain predictor of IGF. In particular, it appeared that increasing the level of C strongly discouraged IGF.

8.3. Overall significance of PISA data

The PISA project has generated significant amounts of data on both the segregation of P and C during irradiation and thermal treatments, and the associated mechanical property changes. The new data cover a range of bulk P levels, irradiation temperatures and fluences, steel types and product forms. In all cases only modest increases of P level on the grain boundary have been observed in commercial steels. Segregation is higher in pre-strained than in unstrained material.

A model for P segregation under irradiation has been developed, and shown to be capable of fitting the experimentally observed changes in P level after irradiation. Significant insight into the development of the microstructure under irradiation has thereby been obtained. In particular, the fraction of point defects surviving cascades is found to be very low.

The model indicates that P reaches the grain boundaries predominantly via the diffusion of P-point defect complexes, and their annihilation at sinks. This leads to a strong dependence of irradiation-induced P segregation on fluence, but any dependence of P segregation on dose rate or irradiation temperature is low. (These dependences are in accordance with data in the literature, and acquired during the PISA program.) The interaction between P and the point defects produced by irradiation does not allow for P leaving a boundary while the flux continues.

It is apparent that the C levels on the boundary reflect changes in carbide precipitation and C trapping in the matrix resulting from irradiation. A dynamic equilibrium is possible between C available in the matrix and C in the boundary, since C can diffuse independently of, and in conjunction with, the point defect flux. There is no evidence in the irradiated steels or from modelling for a relation between C and P segregation in the steels under irradiation.

The comparisons made during PISA between grain boundary chemistry and mechanical properties show that both P and C are important in determining boundary strength. High P levels and / or low C levels are detrimental to boundary strength, and lead to intergranular failure.

A very important result of the PISA program is that the $\Delta T_{41J}/\Delta\sigma_y$ or $\Delta T_{41J}/\Delta H_v$ data analysed give no indication of non-hardening embrittlement in any of the steels examined, even at very high doses. (VB step-cool may be an exception). In some cases, this could be ascribed to the small amounts of P accumulating in the boundaries, but several instances were observed in which the grain boundary P and C levels were such that significant amounts of IGF would be expected. Even in these cases, the embrittlement: hardening ratios showed no signs of segregation-related embrittlement. This suggests that irradiated steels could exhibit IGF without this having a detrimental effect on the resistance to cracking.

Data obtained on sample aged for 2700 days at 290^{o}C gave no evidence of significant P segregation during ageing.

Appendix: Conclusions from Comparison of Auger and FEGSTEM Techniques for Measuring Grain Boundary Composition in Pressure Vessel Steels and Model Alloys

Introduction

Various techniques are used to monitor the changes in grain boundary composition which occur with changes in bulk steel chemistry, thermo-mechanical treatment or irradiation. Two techniques in particular have developed to the extent that quantitative measurements may be made reliably. These are AES (Auger Electron Spectroscopy) and FEGSTEM/EDX (using a field-emission gun scanning transmission electron microscope equipped with an energy-dispersive x-ray analyser). Since the instruments used in AES and FEGSTEM are very different in concept, design and method of operation, the raw data produced by each bear different relations to the actual grain boundary chemistry. Thus different data manipulation techniques are required to represent the grain boundary composition. The data representations are not always such that it is possible to compare a given AES measurement with a given FEGSTEM measurement.

Work Package 7 in the PISA experimental program was designed to compare various techniques for measuring grain boundary composition, and to assess the extent to which they are comparable with each other. Specifically, the objectives of Work Package 7 were to:

- Compare and contrast Auger electron spectroscopy (AES) and transmission electron microscopy (TEM) techniques for measuring grain boundary composition,
- Carry out an inter-technique comparison using material from the PISA programme,
- Suggest and test improvements to experimental procedures, or methods of data analysis, and adopt these procedures if found appropriate,
- Formulate experimental procedures for examination and analysis such that consistent measures of grain boundary composition can be made using different techniques/procedures.

The activities undertaken to fulfil these objectives were:

- A literature review (including data published openly and data made available only to PISA) of existing comparisons between measurements of grain boundary coverage of solutes using AES and FEGSTEM techniques.
- Incorporation of recently-published determinations of inelastic mean free paths for Fe, P and C Auger electrons into revised expressions for evaluating the monolayer P and C levels from measurements using AES
- Assessment of segregant partitioning to matching facets on fracture, and any bias introduced by facet selection methods in AES
- Comparison between on-boundary enrichment measurements and across-boundary composition profiles for measuring monolayer coverages in the STEM
- Comparison between STEM and AES techniques for measuring P monolayer coverages

Quantification

A key aspect of the use of AES to measure solute grain boundary coverage is the conversion of the experimental measurement of the atomic % of an element on a facet to a monolayer coverage. Methods appropriate for C- and P-containing boundaries in steels and iron alloys had been developed over several years at BNFL Magnox. As part of the PISA programme, this methodology has been reviewed. In particular the integral mean free paths (IMFP) for P and C have been updated to match those present in the National Institute of Standards and Technology (NIST) [38], which are derived from the measurements and calculations presented in [39]. The IMFP is an essential parameter in the conversion procedure [40].

- Previously it was determined that, for steels and iron alloys, the complex equation relating monolayers P to atomic% on facet, could be approximated by

  monolayers P ~0.04 x (atomic% on facet)

  The revised IMFPs have not affected this expression. The effect of grain boundary C on the relation between grain boundary P and atomic% on facet was considered explicitly. C was found to affect the relation, but only by a few % of the total as C increased to >10%. The approximate expression was, therefore still recommended for use.
-
- Similar calculations for C had also led to the simplified relation

  monolayers C ~0.04 x (atomic% on facet).

  prior to PISA. The revised IMFPs have changed this ratio to

  monolayers C ~ 0.12 x (atomic% on facet)

  for moderate P levels. (The C level derived from the atomic % on facet is also affected slightly by the atomic % P on the facets.)level.

- The AES data analysis to determine monolayer P, C has been revised in accordance with the findings above.

Aspects Of AES Analysis

The facet selection tests have shown that choosing facets for analysis is best carried out on the basis of the secondary electron image (SEI), if the proportion of intergranular facets is large. If there are many intergranular facets, then locating an intergranular facet from the SEI will not be difficult or time-consuming, and the choice between intergranular facets will be random. A P map of a predominantly intergranular fracture surface will identify the intergranular facets with the highest P levels. This will bias the mean measurement to a higher value than the mean segregation level. The bias will be greater, the smaller the number of facets analysed, as the highest-P facets will be selected first from the P map.

If there are few intergranular facets exposed for analysis, however, locating intergranular facets from the SEI image will be difficult and time-consuming. On the other hand, the P image will emphasise the difference between intergranular and transgranular facets. With few intergranular facets, the opportunity to select a subset of high-P intergranular facets is reduced. At low levels of intergranularity then P mapping is invaluable and not biasing.

The facet matching tests have shown that the assumption that a grain boundary's segregants will partition equally to each fracture surface, is not generally valid. When sufficient boundaries are analysed, however, the distribution of segregant-rich and segregant-poor facets offsets the uneven partitioning, leading to a mean measured boundary composition close to the true mean, and well within the intrinsic boundary – to – boundary variation. When the segregation of P is considered, the actual partitioning varies from 50:50 to ~ 60:40, so the bias due to partitioning reaches an acceptably low value after only a small number of facets have been analysed (say 3-5). When C segregation is considered, the partitioning is so much more variable (from 50:50 to 90:10) that a larger number of facet measurements is required before the chance of significant bias is avoided (say 8-10).

Aspects Of STEM Analysis

The comparison between different methods of measuring grain boundary segregation in a STEM shows that on-boundary measurements will represent the boundary composition if the foil thickness is known or, more conveniently, if a sufficient number of measurements is made, that the measurement locations cover moderate variations in foil thickness about an anticipated mean. If, at the same time, sufficient boundaries are analysed to incorporate intrinsic boundary – to – boundary variability into the data set, then the mean on-boundary measurement will be representative of the material condition. A mean "monolayer" equivalent to the mean on-boundary measurement may be derived using the Fisher et al correction [41] (adapted for the required definition of a "monolayer"). In the current work, the mean of 6 locations on each of 9 boundaries produced a representative measurement. Only 3 boundaries were analysed using the profile method. This also produced a representative material measurement, but actually required a greater total spectrum acquisition time (by a ratio of 4:3). Spectrum acquisition time does not, however, dominate the experimental time in STEM grain boundary analysis: locating and aligning suitable boundaries is the most time-consuming procedure. If, therefore, a steel's prior austenite grain size is small, and a foil contains several suitably-oriented boundaries, then the multiple on-boundary method of analysis is more convenient. If only a few suitable boundaries are present in a foil, then it is more convenient to use the profile method.

Technique Comparison

Within the PISA programme, a Cr-Mo-Ni VVER-1000 steel of type 15Kh2NMFAA was examined using AES and STEM. Two types of STEM analysis were carried out: one technique used a sequence of measurements across each boundary, so that the composition profiles could be used to assess the beam spreading within the thickness of the foil for each boundary; the other technique used a number of measurements on each boundary so that a mean on-boundary measurement would be representative of an average foil thickness (~50nm) and, hence, an average degree of signal dilution. The grain boundaries in the steel were found to be enriched in P, C, Ni, Mn, Mo, Si and Cr, and depleted in Fe. The system was thus typical of RPV, and quite complex in terms of the number of segregants involved.

The results of the different measurement, and data analysis, techniques are summarised in Table **22**. The experimental methodologies, and data analysis techniques used within PISA are shown to yield comparable descriptions of the mean grain boundary P levels in a multiply-segregating system.

Table 22. Comparison Between Results Of Different Techniques For Measuring Grain Boundary P levels In 15Kh2NMFAA steel.

Technique (Laboratory)	Number of boundaries analysed	Number of spectra per boundary	Boundary P level (Mean±Standard Deviation) % monolayer
AES (BNFL Magnox)	35	2*	8.5±3.1
FEGSTEM (AEA Technology)	3	12‡	5.7±1.8
STEM (VTT)	9	6†	9.5±2.2

* one on an intergranular facet, plus one on a nearby transgranular facet to aid in C segregation measurement, and monitor contamination
‡ spectra forming composition profiles across the boundaries
† spectra taken at different locations along the boundaries

CONCLUSIONS/RECOMMENDATIONS

WP7 in the PISA programme has shown that it is possible to obtain consistent measurements of grain boundary composition using different measurement and data analysis techniques so long as

- the boundaries analysed are representative,
- sufficient measurements are taken to account for measurement uncertainties and boundary-to-boundary variation,
- similar definitions of a monolayer (i.e. boundary width) are used in the data reduction procedures.

Choosing representative boundaries in the STEM requires that the (high-angle) boundaries should be aligned parallel to the electron beam, and the foil thickness be accounted for. In the AES, initial P mapping is a neutral procedure for selecting boundaries only when fracture produces very few intergranular facets.

In the STEM, at least 3 different boundaries are required to allow for boundary-to-boundary variability, with 5-10 measurements per boundary to allow for foil thickness effects. In the AES at least 10 boundaries are required to allow for facet orientation effects and uneven solute partitioning during fracture. In both cases, increasing the number of boundaries above the minimum improves the reliability of the measurement.

Within the PISA program, a boundary width of 0.202nm was used to analyse the STEM data.

9. References

1 S.R.Ortner and C.A.English, "Project PISA, Phosphorus Influence On Steel Ageing: Literature Review" Report PISA/R(02)/2001/October/Issue 1.

2. B.Acosta, "LYRA Experiments For PISA: Neutron Metrology And Accumulated Doses Report" JRC Petten Report NSU/CA/BA/05.01.06.01, January 2005.

3. B.Acosta, M.Beers, C.McGirl, F.Sevini and L.Debarberis, "LYRA-05 Experiment for PISA 1 irradiation" Irradiation Report HFR/01/4677, JRC Petten, October 2001.

4. B.Acosta, "LYRA-06 Experiment for PISA B irradiation" Irradiation Report NSU/CA/BA/030701.02, JRC Petten, July 2003

5. B.Acosta, "LYRA-07 Experiment for PISA C irradiation" Irradiation Report NSU/CA/BA/051301.01, JRC Petten, January 2005.

6. R.Langer, "PISA Material Selection and Documentation, WP5 and WP6 Materials" Framatome Report FANP TGM.

7. F.Gillemot, G.Uri, M.Horvath, J. Cowan, B. Acosta, L. Debarberis, M. Beers, C. McGirl, A. Kryukov, M.Brumovsky, J.Brynda, and V. Cerny, "Material Selection", Project PISA Report PISA/R(01)/WP1/D1, Issue 1, July 2001.

8. J.R.Cowan, H.E.Evans, R.B.Jones and P.Bowen, "The grain boundary segregation of phosphorus and carbon in an Fe-P-C alloy during cooling" Acta Materialia, 46 (18) 6565-6574 (1998).

9. J.R.Cowan, H.E.Evans, R.B.Jones and P.Bowen, "The effect of dislocation density and structure on the grain boundary segregation of phosphorus and carbon in a model Fe-P-C alloy" in Proc Workshop on Grain boundaries: Their Character, Characterisation And Influence On Properties" ed. I.R.Harria and I.P.Jones, pub. IOM communications, London 2001, pp.11-26.

10. R.B.Jones, J.R.Cowan,R.C.Corcoran and J.C.Walmsley, "Embrittlement, Hardening And Grain Boundary Composition In An Irradiated And Thermally Aged Fe-P-C Alloy" in "Efects Of Radiation On Materials: 19th Int. Symp. ASTM STP 1366. Eds. M.L.Hamilton, A.S.Kumar, S.T.Rosinski and M.L.Grossbeck, pub. ASTM West Conshohocken, USA (2000) pp.473-491.

11. B.Acosta, "LYRA Experiments For PISA: Neutron Metrology And Accumulated Doses Report" JRC Petten Report NSU/CA/BA/05.01.06.01, January 2005.

12 R B Jones and C J Bolton, "Neutron Radiation Embrittlement Studies in Support of Continued Operation, and Validation by Sampling of Magnox Reactor Steel Pressure Vessels and Components", 24th Water Reactor Safety Meeting, USNRC, Oct. 1996.

13. T.J.Williams, D.Ellis, D.I.Swan, J.McGuire, S.P.Walley, C.A.English, J.H.Venables, and P.H.N.Ray, "The Influence Of Copper, Nickel And Irradiation Temperature On The Irradiation Shift Of Low Alloy Steels "Environmental Degradation Of Materials In Nuclear Power Systems - Water Reactors", ", Proc. 2nd Int. Symp. held September 1985, ANS 1986.

14 K.Chivers private communication

15 Jones, R.B., and Williams T. J., "The dependence of radiation hardening and embrittlement on irradiation temperature" Effects of Radiation on Materials:17th International Symposium, ASTM 1270, Eds D.S. Gelles, R.K. Nanstead, A.S. Kumar, and E.A.Little, ASTM 1996, 569.

16 E D Eason, J E Wright and G R Odette, "Improved Embrittlement Correlations for Reactor Pressure Vessel Steels", NUREG/CR-6551, Nov. 1998.

17 M. Kirk, "Revision of ΔT30 Embrittlement Trend Curves." Presented at the EPRI MRP/NRC PTS Re-Evaluation meeting in Rockville Maryland, August 30, 2000.

18 ASTM E 900-02, "Standard Guide for Predicting Radiation-Induced Transition Temperature Shift for Reactor Vessel Materials, E706 (IIF)," *Annual Book of ASTM Standards*, Vol. 12.02. American Society for Testing and Materials, West Conshohocken, PA.

19. E.A.Little, "Strain Ageing And Neutron Scattering Studies On Irradiated PWR Pressure Vessel Steels" in "Effects Of Radiation On Materials: 12th Int. Symp. ASTM STP 870" Eds. F.A.Garner and J.S.Perrin., pub. ASTM, Phila., USA (1985). pp 1009-1026.

20. "Analysis Of The Behaviour Of Advanced Reactor Pressure Vessel Steels Under Neutron Irradiation" Final Report Of IAEA Coordinated Research Programme 1977-1983. Technical Reports Series No. 265. Pub. IAEA, Vienna (1986) ISBN 92-0-155186-X

21. B. Priest, “Observations On Identifying Trends In The Post-Irradiation Response Of Modern RPV Steels” in Proc. Workshop On Dose Rate Effects In Reactor Pressure Vessel Materials” held Squaw Creek, California, USA, November 2001.
22 Yu.A.Nikolaev, A.V. Nikolaeva, Ya. I. Shtombakh, “Radiation Embrittlement of low-alloy steels. Journal of Pressure Vessel and Piping in press
23. R.J.McElroy, C.A.English, A.J.E Foreman, G.Gage, J.M.Hyde, P.H.N.Ray, and I.A.Vatter, “Temper Embrittlement, Irradiation Induced Phosphorus Segregation And Implications For Post-Irradiation Annealing Of Reactor Pressure Vessels” in “Effects of Radiation on Materials 18th Int. Symp. ASTM STP 1325”. Eds. R.K.Nanstead, M.L.Hamilton, F.A.Garner, and A.S.Kumar. Proc Conf held Hyannis Mass., USA June 1996. Pub ASTM, West Conshohocken USA, 1999. Pp.296-316.
24. G.R.Odette, P.M.Lombrozo, and R.A Wullaert, “Relationship Between Irradiation Hardening and Embrittlement of Pressure Vessel Steels”, Effects of Radiation on Materials: 12th Conference, ASTM STP 870, F.A.Garner and J.S.Perrin Eds. American Society for Testing and Materials, 1985, p.840-860.
25. A.Ballasteros priv comm. 2001.
26 R C Corcoran, S. R. Ortner, I. A. Vatter, and D.D.Jones. Measurements of grain boundary composition in thermally aged PISA samples. PISA/R(11). May 2005.
27. M.Guttman, P.Dumoulin and M.Wayman, “The Thermodynamics Of Interactive Cosegregation Of Phosphorus And Alloying Elements In Iron And Temper-Brittle Steels” Metall. Trans. A, 13A, 1693 (1982).
28 P. Binkele, P. Kizler, S. Schmauder. Atomistic Monte Carlo simulations of the diffusion of P and C near grain boundaries in bcc iron. PISA/R(13). March 2005.
29 A.V.Barashev. Atomic-Scale Modelling and Development of Continuum Theory of Phosphorus Segregation in Pressure Vessel Steels and Model Alloys. PISA/R(14) March 2005.
30 Barashev, A.V., 2005, *Philos. Mag.*, **85**, (2005) 1539-1555.
31 Ackland, G.J., Mendelev, M.I., Srolovitz, D.J., Han, S., and Barashev, A.V., 2004, *J. Phys.: Condens. Matter* **16**, S2629.
32 Barashev, A.V., 2002, *Philos. Mag. Lett*. **82,** 323.
33 Barashev, A.V., Bacon, D.J., and Golubov, S.I., 2000, *J. Nucl. Mater.* **276,** 243.
34 B.A.Gurovich, E.A.Kuleshova, Ya.I.Shtrombakh, O.O.Zabusov and E.A.Krasikov, “Intergranular And Intragranular Phosphorus Segregation In Russian Pressure Vessel Steels Due To Neutron Irradiation”, J.Nucl.Mater., 279, 259-272 (2000).
35. A.V.Nikolaeva, Y.R.Kevorkyan and Y.A.Nikolaev,”Comparison Of Observed and Predicted Data On Radiation Induced Grain Boundary Phosphorus Segregation In VVER Steels," in “Effects of Radiation on Materials, 19th International Symposium, ASTM STP 1366”. Eds. M.L.Hamilton, A.S. Kumar, S.T.Rosinski and M.L.Grossbeck, pub. American Society for Testing and Materials, West Conshohocken, PA, 1999., p 399.
36. S.R.Ortner, R.M.Boothby, G.C.Cattle, J.A.Mace, D.K.Lurcook, R.N.Thomas, I.A.Vatter and W.Hanks, “Microstructural Examination Of Base And Weld Metals”, AEA Technology Report AEAT-1090.
37 K.Chivers Ageing in C-Mn Steels Presentation at ATHENA Workshop Rome October 25th – 27th 2004
38. C.J.Powell and A.Jablonski, “NIST Electron Inelastic-Mean-Free-Path Database”, NIST Standard Reference Database 71, (2000).
39. S.Tanuma, C.J.Powell and D.R.Penn, Surf. Interface Anal., 21, 165, (1994).
40 R.C.Corcoran, D.D.Jones, I.Vatter, S.R.Ortner, and P.Nenonen. Technique Comparison of Auger and FEGSTEM Measurement of Grain Boundary Composition in Pressure Vessel Steels and Model Alloys. PISA/R(12) March 2005.
41 S.B.Fisher, R.S.Scowen and B.J.Lee, private communication February 1996.

European Commission

EUR 23450 EN – Joint Research Centre – Institute for Energy
Title: Project PISA: Phosphorus Influence on Steel Ageing
Author(s): Colin ENGLISH, Nexia Solutions, United Kingdom – coordinator
Ferenc GILLEMOT, KFKI-AEKI, Hungary
Andrew DONALDSON, BNFL-Magnox, United Kingdom
Susan ORTNER, Nexia Solutions, United Kingdom
Peter KIZLER, MPA-Stuttgart, Germany
Milan BRUMOVSKY, NRI Rez, Czech Republic
Reinhard LANGER, FRAMATOME ANP, Germany
Pertti NEONEN, VTT, Finland
Antonio BALLESTEROS, Tecnatom, Spain
Beatriz ACOSTA-IBORRA, JRC-IE, Netherlands
Filippo SEVINI, JRC-IE, Netherlands
David BACON, University of Liverpool, United Kingdom
Sebastian SAILLET, EDF, France
Marta HORVATH, KFKI-AEKI, Hungary
Milos KYTKA, NRI Rez, Czech Republic

Luxembourg: Office for Official Publications of the European Communities
2008 – 90 pp. – 21 x 29.7 cm
EUR – Scientific and Technical Research series – ISSN 1018-5593

Abstract
The integrity of the pressure vessel is vital to the safe operation of a nuclear reactor. It is therefore necessary to monitor or predict the changes in the reactor pressure vessel (RPV) material during operation. Exposure to irradiation (or elevated temperatures) causes the segregation of phosphorus to internal grain boundaries in RPV steels. This, in turn, encourages brittle intergranular failure of the material. The PISA project had the objective of reducing the uncertainties associated with the impact of this failure mechanism on the properties of the RPV, both during service and at the end-of-life.
This report presents the experimental results on the segregation of P and C during irradiation and thermal treatments, and the associated mechanical property changes, generated within PISA. The new data cover a range of bulk P levels, irradiation temperatures and fluences, steel types and product forms. In all cases only modest increases of P level on the grain boundary have been observed in commercial steels. Segregation is higher in pre-strained than in unstrained material. In addition a model for P segregation under irradiation has been developed, and shown to be capable of fitting the experimentally observed changes in P level after irradiation. Significant insight into the development of the microstructure under irradiation has thereby been obtained. Overall, the data and modelling together indicated that relatively small amounts of segregation are likely to occur under most reactor operational conditions in homogeneous commercial steels, and an (unexpectedly) small amount of additional embrittlement likely to derive from this process during reactor service.

The mission of the JRC is to provide customer-driven scientific and technical support for the conception, development, implementation and monitoring of EU policies. As a service of the European Commission, the JRC functions as a reference centre of science and technology for the Union. Close to the policy-making process, it serves the common interest of the Member States, while being independent of special interests, whether private or national.